Carbon dioxide capture by carbon adsorbents derived from waste plastics

Thesis

Submitted in partial fulfillment for the award of degree

of

Doctor of Philosophy

By

BALPREET KAUR

(Registration No.: 951601001)

Under the guidance of

Dr. Haripada Bhunia
Professor
Department of Chemical Engineering,
Thapar Institute of Engineering & Technology (Deemed to be University),
Patiala

Dr. Raj Kumar Gupta
Professor
Department of Chemical Engineering,
Thapar Institute of Engineering & Technology (Deemed to be University),
Patiala

Department of Chemical Engineering
Thapar Institute of Engineering & Technology (Deemed to be University)
Patiala – 147004, Punjab, India
www.thapar.edu

October 2020

Dedicated

To

My Parents,

My Husband

Dr. Harjinder Singh

And

My children

Agam and Mankirat

Certificate

This is to certify that the thesis entitled "**Carbon dioxide capture by carbon adsorbents derived from waste plastics"** being submitted by **Ms**. **Balpreet Kaur (Roll. No. 951601001)** to Department of Chemical Engineering, Thapar Institute of Engineering & Technology (Deemed to be University), Patiala, for the award of degree of **Doctor of Philosophy,** is a record of bonafide research work carried out by her under our guidance and has fulfilled the requirements for the submission of this thesis, which to our knowledge has reached the requisite standard.

The results embodied in the thesis have not been submitted either partially or wholly to any other university or institute for the award of any other degree or diploma.

(Haripada Bhunia)
Professor & Head
Department of Chemical Engineering,
Thapar Institute of Engineering &
Technology (Deemed to be University),
Patiala

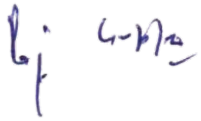

(Raj Kumar Gupta)
Professor
Department of Chemical Engineering,
Thapar Institute of Engineering &
Technology (Deemed to be University),
Patiala

Dated:

Acknowledgements

I would like to thank most sincerely my supervisors **Dr. Haripada Bhunia (Prof. & Head) and Prof. Raj Kumar Gupta**, Department of Chemical Engineering, Thapar Institute of Engineering & Technology (Deemed to be University), for providing me such a valuable research opportunity and for their countless guidance and motivation during the course of my research. I learned a lot from them over the course of this Ph.D. work. Their goal-oriented style of work, passion towards research, work ethic, has been very inspiring for me. Their daily practice of following up on recent scientific literature is something that I also tried to adopt and greatly benefitted. I really appreciate their unconditional support and encouragement towards doing high-caliber research. It's been a great honor to work under their guidance.

I am extremely thankful to **Dr. Prakash Gopalan**, Director, Thapar Institute of Engineering & Technology (Deemed to be University), **Dr. Rafat Siddique**, Dean of Research & Sponsored Projects, Thapar Institute of Engineering & Technology (Deemed to be University) for extending the opportunity to undertake this doctoral research.

I would like to profoundly thank my doctoral committee members **Dr. J. P. Kushwaha** and **Dr. Sudhir K. Singh** of Chemical Engineering and **Dr. O. P. Pandey**, **(Senior Professor & Head)**, School of Physics & Material Science, Thapar Institute of Engineering & Technology (Deemed to be University) for their immense help and guidance in the right direction. My heartful thanks to the staff members of the Department of Chemical Engineering, Thapar Institute of Engineering & Technology (Deemed to be University) for their valuable contribution and moral support.

My sincerest thanks are to **Dr. P. K. Bajpai** (Ex-Distinguished Professor), Department of Chemical Engineering, Thapar Institute of Engineering and Technology, Patiala for providing scientific advice and technical knowledge through many insightful discussions. His valuable comments and suggestions helped me a lot to improve my manuscripts.

My endless thanks go to Dr. Deepak Tiwari, Dr. Jasminder Singh, Dr. Dev Kumar Mandal, Mr. Saudagar Balasaheb Dongare and Mr. Sunil Sable for their assistance and support at

various stages of my research work. I would also like to express my deepest gratitude to my husband Dr. Harjinder Singh who always encouraged me and supported me to accomplish this task. Words cannot express how grateful I am to my mother-in-law, my mother and father for all the sacrifices they made on my behalf. Special thanks to my beloved children, Agamjot Singh, and Mankirat Singh, for enduring with me for not giving them sufficient time and always cheering me up during difficult times.

Finally, I thank the almighty God for his sufficiency and letting me through all the difficulties.

(Balpreet Kaur)

Abstract

In the present era, one of the major threats to environment is climate change and the well known and accepted basis for this is greenhouse gas (GHG) emissions. CO_2 is the key contributor promoting global warming and subsequently affecting the climate as manifested by frequent occurrence of floods and droughts, progressive rise in temperature and sea levels, heat waves and melting of glaciers. To economically sequester CO_2, it is imperative to comprise cost-effective capture for which the adsorption-based post-combustion CO_2 capture has been identified as a promising alternative due to its lower energy requirements, cost-effectiveness, and simplicity in use at a broad range of temperatures. However, the main challenge in successfully commercializing adsorption technology is the development of effective and low-cost adsorbents. Further, plastic waste generation is another major problem that is causing a deleterious effect on our environment. It is estimated that approximately 15,000 tonnes of plastic wastes are generated every day in India and polyethylene terephthalate (PET) waste takes around 500-700 years to biodegrade, therefore environmentalists are seriously concerned about its disposal.

Literature studies indicate that carbons from PET wastes especially chemically activated ones have immense potential to adsorb CO_2 due to generation of micro/meso pores post carbonization. Also, it has been observed that majority of the CO_2 capture studies on PET-based adsorbents have been performed thermogravimetrically which is a suitable method for preliminary studies and cannot be implemented on large scale at industry level. Moreover, in this method adsorption is measured on weight gain basis which may involve higher component of error due to adsorption of other gases. Therefore, there is a need to perform CO_2 adsorption studies in a packed column which can be scaled up. Hence, in current study our aim is to prepare porous carbons from PET, post-consumer plastic waste and evaluate its CO_2 adsorption capacity under dynamic conditions by performing breakthrough experiments.

Fig. 1 shows the schematic of overall thesis work.

O-enriched porous carbonaceous adsorbents have been developed from low cost, abundantly available polyethylene terephthalate (PET) waste with high carbon content by directly carbonizing at different temperatures (500 to 800 °C) and then chemically activating using variable impregnation ratios of KOH to carbon (1 to 4). The prepared carbon adsorbents were

characterized for their textural and surface chemical properties using nitrogen sorption, CHN, FTIR, XRD, SEM, HRTEM, TPD, and XPS techniques. Further, to assess their CO_2 adsorption-desorption performance under dynamic conditions, breakthrough experiments were conducted in fixed-bed adsorption set up. Porous carbon obtained at 700 °C with KOH to carbon mass ratio of 3 (Act-3-700) exhibited best textural properties with BET surface area of 1690 $m^2\ g^{-1}$ and micropore volume of 0.78 $cm^3\ g^{-1}$ and showed highest CO_2 uptake of 1.31 mmol g^{-1} at 30 °C and 12.5% CO_2 concentration. Five adsorption-desorption cycles establish adsorbent's remarkable stability and regeneration. The kinetics of adsorption process was studied using Lagergren's pseudo-first-order model, pseudo-second, and fractional order, Elovich, and Avrami models. Among these five models, fractional-order model best explained the CO_2 adsorption kinetics. Further, three isotherm models were used to analyze the equilibrium data and Freundlich isotherm showed a superior fit, thus confirming the heterogeneous nature of adsorbent's surface. Negative values of Gibbs free energy ($\Delta G°$) and adsorption enthalpy ($\Delta H°$) indicate the spontaneous and exothermic nature of adsorption process. Thermal energy needed for desorbing CO_2 from the activated adsorbent was found to be 1.34 MJ per kg CO_2, which corresponds to ~11.84% energy penalty. The average value of isosteric heat of adsorption was estimated to be 12.08 kJ mol^{-1}, indicating predominance of physisorption. Adsorption column breakthrough profiles were modeled using Linear Driving Force (LDF) approximation for mass transfer. Model equations were solved using the Method of lines in MATLAB environment. Results show that the model closely approximated the column breakthrough curves for different CO_2 concentrations (5%-12.5%) and different adsorption temperatures (30-100°C).

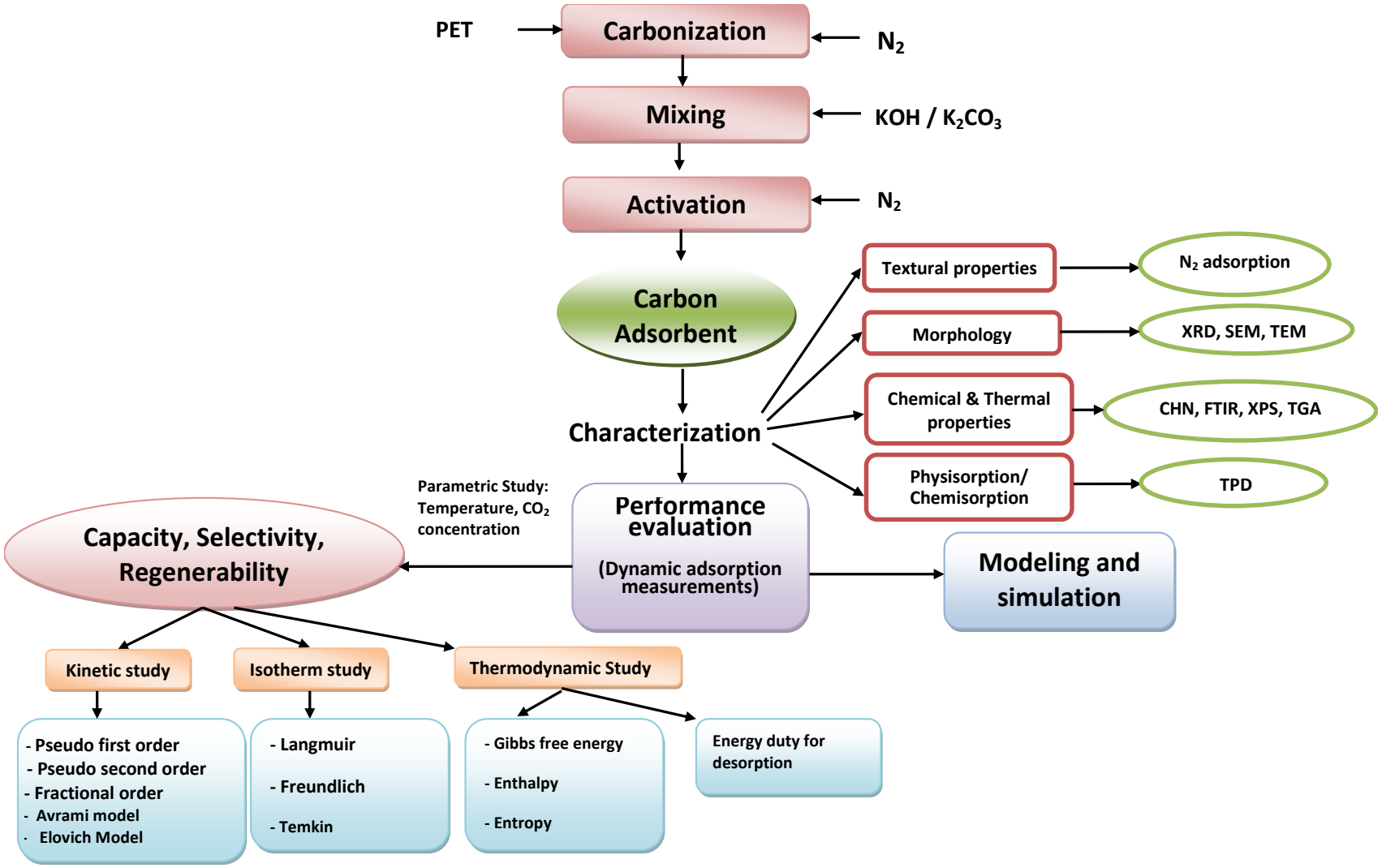

Fig. 1 Schematic of overall thesis work

TABLE OF CONTENTS

LIST OF FIGURES

LIST OF TABLES

LIST OF SYMBOLS

α	initial adsorption rate, mmol $g^{-1}s^{-1}$
C_b	bulk phase concentration of CO_2, mol m^{-3}
C_s	concentration of CO_2 in equilibrium with surface concentration, mol m^{-3}
d_p	diameter of the particle, m
d_b	diameter of bed, m
D_{ax}	axial dispersion coefficient, m^2 s^{-1}
$D_{m,i}$	molecular diffusivity of component i, m^2 s^{-1}
$D_{m,j}$	molecular diffusivity of component j, m^2 s^{-1}
u_i	interstitial velocity, m s^{-1}
u_s	superficial velocity, m s^{-1}
k_f	film mass transfer coefficient, m s^{-1}
y_i	molar fraction of component i
P_t	total pressure, atm
q_i	adsorbed phase concentration of component i, mol kg^{-1}
Q_v	Volumetric flow rate of gas in ml min^{-1}
m_a	mass of adsorbent, g
C_o	concentrations of CO_2 at inlet, mmol ml^{-1}
C	concentrations of CO_2 at the outlet, mmol ml^{-1}
T	temperature, ^oC
x	axial distance along the column, m
M_i , M_j	molecular weight of component i and j, g mol^{-1}
R_g	universal gas constant
a_p	radius of the particle, m
T_i	feed temperature, K
P	CO_2 partial pressure, atm
K_F	Freundlich constant for adsorbate, mmol $g^{-1}atm^{-1/n}$
K_L	Langmuir constant, atm^{-1}
K_T	Temkin constant, atm^{-1}
k_1	pseudo-first order rate constant, min^{-1}
k_2	pseudo-second order rate constant, g $mmol^{-1}$ min^{-1}

k_n	fractional order rate constant
k_a	Avrami constant, min^{-1}
$q_{t(\exp)}$	Amount of adsorbate adsorbed at equilibrium determined experimentally, mmol g^{-1}
$q_{t(pred)}$	amount of adsorbate adsorbed at equilibrium as predicted by model, mmol g^{-1}

Dimensionless numbers

Re	Reynolds number = $\frac{u_s d_p \rho_g}{\mu_g}$
Sc	Schmidt number = $\frac{\mu_g}{\rho_g D_m}$
Sh	Sherwood number = $\frac{k_f \times d_p}{D_m}$

Greek letters

ε_b	bed voidage
ε_p	particle porosity
$\frac{\varepsilon_i}{\kappa}, \frac{\varepsilon_j}{\kappa}$	Lennard Jones parameter for pure gases, K
$\frac{\varepsilon_{ij}}{\kappa}$	Lennard Jones parameter for gas mixture, K
σ_i, σ_j	collision diameter for pure gases, Å
σ_{ij}	collision diameter for gas mixture, Å
μ_i, μ_j	viscosity of pure gases, kg $(m.s)^{-1}$
μ_g	viscosity of gas mixture, kg $(m.s)^{-1}$
ρ_g	density of gas, kg m^{-3}
Ω_μ	collision integral of pure gas
Ω_{ij}	collision integral of gas mixture
ρ_p	density of particle, kg m^{-3}

LIST OF ABBREVIATIONS

ASU	Air separation unit
AOS	Amino-organo siloxanes
A%	Relative area percentage
B. E.	Binding energy
BET	Brunauer-Emmett-Teller
BJH	Barrett-Joyner-Halenda
BMC	Basic magnesium carbonate
COP	Conference of parties
CNT	Carbon nanotubes
CR	Catalytic reduction
DEA	Diethanol amine
DTG	Derivative thermogravimetric
ESP	Electrostatic precipitator
FDG	Flue gas desulphurization
FTIR	Fourier transform infrared
FWHM	Full width at half maximum
GHGs	Greenhouse gases
Gt	Gigatonnes
HFC	Hydrofluorocarbons
HMS	Hexagonal mesoporous silica
IPA	Isopropanol amine
IEA	International energy agency
IGCC	Integrated gasification combined cycle
IPCC	Intergovernmental panel on climate change
KCA	Potassium carbonate activated
LDF	Linear driving force
MDEA	Methyldiethanol amine
MEA	Monoethanol amine
MCM	Mobil crystalline material
MOFs	Metal-organic-frameworks
MOL	Method of lines
MWCNT	Multi-walled carbon nanotubes

NLDFT	Non-local density functional theory
OTM	Oxygen transport membrane
PEI	Polyethyleneimine
PET	Polyethylene terephthalate
ppm	Parts per million
PL	Potassium lysinate
PSA	Pressure swing adsorption
PSD	Pore size distribution
PTSA	Pressure temperature swing adsorption
SBA	Santa Barbara amorphous
SWCNT	Single-walled carbon nanotubes
TEM	Transmission electron microscopy
TG	Thermogravimetric
TSA	Temperature swing adsorption
VSA	Vacuum swing adsorption
wt%	Weight percent

Chapter 1 – Introduction

1.1 Greenhouse gas emissions and global climate change

The immense requirement of energy due to rapid industrialization and explosive population growth in the present era has led to tremendous use of fossil fuels [1]. This augmented usage of fossil fuels due to anthropogenic activities has elevated the release of primary greenhouse gases (GHGs) or heat trapping gases in the environment leading to global warming and severe climatic conditions [2]. In 2014, IPCC endorsed the above stated fact through their report. Surprisingly, CO_2 holds the foremost share of about 76% of the total source of GHGs and is found to be the most worrisome anthropogenic greenhouse gas liable for causing damaging impacts on our environment [3, 4]. Besides, CO_2 concentration has drastically increased from ca. 280 ppm in 1750 to 412 ppm in 2019 and is expected to touch levels of 570 ppm by 2100 indicating a huge leap of around 45% in the last 250 years. These alarming levels of CO_2 have led to thinning of polar ice caps, heat waves, increase in acidity of oceans, uneven weather patterns, heavy rainfall, and droughts. Also, an average global temperature rise in the range of 2-6 °C is envisaged towards the end of this century. This will lead to grim consequences and therefore a reduction in GHGs by minimum 50% is required by 2050 [5].

Further, rise in CO_2 emissions has compelled the developing countries to build up sound policies on energy consumption and opt for CCS and clean energy technologies to curb environmental pollution. For achieving this, the government needs to incur cost on capturing and storage of CO_2. Besides, there is a need of efficient infrastructure for energy conversion to adequately deliver various forms of clean energy at affordable prices. Thus, it has affected the growth and economy of all the developed and developing nations and subsequently the individuals [6]. Hence, CO_2 concentration needs to be stabilized below 450 ppm to circumvent the abrupt rise in mean global temperature. Carbon dioxide is released into environment majorly from mega point sources like coal based power plants or industrial units, refineries, iron and steel manufacturing units [7], transportation and also from upcoming areas like hydrogen purification from biomass. Fossil fuel-based power plants contribute to circa 40% of the total CO_2 emissions [8] and therefore, they need immediate consideration for forthcoming CO_2 reduction [9]. Fossil fuel combustion alone meets around $4/5^{th}$ of the world's commercial energy demand and in turn, releases 3×10^{13} kg of CO_2 per annum in the atmosphere [10]. Since the demand for electricity is increasing, power generation will be responsible for about 50% increase in global CO_2 emissions within 2000 and 2030.

Trends in CO_2 emissions at global level during the years between 1960 and 2019 are shown in Fig. 1.1.

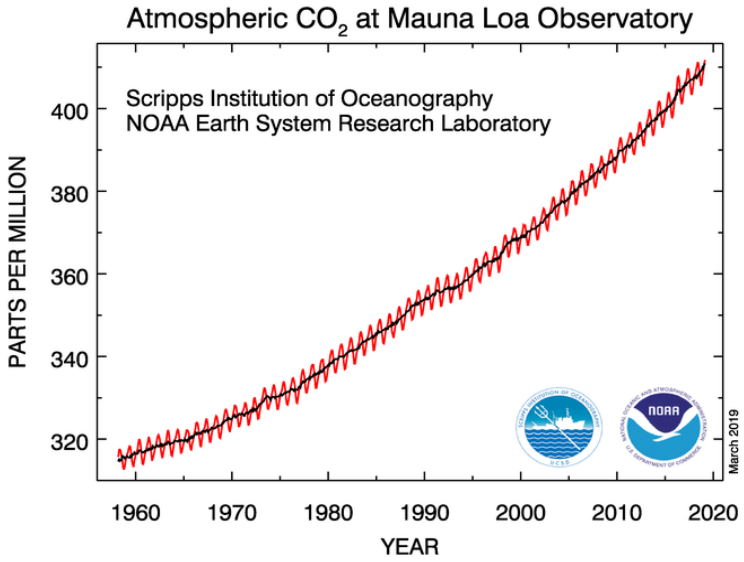

Fig. 1.1 Global trend of greenhouse gas emissions from 1960 to 2019 [11]

1.2 Pathways for CO_2 mitigation

In order to avoid the serious consequences due to CO_2 emissions, an agreement was signed by COP in Paris (UNFCCC, 2015) to combat the change in climate and to strengthen the steps or measures required for sustainable low carbon future. Also, their main motive was to stabilize the average temperature rise of the globe below 2 ^{o}C, rather near to 1.5 ^{o}C towards the end of the 21st century. Various strategies employed for reducing CO_2 concentrations are:

1. Reducing energy demand through the usage of efficient and improved energy conversion devices [12].
2. Increased usage of renewable energies, hydrogen, and nuclear power.
3. Decarbonization of power generation from fossil fuels.
4. Increasing vegetation and forests on land to provide improved air quality.
5. Carbon dioxide capture and sequestration (CCS) [13, 14].

1.3 CO_2 capture and sequestration

CCS has been acknowledged as a promising solution as it possesses immense potential to control the unregulated release of CO_2 from mega point sources [15]. As per reports of International Energy Agency (IEA), CCS will have to contribute about 20% reduction of emissions to cut down the global GHG emissions by 50% till 2050 at a nominal cost. Besides,

The IPCC report (2018) maintains that without CCS, the price of achieving long-run climate goals is almost 140% more expensive. Despite of recent thrust in renewable energy options like solar, wind etc., fossil fuels would still provide 60% of the world's primary energy by 2040. This confirms the urgency at which carbon capture and sequestration (CCS) must be applied to power and wider industry. If good emission reduction incentives are offered by the governments, CCS presents a very workable option to reduce CO_2 emissions. It has been estimated that ca. 5.1 Gigatonnes (Gt) of CO_2 needs to be captured per year and stored up by 2050. This would account to about 14% of the total requirement for stabilization of global temperature. This can be further improved by adopting the ETP BLUE Map scenario through which global CO_2 emissions could be halved and it would contribute to 19% of total emissions reductions in 2050 [16]. In this scenario, 10.4 gigaton of CO_2 per year would be captured and stored in 2050.

CCS technology involves capturing of major portion of the CO_2 gas (~ 90%) released from the utility and industrial plants especially those related to energy sector, thus inhibiting the inflow of carbon dioxide into the atmosphere. The captured CO_2 is transported all the way through pipelines and then compressed and stored in appropriate geological sinks such as oceans, depleted oil or gas fields and coal beds which are unminable. The technologies for CO_2 transport are well established. The CO_2 pipelines stretch covers more than 6500 km globally majority of which are connected with enhanced oil recovery operations in the U.S. [17]. CO_2 capture is applied mainly on mega point sources e.g. oil refineries and power generation plants as capturing of CO_2 from small and scattered point sources is rather difficult and not an economically viable process. Around 37 major CCS projects have been deployed worldwide out of which 17 are operating and rest others are either in construction stage or development stage. Fig. 1.2 shows the CO_2 capture capacity and the current status of large scale CCS projects at a global level from the year 2000 to 2019.

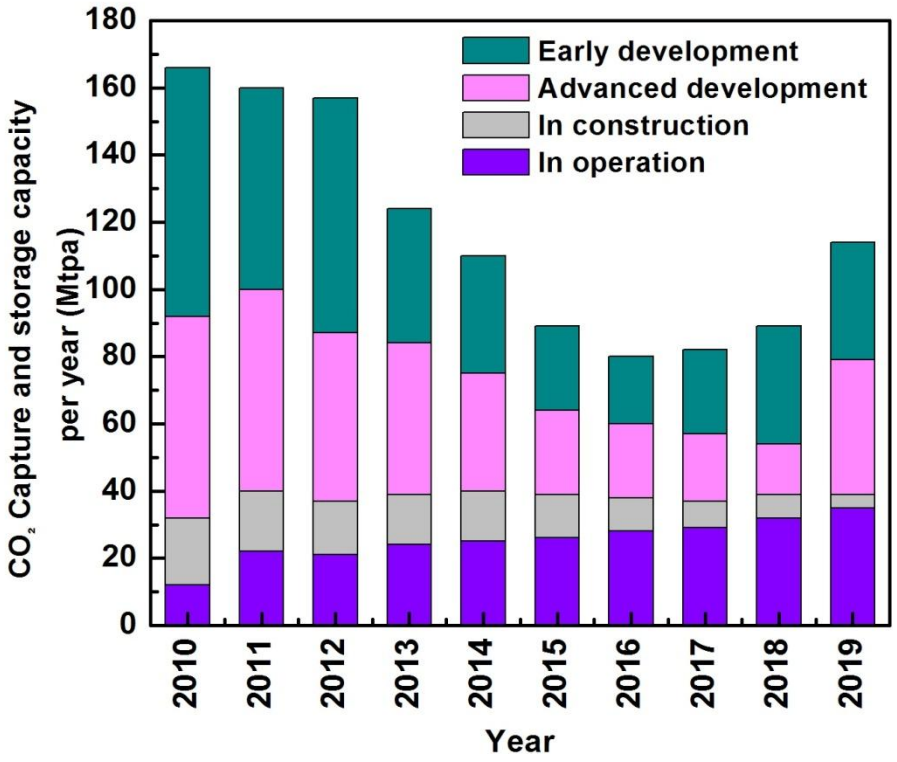

Fig. 1.2 CO_2 capture capacity of large scale CCS projects at a global level [18]

1.3.1 CO_2 capture technologies

Carbon capture has been acknowledged as a promising technology as well as essential tool for controlling the unregulated release of CO_2 into the atmosphere from the point sources [19]. The proportions of components present in the flue gas released from the coal-fired plants are summed up in Table 1.1. It clearly indicates an unacceptable percentage of CO_2 in the exit gas stream, and therefore this issue should be addressed at priority.

Table 1.1 Flue gas stack **c**omposition in coal fired power station [20]

Component	Units	Composition in flue gas
Nitrogen	volume %	70-80
Carbon dioxide	volume %	11-16
Oxygen	volume %	5-12
Water vapor	volume %	3-6
Oxides of sulphur	ppm	0-4000
Oxides of nitrogen	ppm	200-800
Carbon monoxide	ppm	50-100
Suspended matter	g m^{-3}	5-20

Fig. 1.3 shows the capturing of carbon dioxide from gaseous emissions via three approaches [21].

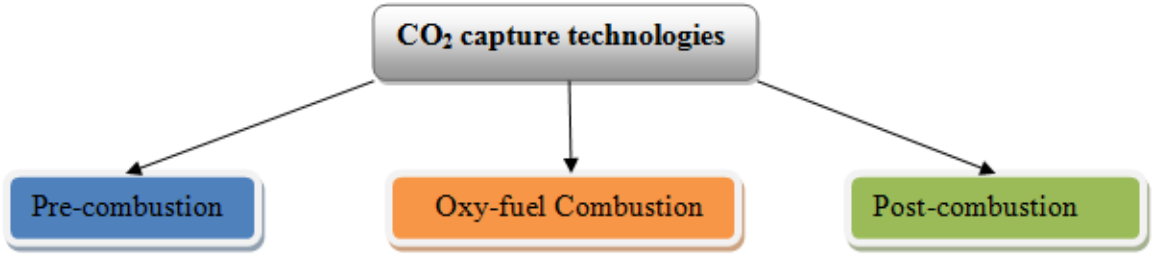

Fig. 1.3 Technological alternatives for CO_2 capture

1.3.1.1 Pre-combustion

In this technique fossil fuels are initially fed to the gasifier for gasification or partial oxidation of fuels prior to combustion [22]. This produces a mixture consisting mainly of carbon monoxide (CO), hydrogen (H_2), small amount of carbon dioxide and traces of methane. This mix is popularly identified as syn-gas which is further heated in a steam producing boiler (shift reactor) to generate CO_2 and hydrogen. Various steps for the process are shown in Fig. 1.4.

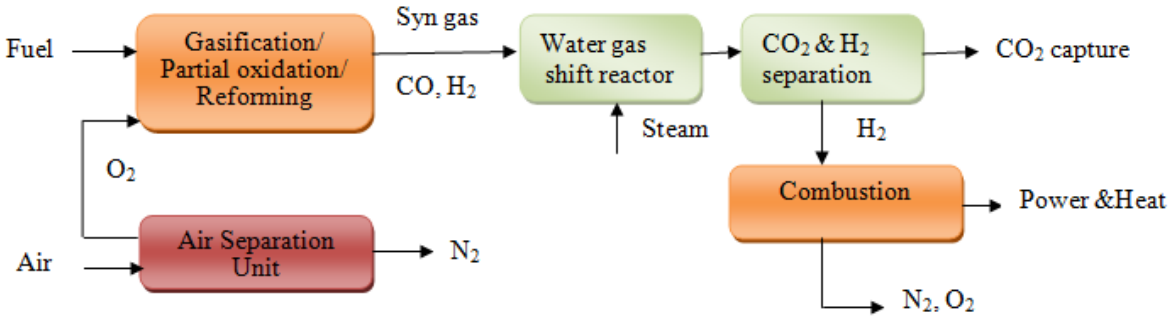

Fig. 1.4 Technology concept of pre-combustion CO_2 capture

The CO_2 is separated from the mixture and hydrogen finds its application as a fuel for combustion purpose, electricity generation, for powering cars and heating homes with almost zero emissions. The running expenses involved in carbon capture facilities depend mainly upon the extent of CO_2 concentration and its partial pressure in the exit stream. Fertilizer units, hydrogen generation plants, and integrated gasification combined cycle power plants majorly employ this technique [23].

1.3.1.2 Oxy-fuel combustion

Oxy-fuel combustion is a remarkable alternative for capturing carbon dioxide from both the fuel gas as well as flue gas by simply modifying the combustion process. This technique utilizes pure oxygen rather than air for burning fuel which is sent through an air separation unit (ASU). As a result, higher concentration of CO_2 gas is released in the flue gas. This process is demonstrated in Fig. 1.5.

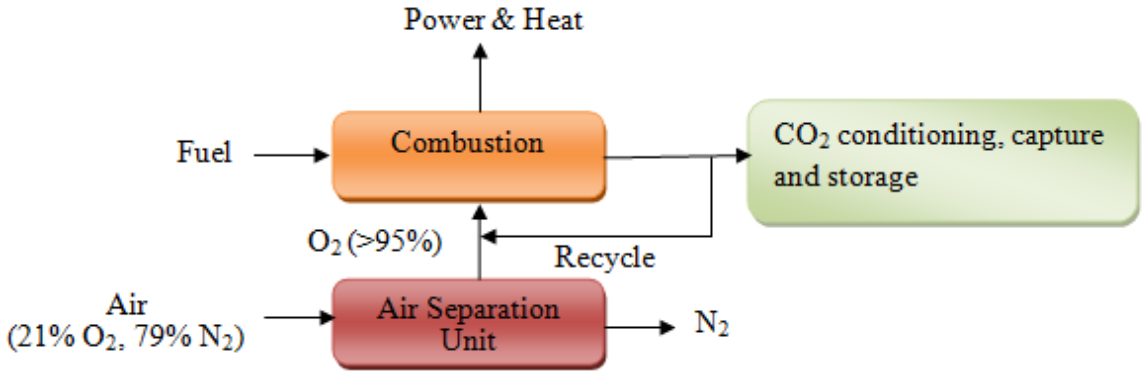

Fig. 1.5 Technology concept of oxy-fuel combustion

The CO_2 rich flue gas can be conditioned or compressed for storage without incurring much expense. However, the oxygen requirement in this process is almost tripled in comparison to any conventional IGCC plant of similar size which makes the technique expensive due to additional cost incurred on air separation units [24]. Also, this high purity oxygen stream is mixed with recycled flue gas before sending to the combustion unit in order to avoid overheating caused due to the combustion of coal in pure oxygen [25].

1.3.1.3 Post-combustion capture

Post-combustion capture works on the basis of CO_2 separation from the flue gas consisting mainly of nitrogen, nitrogen oxides and sulfur oxides which is generated during the combustion of fuels. Fig. 1.6 shows the process flow diagram for post-combustion capture. Flue gases released after combustion process are firstly pretreated by passing through various air pollution control devices such as catalytic reduction system (CR), electrostatic precipitator (ESP) and flue gas desulphurization (FGD). Nitrogen oxides can be removed through selective catalytic reduction in CR and the concentration of particulate matter fly ash can be removed with an ESP. Finally, FGD helps to separate sulfur oxides coming in the exhaust flue gas stream.

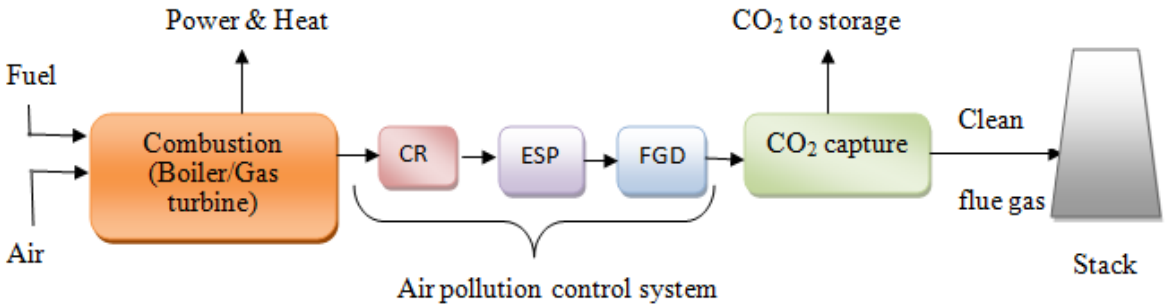

Fig. 1.6 Technology concept of post-combustion CO_2 capture

As the partial pressure of CO_2 (0.12 - 0.15 atm) is low and the temperature of flue gas is high, these conditions stand as a technical barrier in the path of a cost-effective capture process. In spite of all these limitations, this technology has been accepted worldwide. Since the majority of the power plants are coal-fired, the technological ease in retrofitting it to existing plants makes it a viable option in capturing CO_2 [26]. Also, the power plants are able to operate smoothly inspite of faults in the capturing system [27]. Most employed post-combustion capture systems are namely a) absorption using liquid solvents [28] (b) membrane systems [29] (c) cryogenic separation [30] (d) biological fixation [31] and (e) adsorption using solid materials [32].

However, the advances in post-combustion CO_2 capture technologies can make it less energy intensive along with higher recovery of CO_2 from large volumes of flue exhaust. One such upcoming technology is chemical looping (CL). CL is a concept that uses certain intermediate compounds like metal oxides which can potentially convert hydrocarbon fuels into other chemicals, electricity or hydrogen along with capturing of CO_2 at a very meager cost. Post combustion chemical looping process uses two reactors for undergoing carbonation-calcination reactions as shown in Fig. 1.7. For carbonation reaction, the first reactor is loaded with calcium oxide (CaO) which reacts with CO_2 gas from flue gas desulfurization unit to form calcium carbonate ($CaCO_3$), thus causing *in situ* capture of CO_2 without dilution [33]. This product is further fed to other reactor for calcination reaction, where $CaCO_3$ calcines at high temperature (> 900 ^{0}C) to yield high purity CO_2 which can be conveniently transported at appropriate storage sites. Besides, calcium oxide is also formed which is recycled to first reactor and thus the loop gets completed. Oxy-combustion of coal within the calciner is typically used as a source of heat for the calcination reaction. Heat can be recovered from the exothermic carbonation reaction, and from the gas and solid streams at high temperatures, to generate

additional electricity from the power plant. As a result, chemical looping technology has the potential to be thermodynamically more efficient than a conventional post-combustion CO_2 capture process using amines and impose lesser energy penalty [33].

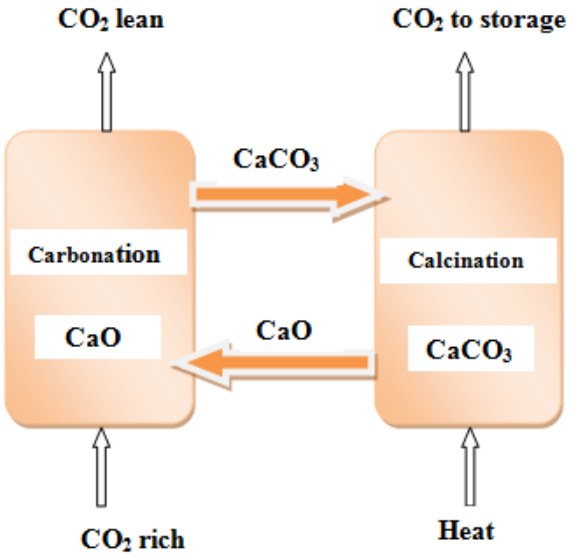

Fig. 1.7 Chemical looping for post combustion CO_2 capture

Advances in capture techniques from fossil fuels with time to commercialization are represented in Fig. 1.8.

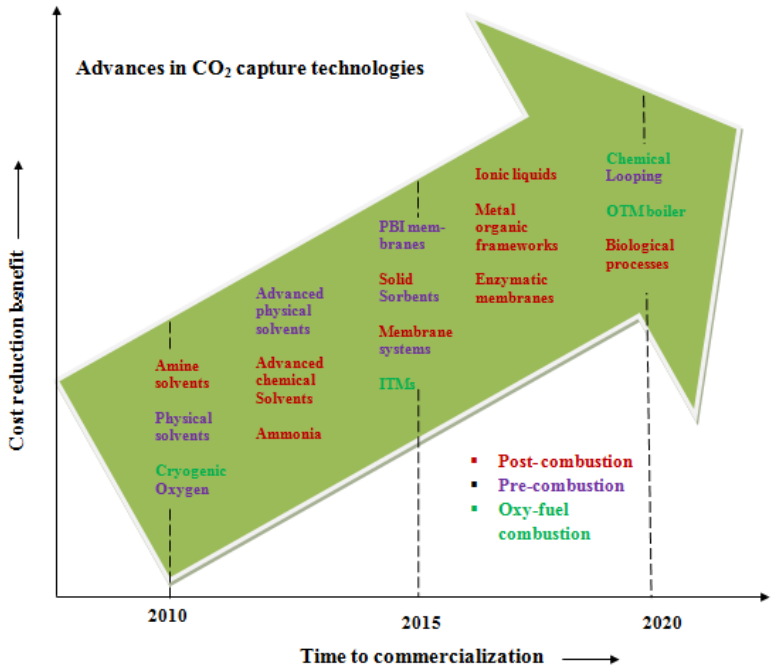

Fig. 1.8 Advances in fossil energy CO_2 capture technologies with time to commercialization [34]

*OTM – O_2 Transport Membrane and ITM – O_2 Ion Transport Membrane

1.3.1.3.1 Absorption

Among the several post-combustion capture processes, solvent-based absorption is considered the best available and mature technology for CO_2 separation/removal from flue gases and has blossomed considerably [35, 36]. In this process, CO_2 is absorbed in a liquid solvent which forms a bonded compound with CO_2. Later the solvent is recovered from the compound by heating and further reused in the next absorption cycle. It is mainly of two types: physical and chemical depending on the way how CO_2 solubilizes in the solution without chemical reaction or with chemical reaction. CO_2 absorption is preferred with physical solvents when the CO_2 partial pressure is high (>10 bar) and operating temperature is low [37]. On the other hand, chemical absorption is favored at moderate conditions, i.e. pressure of about 1 bar and temperature of ca. 40-50°C [38]. Commonly used physical solvents are Rectisol, Selexol, Purisol, Sepasolv-MPE and Morphysorb. MEA, DEA, and MDEA are widely used chemical solvents for CO_2 absorption at industrial level but they suffer from the drawbacks of CO_2 such as high equipment corrosion rate, amine degradation due to presence of SO_2, NO_2, HCl, HF, O_2 and other impurities, volatility at higher temperatures, requirement of quite tall absorption-desorption columns and high energy requirement for solvent regeneration [39]. In recent times, amino acid salts have drawn attention due to their low volatility and ability to resist oxidative degradation [40]. The amino acids of sarcosine, arginine, proline, and glysine mixed with reactive metals like potassium and sodium are extensively used for CO_2 absorption. Koutsianos et al. [41] first reported methanol as an alternative to water which can enhance the ability to facilitate CO_2 transport in polyethyleneimine based sorbents. The selection of methanol was made on the basis of Hansen solubility parameter (HSPs) which describes the interaction of a solvent molecule with others of its kind. These parameters for methanol were quite close to that of water. PEI based sorbent when exposed to methanol saturated CO_2 at 25 °C exhibited mass uptakes of CO_2 of about 0.3g g^{-1}. The possible reason for this was attributed to the formation of diffusive intermediates involving a methanol molecule, a primary amine group of PEI, and a CO_2 molecule which enhanced the ability to facilitate CO_2 transport.

Though absorption is known to be the most established technology, it will no longer be a preferred post-combustion technology as the regeneration of the solvent imposes high energy penalty.

1.3.1.3.2 Membrane technology

Membrane technology is being successfully used by the industry from the last four decades. Gas separation via membranes works on the principle of selective permeation of a particular component (e.g. CO_2) through the membrane material and retaining the remaining components. Membranes made from organic (polymeric materials), inorganic, mixed or hybrid materials are generally used for capturing CO_2 in post-combustion process [42]. It can be used independently or in conjunction with absorption where it acts as a contactor of CO_2 gas and amine solution. CO_2 gas after passing through the membrane gets absorbed in amine solution leaving behind other impurities in the gaseous phase.

Membrane separation has been acknowledged promising due to its operational and maintenance simplicity, compactness, energy efficiency and cost-effectiveness [43, 44]. However, high degree of CO_2 separation cannot be achieved through membranes due to lean concentration/ low partial pressure of CO_2 gas in flue exit. Various other factors such as life and cost of membranes, handling of membranes at high temperature of flue gas, multiple stages and recycle streams to attain high CO_2 capture efficiency and impact of various impurities on membrane performance and stability need to be resolved before scale up of this technology. Thus, it becomes imperative to develop membranes from novel materials for efficient separation [45]. The simplified schematic of membrane separation technique is illustrated in Fig. 1.9.

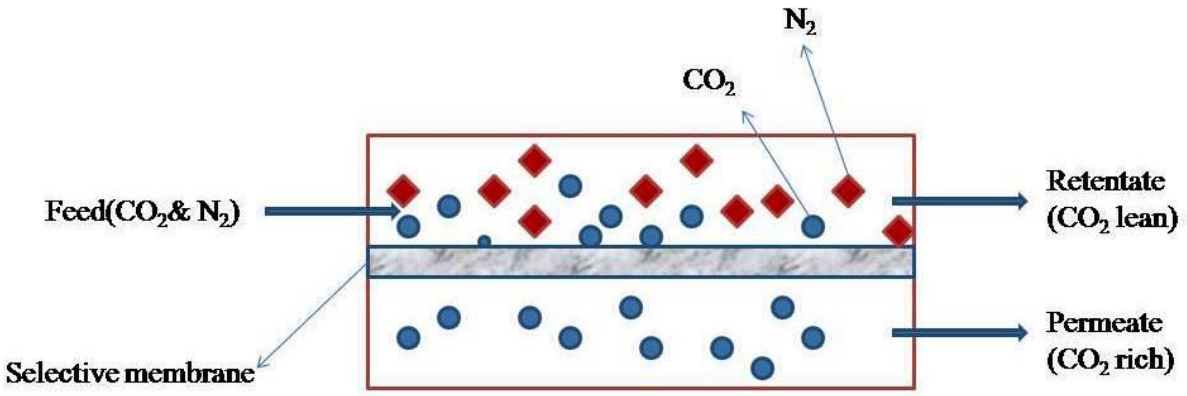

Fig. 1.9 Simplified schematic of the membrane separation technique

1.3.1.3.3 Cryogenic distillation

In this technique flue gases are separated on the basis of freezing points of the components and the desired product is liquefied by varying the temperature and pressure. At atmospheric pressure, the temperature below -73.3 ^{o}C is required for condensing CO_2. Heat exchangers,

compressors, cold traps, and Joule-Thompson valves are used to obtain these cryogenic temperatures [30]. Presently, cryogenic separation is obtained by desublimating CO_2 on the fins of the heat exchangers or on the packed beds [46, 47]. In the former case, the liquid CO_2 is recovered by further heating and pressuring the solid CO_2 and in the latter case fresh gas stream is introduced to the column in order to raise the temperature and improve the concentration of the CO_2 gas recovered from packed bed. Fig. 1.10 shows the cryogenic separation of CO_2 from flue gas in a distillation tower after removal of undesired components. The N_2 exits the distillation tower after absorbing heat from gas mixture coming from heat exchanger. CO_2 gets liquefied or solidified and collects at the bottom [48].

The advantages of this process are a) liquid CO_2 can be easily transported through pipelines, and b) high purity CO_2 (>99.95%) is obtained. But the following disadvantages limit its usage in practical applications: a) it is quite energy-intensive as there is continuous usage of energy for maintaining very low temperature b) the other gases like NO_x, SO_x, oxygen and water vapors need to be removed before initiating the distillation [48]. On the whole, the drawbacks of this process make it cost-inefficient.

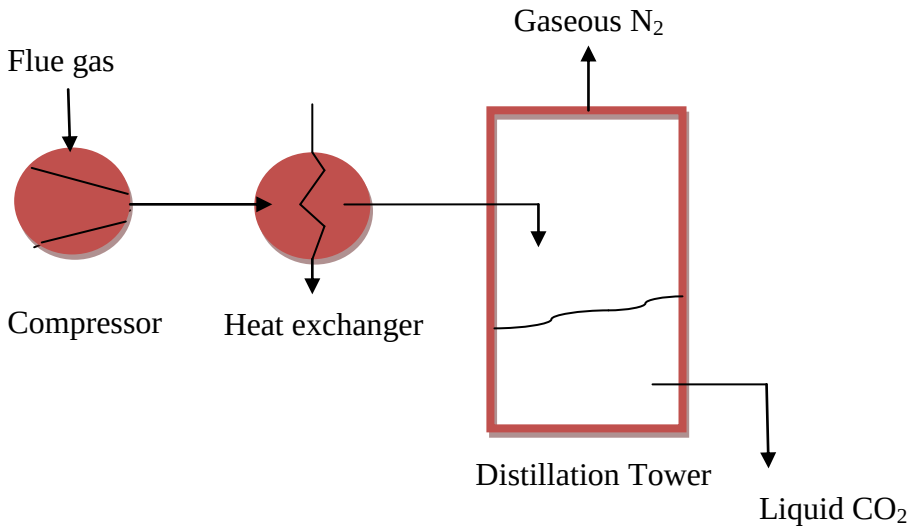

Fig. 1.10 Cryogenic separation of CO_2 from exhaust flue gas

1.3.1.3.4 Biological fixation

Apart from existing physical and chemical methods, biological and biochemical methods have also been explored for CO_2 separation by many researchers [31, 49]. Biological species such as algae, seaweeds, cyanobacteria, and even autotrophic bacteria utilize CO_2 (as carbon source)

emitted from industrial processes or power plants to produce bio-fuels and numerous bio-chemicals [30]. Algae has the capability to absorb CO_2 present in the flue gas exhaust and results in enhanced growth in the presence of sunlight, nutrients, metals (trace elements) and nitrogen. Another benefit of algae is that it grows in moist environment and therefore the flue gases can be directly passed through the algal medium. Inspite of these advantages algal cultivation for sequestration of CO_2 faces following main challenges: high operating cost, limited availability of sunlight, high temperature and varying composition of flue gas [31].

1.3.1.3.5 Gas hydrate separation

Gas hydrate based separation is an upcoming technique with an immense potential for efficient and selective post-combustion capture of CO_2 from flue exhaust. Gas hydrates recognized as clathrates are physical solids formed from water and hence they resemble ice. The hydrogen bonds in the water molecules freeze and form a cage like structure which possesses the ability to trap small molecules of gases like carbon dioxide, hydrogen, nitrogen, methane, etc [50]. Here water behaves as 'host' and capture the 'guests' which are gas molecules or any other non-polar hydrophobic compounds present in flue gas mixture. The clathrate formation takes place only at certain specific conditions such as low temperature and high pressure. Besides, CO_2 gas has much higher affinity for water than other gas molecules and hence the host becomes enriched with more CO_2. Later, the CO_2 gas can be separated from the cage either by heating or by releasing the pressure.

Low energy penalty is the main advantage of this technology, however still lot of research is required to implement it at large scale [51]. One of the problems faced during hydrate formation is of agglomeration of the crystalline hydrates at the interface which substantially reduce the conversion of water to hydrates (almost < 20%). Also, stirring cost may significantly add to the overall processing costs if continuous stirred tank reactors are used on commercial scale.

1.3.1.3.6 Adsorption

Though absorption is considered to be the most matured technology, yet it suffers from several drawbacks which have been well documented in the literature such as low CO_2 loading, low gas/liquid contact area, and severe absorbent corrosion problems. These limitations have impelled the researchers to search for a better technological option which can address the problem of CO_2 capture. One viable route is adsorption which has been recognized as an attractive substitute of absorption due its simplicity and availability of variety of adsorbents

[52]. In addition, it is a cost-efficient technology as it can be put into practice in the existing power plants and also accomplishes the objective of reducing energy penalty.

Adsorption is a very natural phenomenon in our daily lives. Even common solids have the ability to adsorb moisture and gases to some extent. For example, the groceries and bakery products lose their crispness and dried porcelain crucible gains weight in humid days which is due to adsorption of moisture from air. However, only certain solids possess specific surface properties and sufficient adsorptive capacity for their application at industrial level. At large scale, adsorption finds in gas separation, dehumidification of air and other gases, deodorization and removal of impurities like CO_2 from gas mixtures. The adsorbent properties such as specific surface area, distinct pore structure, polarity, surface functionalized groups etc. are the key factors that decide the ideality of an adsorbent in capturing CO_2. Further, thermodynamic properties of the material govern efficient transfer of gaseous phase onto solid phase. Depending upon the surface properties of the adsorbent, the adsorbate molecules may temporarily retain on surface or may form chemical bonds with adsorbent. The former retention is known as physical adsorption and later as chemical adsorption.

Flue gas treatment involves selective retention of CO_2 from mixture of various gases on the adsorbent, subsequently followed by regeneration. The latter step is accomplished by various options like heating the adsorbent at high temperature, reducing pressure below atmospheric, passing electric current, purge gas stripping and displacement desorption [53].

An effective adsorbent is expected to possess following characteristics: (1) low cost and easy availability, (2) high working capacity and preferential selectivity of CO_2 over N_2, (3) easy regenerability, (4) stability, (5) faster reaction kinetics, and (6) good abrasive resistance in packed beds [54, 55]. The main adsorbents generally used are: fuller's earth, active clays, bauxite, bone char, gas-adsorbents, molecular sieves, activated carbon and synthetic polymeric adsorbents [56, 57].

1.4 Thesis motivation and objectives

Adsorption emerges to be a propitious and promising technology for CCS due to its potential to capture carbon dioxide from major point sources and thus contribute in mitigation of climate change. However, the main challenge behind successfully commercialization of adsorption technology is the development of effective and low-cost adsorbents. Lower surface areas and hydophobicity limit the use of conventional adsorbents for high-performance CO_2 capture.

Amine functionalization and heat treatment appeared as remedial methods which helped to improve the CO_2 adsorption capacity as well as regenerability of these adsorbents but they had to face problems like pore blockage and poor stability. In lieu of this, carbon-based adsorbents gained attention due to their well-developed pore structures, easy availability, low energy requirements, and low costs. Also, development of adsorbents from plastic waste especially PET waste has not been taken much into consideration, though it is a great menace to the society because of its non-biodegradability, abundant littering, inefficient collection, and limited recycling capabilities. PET is highly recyclable, but the weight of the containers causes high frequency of collections which leads to increase in the transport costs. In addition, it needs to be segregated into different grades and colors that make its recovery inefficient and expensive [58]. To handle its disposal problem, researchers came up with another useful alternative of converting this waste into a valuable product such as activated carbon for solving one more environment issue i.e. CO_2 capture. Several factors such as well-developed pore structure, high surface area whose values reach even higher than those of commercial AC, ability to modify surface characteristics and porosity by incorporating hetero atoms, easy availability and low cost support its selection as a precursor for synthesis of AC for CO_2 capture [59, 60].

In addition, substantial work has not been done to modify the carbon adsorbents obtained from PET wastes by physical and chemical activation for CO_2 capture. It was also observed that most of the researchers tried to assess the static CO_2 uptake of developed adsorbents which holds less relevance to CO_2 capture from flue exhaust gases in real-life applications. To overcome this gap, carbon adsorbents were developed from PET waste, chemically activated and then investigated for CO_2 adsorption studies under dynamic flow conditions by different CO_2 concentrations (5-12.5%) and temperatures (30-100°C). Further, for better understanding of the adsorbents and adsorption process, mathematical modeling and simulation has been performed, that considers all relevant transport phenomena and saves experimental time.

The main objectives of thesis are:

- ✓ Development of carbon adsorbents from waste plastics (PET wastes), having specific pore structures and surface areas.
- ✓ Activation (physical/chemical) of adsorbents for its modification.
- ✓ Performance evaluation of adsorbents on fixed-bed column at different conditions of temperature and CO_2 concentration.
- ✓ Comparison of experimental data with equilibrium and kinetic models.

- ✓ Modeling and simulation of the fixed bed adsorption process.

1.5 Thesis overview

Microporous carbon adsorbents were prepared from polyethylene terephthalate (PET) waste by direct carbonization and then activation with KOH activation for CO_2 capture studies. The developed adsorbents were characterized for textural properties by nitrogen adsorption/desorption, morphology by XRD, SEM and HRTEM and chemical & thermal properties by FTIR, XPS and CHN analysis. In addition, to evaluate their CO_2 adsorption-desorption performance column breakthrough experiments under dynamic flow conditions were conducted in a fixed-bed set-up designed for adsorption studies. Regenerability studies were conducted to assess the ability of adsorbents to perform in long term. Also, kinetics and thermodynamics of CO_2 adsorption were assessed. Further, equilibrium uptakes were fitted to different isotherm models. Heat duty required for regeneration of the adsorbent was also evaluated. Adsorption column breakthrough profiles were modeled using linear driving force (LDF) approximation for mass transfer. Model equations were solved using the Method of Lines in MATLAB environment.

The overall thesis consists of **six chapters**.

Chapter 1 is the introduction which highlights the recent environmental issues of global warming and climate change. It raises concern over the alarming levels of CO_2 in the atmosphere and their adverse impacts on environment. Various mitigation pathways for CO_2 emissions have been briefed along with description of available CO_2 capture technologies. The main focus is on post-combustion CO_2 capture via adsorption. At the end of chapter, the problem statement is defined and the objectives of the research are specified.

Chapter 2 presents the review of literature which includes elaborate study of numerous solid adsorbents developed for capturing CO_2 and their adsorption performance under different conditions. Among them, activated carbons synthesized from waste materials have been more emphasized in the current research work.

Chapter 3 is materials and experimental methods which covers the specifications of materials and reagents used in current study along with the experimental methods employed for characterization of adsorbents and their performance evaluation. Further, the description of fixed-bed adsorption set-up used for performance evaluation is given. The theoretical aspects of

thermodynamics, kinetic as well as isotherm models have been elaborated together with mentioning of software used for simulation.

Chapter 4 describes the development of carbon adsorbents from polyethylene terephthalate (PET) waste by carbonization followed by chemical (KOH or K_2CO_3) activation. The chapter presents the details of characterization, performance evaluation for CO_2 adsorption and the factors affecting the later. Further, the inference of results is correlated with their surface, textural and chemical properties. The optimal sample was subjected to dynamic adsorption study in the fixed bed reactor at different adsorption temperatures using gas composition (CO_2 & N_2) similar to flue gas. The maximum adsorption capacity of 1.31 mmol g^{-1} was obtained for Act-3-700 (optimized sample) at 30 °C and 12.5% CO_2. Further, in this chapter complete kinetic analysis, isotherm study and thermodynamic investigations for CO_2 adsorption were performed on the optimal sample. In the last, energy penalty for complete process was also determined. Fractional-order best explained the kinetics of adsorption and Freundlich model fitting along with high values of isosteric heat supported the adsorbent's surface heterogeneity. At all adsorption temperatures, negative values of Gibbs free energy as well as enthalpy were obtained which confirm the spontaneity of adsorption process and substantiate the exothermic nature of process respectively. The energy needed for desorbing 1 kg CO_2 from the activated adsorbent was found to be 1.34 MJ, which corresponds to 0.0576 kg CO_2 (~11.84% energy penalty).

Chapter 5 covers the mathematical modeling of the fixed-bed adsorption. In this chapter fixed-bed adsorption of CO_2 on developed carbon adsorbent was modeled using LDF approximation. Further, the model was simulated in MATLAB using the Method of Lines and validated with the experimentally obtained data. The fixed bed model for CO_2 adsorption on the optimized adsorbent sample (Act-3-700), satisfactorily described the experimental adsorption behavior. The model predicted breakthrough curves at different concentrations of CO_2 in feed (5-12.5 vol %) and temperatures (30-100 °C) matched closely with the experimentally generated results.

Finally, chapter 6 summarizes the conclusions derived from the experimental and theoretical data and also presents the scope of future work.

In the last part of thesis, list of cited references has been provided.

Chapter 2 – Literature Review

2.1 Adsorption technology

Adsorption is a process that involves selective retention of component(s) of a mixture on a solid surface because of interactive forces between the adsorbent and adsorbate molecules. If the forces of interaction are caused by weak van der Waals or electrostatic forces, the type of adsorption is called physical adsorption (physisorption). In contrast, if the interaction is by virtue of chemical bonding between the solute and the solid surface, the type is called chemical adsorption (chemisorption). Adsorption is an exothermic phenomenon releasing substantially larger heat during chemisorption in comparison to physisorption. Once the undesired component (CO_2) has been captured, it needs to be removed with an intention that the adsorbent can be reused in cyclic adsorption processes. This can be accomplished through regeneration or desorption and the favorable factors for desorption are higher temperature and lower pressure. Adsorbent bed can be regenerated by using several cyclic adsorption methods like temperature or thermal swing adsorption (TSA), purge-gas stripping, pressure swing adsorption (PSA) including vacuum swing adsorption (VSA), or by combination of TSA and PSA processes. In thermal and pressure swing techniques, the adsorbent can be desorbed by elevating the temperature or by depressurizing the bed in the respective techniques. Both these processes find application in capturing CO_2 at industrial level especially from mega point sources. TSA requires comparatively more time for completing the individual cycle than PSA, yet it is considered more promising as the energy requirement can be substantially reduced in TSA plus it generates high purity CO_2 with good amount of adsorbate recovery (exceeding 80%) [61]. However, selection of the adsorbent performs a crucial and decisive role in the design of a cyclic adsorption process.

2.2 Type of adsorbents

Physical properties of an adsorbent play a crucial role in capturing CO_2. An ideal adsorbent is expected to possess the following attributes: low cost, high adsorption capacity, selectivity, adequate mechanical strength, easy regenerability, stability, faster kinetics and low energy requirement [54]. Possession of even few characteristics makes the adsorbent viable for practical use. An extensive range of materials have been prepared by the researchers and examined for CO_2 adsorption namely amines [62], zeolites [63], metal-organic-frameworks (MOFs) [64], silicas [32], alkali metal carbonates [65], carbon nanotubes [66] and activated

carbons from biomass and synthetic polymers [67-69]. Therefore, it is rather challenging to develop an adsorbent which can efficiently capture CO_2 from a mixture of gases exiting from the flue as the pressure of the CO_2 gas is quite low (~1 atm) and concentration (~15%) is also appreciably low in comparison to N_2 (~70%). Ultimately, the performance of the adsorbent will play a decisive role in its selection.

2.2.1 Metal-organic frameworks based adsorbents

Recently, a new class of hybrid microporous materials came into existence with exceptional structural flexibility and immense capacity to adsorb gases. These are known as metal-organic frameworks (MOFs) as they consist of nodes of inorganic metals coordinating with organic groups which subsequently form either single or multidimensional open structures. Besides, these materials are known to possess high surface area, outstanding porosity, good crystallinity along with chemical stablility and tunablilty. Apparently, their unique properties make them approving as well as demanding in field of CO_2 capture [70]. Widely used MOFs in area of CCS are MOF-5, MIL-53, HKUST and SNU.

Zhen et al. [71] prepared composite from melamine formaldehyde sponge (MS) monolith as a porous carrier loaded with MOF to be used as adsorbent for CO_2 capture studies in a fixed bed. For synthesizing the composite, the copper metal ions were firstly dissolved in methanol and the solution was poured over MS which was previously coated with polyvinyl alcohol for better strength. Thereafter the organic molecules were introduced inside the pores of MS which coordinated with the metal ions. The *in-situ* growth of MOFs initiated the pores forming a fine network in the bed and later breakthrough experiments were performed for investigating its CO_2 adsorption ability. At 20 °C, the adsorbent loaded with 5 g of MOFs per gram of porous carrier displayed maximum capture capacity of about 1.02 mmol g^{-1} of CO_2. The bed was desorbed by purging CO_2 free air (simulated) for 10 min continuously through the column.

For further improvement in the capture performance of MOFs or MILs, basic functional moieties may be introduced inside their framework which may help to achieve more effective adsorption of acidic carbon dioxide. Yoo et al. [72] modified the pristine MIL-101 by loading it with polymethacrylamide (MA) and then polymerized to obtain poly-MA. Further, it was reduced with lithium aluminum hydride to insert amide ($-NH_2$) group. The modified adsorbent showed improved CO_2 adsorption as well as selectivity as compared to immaculate MIL. Even at low pressure of CO_2 the modified adsorbent showed capture capacity of 1.4 mmol g^{-1} under

static conditions. In a recent study, Siegelman et al. [73] functionalized a metal−organic framework with cyclic diamine and produced an adsorbent capable of capturing more than 90% CO_2 from a humid natural gas flue emission stream by performing breakthrough experiments in a fixed bed reactor. This synthesized material enabled CO_2 adsorption capacity of 2.4 mmol g^{-1} at 40 ^oC and the adsorbent was regenerated at 140 °C. Also, the studies suggested the role of water in enhancing the CO_2 capture in developed adsorbent due to hydrogen-bonding interactions with the ammonium carbamate chains formed after CO_2 adsorption thus providing thermodynamic push for CO_2 binding.

However, from industrial applications point of view, MOFs are less feasible as adsorbents for CO_2 as they have high affinity for moisture and flue gas contains good amount of water vapors which once adsorbed cannot be completely desorbed. Besides, they suffer from structural instability of metallic ions and/ or hydrogen bonding which limits its use in fossil fuel based plants for CO_2 capture.

2.2.2 Silica based adsorbents

Ordered mesoporous silica was first synthesized in 1992 at Mobil Oil Corporation and since then they are in demand because of their excellent properties like remarkable surface area, higher pore volume, tunable pore size, and easy functionalization ability. These materials can be synthesized through various methods such as sol-gel, chemical etching, templating and microwave-assisted techniques. M41S was the first mesoporous silica to be developed and further research led to the preparation of Mobil Crystalline Material (MCM), and other popular variants like Santa Barbara Amorphous (SBA), Michigan State University (MSU) and Mesoporous Silica-Hexagonal (HMS) [74, 75].

Xu et al. [62] were the foremost researchers to thermogravimetrically investigate the adsorption behavior of CO_2 on mesoporous silica, MCM-41 impregnated with a polyethyleneimine (PEI). They later investigated the effect of the method of preparing and loading of PEI on CO_2 adsorption capacity [76]. Wet impregnation and mechanical mixing were used for the preparation of adsorbent and the former method resulted in CO_2 uptake of 2.54 mmol g^{-1} whereas the latter produced uptake of 2.25 mmol g^{-1}. Also, the adsorption capacities improved with dispersion of PEI into the molecular sieves. In another study [77], the effect of moisture on amount of CO_2 adsorbed was also studied. The capacity increased with the amount of moisture. The increase in uptake of CO_2 was higher for 10% moisture in comparison to 16% moisture.

However, when feed concentration of moisture exceeded the CO_2 concentration, the adsorption capacity did not improve further.

Zelenk et al. [78] synthesized amino functionalized mesoporous materials (MCM-41) by co-condensing amino-organo siloxanes (AOS) with tetraethyl orthosilicate (TEOS) in varying ratios. The ratio of AOS:TEOS in the mixture were maintained to be 3, 5, 10, 20 and 30 wt%. Symmetrical (hexagonal) porous silica materials were obtained at smaller AOS:TEOS ratios and disordered and non-porous silica particles were obtained at higher ratios. Investigations revealed that adsorption took place on amine active centers primarily via physisorption. The effect of increase in concentration of AOS was clearly visible from superior CO_2 adsorption capacity and the sample consisting of 10 wt % AOS exhibited utmost CO_2 uptake of 0.67 mmol g^{-1} at 25 °C determined gravimetrically. The sample was regenerated by heating it up to 70 °C in nitrogen atmosphere which led to the removal of CO_2.

Mesoporous carbon was developed from chitosan following hard template route and then impregnated it with pentaethylenehexamine (PEH) [79]. The prepared adsorbent displayed improved CO_2 adsorption and was more selective towards CO_2. CO_2 adsorption measurements were performed on TGA/DTA system and the highest CO_2 uptake achieved by the adsorbent at 373 K was 3.72 mmol g^{-1}. For recycling the adsorbents, CO_2 was replaced with pure nitrogen flow for 2 h.

Dey et al. [80] synthesized mesoporous SBA-15 by functionalizing with polyethyleneimine for gravimetric evaluation of CO_2 uptake. The optimum sample (50 wt% of amine loading) adsorbed 3.09 mmol g^{-1} with 10% premoistened CO_2 at 348 K. For regeneration of samples dry nitrogen was purged at 393 K. The prepared adsorbent showed remarkable stability over 60 adsorption/desorption cycles during 65 hours of operation of temperature swing adsorption.

On the whole, silica materials have proved to be promising for capturing CO_2 majorly due to presence of interconnected meso and macropores and low energy requirement. However, the low hydrolytic stability of Si-O-Si bond when used for capturing carbon dioxide from moist flue gases causes many problems and hence limits its use in industrial applications.

2.2.3 Zeolite based adsorbents

Zeolites represent a class of highly crystalline and porous structures of aluminosilicate materials consisting of the alkali and alkaline-earth metals [81]. These materials exhibit an open 3-D

structure with cations balancing the electrostatic charge of the alumina, silica tetrahedra and contained water. Their structure resembles a honeycomb due to which they acquire high internal surface area and pore volumes. Zeolites behave as remarkable molecular sieves and hence can selectively separate CO_2 from mixture of gases. They have been used in TSA and PSA processes successfully at moderate or high-temperature conditions [82]. However, they are brought in usage generally at pressures higher than 2 bar.

Researchers had always been keen to investigate the adsorption behavior of zeolites. In this context, Li et al. [83] studied the adsorption behavior of six types of commercial variants of zeolites namely NaA, NaX, CaA, CaX, ZSM-5 and Y type for separating CO_2 from methane. Larger CO_2 adsorption amount and highest CO_2 affinity were shown by NaX and CaA respectively at 0.1 MPa. IAST model predicted CO_2 selectivity was reported to be 76 for NaX and 74 for CaA at 0.1MPa. Moisture greatly influences the adsorption performance as the adsorbing ability of zeolites gets much weakened. Also, their usage is restricted at room or low temperature. Further, low CO_2 over N_2 selectivity is yet an additional limitation of zeolites in flue gas applications. To tackle these issues, researchers have modified zeolites by impregnating amines into their porous structures [54].

Madden et al. [84] prepared modified β-25 zeolite by physically impregnating with amines. The synthesized adsorbent was fed to a fixed bed for investigating the CO_2 adsorption/desorption performance. The adsorbent displayed a substantially higher CO_2 uptake up to ~4.7 mmol g^{-1} at adsorption temperature of 35 °C. Besides, the sample desorbed at a quite low temperature of around 60 °C indicating supremacy of physisorption. The externally added moisture also proved to be beneficial as it improved the CO_2 adsorption capacity by nearly 20%.

Chen et al. [85] synthesized mesoporous zeolite and wet impregnated with polyethylenimine (PEI) for functionalization. The results indicated that the PEI impregnated sample was more selective towards CO_2 than N_2 and exhibited superior CO_2 capture capacity even at 100 °C and low CO_2 concentration.

To further perk up the CO_2 adsorptive performance of zeolites, they need to be modified in the nanoscale range [2]. Jiang et al. [86] synthesized type-T zeolite nanoparticles with an average pore size 3.6 Å×5.1 Å, slightly larger than the size of CO_2 molecules (3.3 Å). The prepared adsorbent was investigated for CO_2 capture studies in a fixed bed apparatus. At 288 K and 1 bar, the adsorbent displayed CO_2 adsorption capacity of ~4 mmol g^{-1}. Subsequently, bed was

desorbed at 318 K and 1 bar under nitrogen flow. Shakarova et al. [87] developed nanocrystals of size circa 100 nm which showed CO_2 adsorption of 5 mmol g^{-1} at 20 °C and 1.003 bar.

Nguyen et al. [88] successfully synthesized mesoporous Linde Type A (LTA) zeolites by adding a known quantity of surfactant to the reactants during mixing. The larger mesopores in LTA zeolites were capable of trapping CO_2 molecules, displaying high uptake of 2.3 mmol g^{-1} at 60 °C measured under dynamic flow conditions in a TGA. The samples showed good stability over 10 adsorption runs & desorption after regeneration at 150 °C under nitrogen flow. Zeolite (ZSM-5) was synthesized by wet impregnation method via organic template route [89]. Mesoporous adsorbent exhibited specific surface area of ca. 400 m^2 g^{-1} and showed CO_2 uptake of 0.9 mmol g^{-1} along with improved selectivity at 10% CO_2 concentration.

Zeolites have shown promising results in CO_2 separation from mixture of gases. However, these materials have great affinity for water molecules which get trapped in the micropores, subsequently blocking the admittance of carbon dioxide and thus affecting CO_2 adsorption capacity. As a consequence, very high temperatures (> 300 °C) are required for regeneration of the adsorbent which is responsible for imposing large energy penalty [90] and thus limiting its widespread applicability [91].

2.2.4 Hydrotalcite adsorbents

Depending upon the operating temperatures, the solid materials used for CO_2 adsorption can be categorized as low, intermediate or high temperature adsorbents. The low temperature adsorbents generally operate below 200 °C and specific examples of this category are carbonaceous adsorbents, MOFs or MILs and zeolites. On the other hand high temperature adsorbents namely alkali metal oxides/hydroxides and hydrotalcites can suitably perform at temperatures above 200 °C. From the latter category, hydrotalcites have shown great potential for CO_2 capture in intermediate as well as high temperature range. Hydrotalcites are principally ceramic materials which constitute a huge group of basic and anionic clays. These are double layered structures formed from a cationic layer of metallic oxides and an anionic layer of weakly held carbonates. Because of its anion exchange ability, they acquire remarkable adsorptive and catalytic characteristics.

Recently, a new composite has been developed from mixing of a commercial variant of hydrotalcite and a geopolymer for assessing CO_2 adsorption in intermediate temperature range of 200 to 400 degree C [92]. The adsorption capacity for CO_2 was achieved in the range of 0.38-

0.46 and 0.109-0.145 mmol g^{-1} for commercial variant of hydrotalcite and the composite respectively at 200 degree C. However, the capture capacity of geopolymer was just 0.052 mmol g^{-1}.

Chen et al. [93] modified the lithium-aluminium based hydrotalcite for capturing CO_2 by calcination followed by treatment with KOH/C_2H_5OH and subsequent functionalization with polyethyleneimine. PEI loading on adsorbent much affected the capture performance. The adsorbent sample without PEI impregnation showed capture capacity of 0.58 mmol g^{-1} whereas the same sample loaded with 40% PEI exhibited CO_2 uptake of 1.72 mmol g^{-1} at 50 degree C evaluated thermogravimetrically. Also, the sorbents were regenerated at 150 degree C under nitrogen flow after completion of each adsorption cycle and regenerability was assessed for 7 cycles.

Khalkhali et al. [94] studied the structural morphology of the hydrotalcite based oxides (HBOs) or double layered oxides by means of atomistic simulation method. The analyses revealed that the HBOs were crystalline in nature exhibiting structural resemblance with magnesium oxide. Further, to investigate the effect of morphology on CO_2 adsorption behavior, amorphous as well as crystalline HBOs were simulated which represented the hydrotalcites produced at lowest and highest calcination temperatures. Analysis revealed that the amorphous hydrotalcites showed better dynamic CO_2 adsorption behavior than the crystalline ones. This may be attributed to the random array of CO_2 molecules in the adsorption layer which assisted in easy adsorption and desorption whereas in latter case the hydrotalcite surface behaved as a contaminating layer which restricted the adsorption of CO_2 molecules and thereby reduced its capture capacity. Conclusively, the amorphous HBOs displayed enhanced physisorption behavior.

Hydrotalcites are promising adsorbents for CO_2 capture in intermediate as well as high temperature range. These materials are quite cheap and easy to synthesize both at laboratory level and industrial scale. However, the thermal evolution of these materials, with the formation of mixed oxides with high surface area and potential to regain the original hydrotalcite structure is crucial for enhancement of the CO_2 capture capacity [95].

2.2.5 Metal based adsorbents

Another class of sorbents which has proved to be beneficial for high temperature applications is metal based adsorbents. These materials possess the potential to capture carbon dioxide owing to presence of more basic sites on their surface and faster reaction kinetics in the high

temperature regime of 300-900 °C [96]. They can be used either as oxides/hydroxides or carbonates/bicarbonates of alkali metals and alkaline earth metals or in amalgamation with other minerals for adsorption of CO_2. Besides, they may exist in hydrated or non-hydrated form. For alkali metals, the affinity for CO_2 increases as we move from lithium to cesium in the periodic table. For any metal from this category, CO_2 released in flue exhaust combines with its oxides at specific temperatures to form carbonates which decompose to metal oxides at higher temperatures during regeneration step.

Literature reveals that numerous metallic oxides namely CaO, MgO, Na_2O, K_2O, MnO and PbO have been explored as adsorbents for capturing CO_2, however CaO and MgO have been extensively studied. Guo et al. [97] synthesized MgO nanoparticles for trapping CO_2 by calcination of various organomagnesium compounds and also investigated the effect of individual precursor on CO_2 capture capacity. MgO nanoparticle formed from magnesium oxalate dihydrate adsorbed maximum amount of CO_2 which was reported to be around 4.4 mmol g^{-1}. In another study minerals of magnesium were used as precursors to prepare low cost adsorbents for capturing CO_2 at high temperatures and their adsorption performance was studied in a fixed bed reactor [98]. For regeneration of the sorbent, bed was heated to 400 °C and maintained at this temperature for 30 min. Four different mineral precursors namely Magnesite (Ma), Brucite (Br), Bischofite (Bi), and Hydromagnesite (Hm) were calcined at 750 °C, 650 °C, 600 °C, and 550 °C respectively for adsorbent preparation. However, Hm and Br based basic magnesium adsorbents demonstrated significant CO_2 equilibrium uptakes of around 1.73 mmol g^{-1} and 1.67 mmol g^{-1} respectively, at 200 °C.

Pichardo et al. [99] prepared CaO based adsorbents via solution combustion technique using hydrated calcium nitrate (CN) and urea as precursors. The mass ratios of CN to urea varied from 1:1 to 1:5/2. The CaO nanopowders obtained from combustion were ball-milled for augmenting the surface properties. The finally obtained adsorbent showed remarkable CO_2 capture capacity of 9.31 mmol g^{-1} measured using a TGA/DSC apparatus at 298 K and standard atmosphere pressure. Gao et al. [100] developed CaO based adsorbents supported on charcoal via three different routes namely sol-gel, wet impregnation and manual mixing in order to achieve improvement in their CO_2 capture capacity. Investigations revealed that charcoal impregnation inhibited the formation of crystalline calcium oxide which helped to improve its capture capacity. Optimum adsorbent sample was developed with CaO to charcoal mass ratio of 4:1 through sol-gel method which exhibited initial adsorption capacity of ~15 mmol g^{-1} at 600 °C and later maintained it at 8.0 mmol g^{-1} after 15 cycles of adsorption/desorption.

Sengugta et al. [101] developed K_2CO_3/Al_2O_3 based adsorbents via single-step impregnation (SI) and multi-step impregnation (MI) and then examined their adsorption-desorption performance in a fixed bed reactor. The adsorbent prepared through multi-method enabled uniform dispersion of active species (K_2CO_3) in the macropores without causing blockage of narrower mesopores thus resulting in higher adsorption capacity. On the other hand sample prepared through SI method suffered from blockage of narrower mesopores due to excessive growth of K_2CO_3 thus limiting the accessibility of CO_2 in the pores. Adsorbents prepared with K_2CO_3:Al_2O_3 mass ratio of 1:1 by MI and SI methods exhibited maximum CO_2 uptake of 3.12 and 2.1 mmol g^{-1} and regeneration efficiency of about 65 and 56%, respectively, at 130 °C in multi-cycle testing.

To summarize, good thermodynamic properties and faster kinetics are the strengths of metal based adsorbents however for industrial applications the sorbent should possess excellent mechanical strength so that the decay of sorbents caused due to sintering and attrition may be reduced [96].

2.2.6 Carbonaceous adsorbents

Solid physical adsorbents predominantly consist of carbonaceous materials for example activated carbon, carbon nano-materials, graphene and carbon molecular sieves. Apart from being rich in carbon content, these carbonaceous materials possess faster adsorption kinetics due to physical adsorption, excellent stability and thermal conductivity, easy regenerability, and bare minimum cost. Since these characteristics are highly desirable for any adsorbent and assist in improving its CO_2 capture capacity, therefore number of studies have been performed on them [102, 103]. However, textural properties and subsequently adsorption performance of these adsorbents depend upon the kind of precursor used for its synthesis. Different activated carbons have been derived from various sources for example coal or its byproducts [104], biomass (rice husk, coconut shells, almond shells, olive stones, bagasse) [67, 68] and household wastes such as plastic wastes.

2.2.6.1 Commercial activated carbons

Remarkable surface areas and fine pore size distribution are the key features which support activated carbons in achieving good CO_2 capture capacities [105]. To overcome few limitations of these adsorbents like inferior mechanical strength leading to high attrition in a fluidized bed and leaching of active sites in presence of high moisture content, researchers have worked on its

modification/activation to improve the surface affinity toward CO_2 and successfully achieved it [54, 106]. Therefore, commercial activated carbons have been used in various studies related to capturing of post-combustion carbon dioxide emissions from flue gases using PSA and TSA techniques [107, 108].

Al-Maser et al. [10] examined the adsorption behavior of two commercial grades (sorbent-1 and sorbent-2) of activated carbon for CO_2 capture in a fixed bed rector. To remove the adsorbed CO_2 or traces of oxygen, pure nitrogen was purged in the bed for 2 h. Investigations revealed that the cycle time reduced when a typical adsorption/desorption experiment was performed at high feed rate and elevated temperature. The utmost CO_2 uptake of 0.0254 g g^{-1} adsorbent was achieved at a partial pressure of 0.0417 atm.

Plaza et al. [109] tested commercial grade activated carbon, Norit R2030CO2 as an adsorbent for CO_2 under post-combustion conditions in a fixed-bed adsorption set up. Bed of solids was regenerated before each experiment by heating the bed up to 100 °C for one hour along with arrangement of nitrogen purging. The material showed good CO_2/N_2 selectivity, remarkable cyclic ability over 10 adsorption/desorption cycles and easy regenerability. Three different regeneration techniques were tried and the highest adsorption of 1.9 mol kg^{-1} along with 97% recovery was obtained in an hour. The sequence followed for CO_2 recovery was VTSA > VSA > TSA. Cheng-Hsiu et al. [38] assessed the CO_2 adsorption performance of super activated carbon MAXSORB (commercial grade). The carbon exhibited CO_2 uptake capacity of 32 mmol g^{-1} at a pressure of 3.2 MPa.

2.2.6.2 Carbon adsorbents from waste materials

Relatively higher cost limits the use of commercial activated carbon as adsorbents. Because of this reason, the researchers have gained interest in producing activated carbons from waste materials and investigating them for CO_2 capture; may be biomass wastes or industrial wastes. Biomass wastes such as sugarcane bagasse, lotus stem waste, coconut coir, waste tea, peanut shells, etc. have been successfully utilized for preparing activated carbon for CO_2 capture [110]. Palm oil, wastewater treatment sludge and coal fly ash from thermal plants are major industrial wastes investigated by researchers.

In order to prepare activated carbon from any precursor, it needs to go through two main steps. In the first step, the raw material is carbonized at high temperature in an inert atmosphere and then the resultant char is activated either physically or chemically. Physical activation takes

place in the presence of oxidants for example steam, air or CO_2 in the temperature ranging from 800 to 1000 °C [20]. Alternatively, chemical activation involves impregnation of appropriate dehydrating agents like NaOH, KOH, $ZnCl_2$, H_3PO_4, etc. before activation in the temperature varying between 600 and 800 °C. During carbonization, the carbonaceous material thermally decomposes and eliminates volatile compounds producing fixed carbon but with limited pores. Further, the oxidizing reactions taking place during activation not only enlarge the existing pores created during carbonization but also help to form new pores [111].

Moroto et al. [112] developed activated adsorbents derived from fly ash for CO_2 capture via steam activation. Amine compounds were infused into the carbonized samples and then activated at 850 ^oC resulting in surface area of 1075 m^2g^{-1}. The highest CO_2 adsorption uptake of 1.56 mmol g^{-1} was obtained at 30 ^oC for the amine impregnated activated carbon determined thermogravimetrically. For desorbing the sample nitrogen gas was purged at 100 ml min^{-1} at the same temperature set for adsorption. The reported values of adsorption capacities were higher than their earlier published capacities for non-activated fly ash carbons. In another study, lithium-based adsorbents were developed from fly ash for investigating the CO_2 uptake capacity at high temperatures (400-650 ^oC) with simultaneous addition of K_2CO_3 (0-40 mol%). The maximum reported CO_2 uptake was 2.43 mmol g^{-1} at 600 ^oC using 40 mol% K_2CO_3 [104]. To regenerate the adsorbent, 100% N_2 was made to flow at the same adsorption temperature. Also, the lithium-based adsorbents were almost completely regenerable and exhibited stability over 10 sorption cycles.

Deng et al. [67] prepared activated carbons from sunflower seed shells (SSS) and peanut shells (PS) for CO_2 capture study using KOH for activation. The adsorbent samples prepared from SSS and PS respectively exhibited CO_2 adsorption capacities of 64.24 and 67.76 mg g^{-1} at 25 ^oC and 1 bar. Inspite of lower BET surface of SSS based adsorbents than PS derived adsorbent; the highest capacity was obtained for latter samples due to higher micropore volumes.

Large surface area adsorbents were prepared from sugarcane bagasse by impregnating it with urea for nitrogen enrichment and then activating with KOH in the temperature range of 500-800 ^oC. Under static conditions, CO_2 uptake of 4.8 mmol g^{-1} was obtained at 25 °C and 0.986 atm using 15 wt% urea and KOH:carbon mass ratio of 2 [113]. For testing the cyclic stability, the adsorbed sample was firstly degassed for 6 h and then desorbed at 110 ^oC.

Lotus stem waste was used for preparing porous carbon adsorbents for evaluating CO_2 capture performance [114]. The adsorbent samples showed huge surface area up to 2893 m^2 g^{-1} along

with exhibition of large micropore volume of 1.59 cm^3 g^{-1}. Maximum 3.85 mmol g^{-1} of CO_2 was absorbed at ambient temperature and pressure.

Li et al. [115] developed low-cost porous carbons from waste wool with an aim to selectively adsorb CO_2. The pre-carbonised wool (at 300 ^oC) was impregnated with KOH in the ratio of 3:1 for activation. The optimum sample showed CO_2 uptake of about 3.7 mmol g^{-1} at 0 ^oC and 2.78 mmol g^{-1} measured thermogravimetrically at 25 ^oC.

In another study, waste carpet materials were carbonized and then chemically activated with KOH for preparing adsorbent samples with an intention of capturing CO_2. A unit gram of adsorbent sample was able to adsorb maximum 3.13 mmol of CO_2 at 30 °C and minimum 0.7 mmol at 100 °C, using 100% pure CO_2 by thermogravimetric method [116]. Regeneration was conducted at the same temperatures for 15 min by replacing CO_2 gas with N_2 at a flow rate of 100 ml min^{-1}.

2.2.6.2.1 Carbon adsorbents from waste plastics

Since 1950, the production of synthetic plastic in India exceeded 8 billion metric tons which led to the generation of 6.3 billion metric tons of non-degradable plastic waste. Data indicates that only 9% waste has been recycled and 12% incinerated [117]. The remaining plastic waste is dumped in the landfills or is littering in the environment. If the current rate of production persists, it is expected that around 12 metric giga tons of plastic waste will accumulate in the environment which approximates to ~15000 tons of collection per day. These are alarming values and hence disposal of plastic waste has turned out to be a global concern.

Various environment related issues have been raised due to the non-biodegradabilty and unskilled reprocessing of waste plastics: 1) Release of toxic emissions such as dioxins, carbon monoxide, amines, carbon tetrachloride etc during burning of plastics. 2) Landfilling occupies expensive land and also makes it infertile due to its barrier properties. 3) Harmful metals such as lead and cadmium used as additives in synthesis of packaging films leach out from landfills. Some of the viable options for addressing this problem are incineration and recycling of waste by physical means [118]. However, both these processes are cost-intensive and economically less viable due to precincts of toxic emissions released and segregation of wastes.

Another important environmental concern is global warming owing to excessive usage of fossil fuels in transportation and energy generation. This releases huge amount of CO_2 - a greenhouse

gas which is a prime contributor to global temperature rise [119]. Hence, it needs to be captured.

The challenges of plastic waste management and CO_2 capture can be simultaneously addressed by the synthesis of adsorbents from plastic wastes for capturing CO_2 [120]. This has been attempted by many researchers via pyrolysis or carbonization techniques using various activating agents [121]. Apart from activated carbons obtained from natural resources such as coal and biomass, synthetic polymer wastes have gained attention as carbon precursors because of their high surface area, low cost, ability to modify surface characteristics and porosity [122].

Sneddon et al. [123] prepared novel absorbent from poly(vinyl chloride) (PVC) waste for carbon capture. Aminated PVC was supported on SBA-15 (mesoporous silica) and tested gravimetrically on a microbalance for CO_2 adsorption from simulated flue gas (CO_2/N_2 mixture). Maximum CO_2 uptake obtained by the composite is reported to be 0.50 mmol g^{-1} at 25 °C and the samples were regenerated at 75 °C for 2 h. Ethylenediamine claimed to be the best aminating agent for PVC resulting in highest CO_2 uptake.

Polycarbonate waste in the form of used CDs and DVDs was carbonized and later activated with either KOH or CO_2 [60] . Structural properties of the samples improved many folds with both the activating agents. Maximum and minimum BET surface areas obtained were 2240 m^2 g^{-1} and 500 m^2 g^{-1} respectively. Developed carbons exhibited good adsorption properties towards CO_2, H_2, and C_6H_6. Highest CO_2 uptake of 3.3 mmol g^{-1} was achieved at 298 K and 850 mm Hg pressure under static conditions.

Fu et al. [124] transformed waste polystyrene foam to hyper-crosslinked porous polymers (HCPs) using 1,2-dichloroethane. Highest surface area and pore volume obtained was 572 m^2 g^{-1} and 0.53 cm^3 g^{-1} respectively. Also, all the HCPs showed good thermal stability. The optimum sample exhibited CO_2 uptake as high as 1.98 mmol g^{-1} along with CO_2/N_2 selectivity of 23.4 at 25 ^oC and 1.13 bar.

Polyurethane foam waste was used to prepare porous carbon material and investigated for the capturing of CO_2 [125]. Effect of governing parameters like carbonization temperature, impregnation ratio, and activation temperature was studied for the sake of controlling pore size distribution and content of nitrogen with a motive to capture maximum CO_2. The sample pre-carbonised at 400 ^oC and activated at 700 ^oC maintaining KOH:carbon ratio of 2 showed adsorption capacity as high as 6.67 mmol g^{-1} at 25 ^oC and 4.33 mmol g^{-1} at 0 ^oC and ~1 atm.

The prepared carbon adsorbents exhibited good regeneration ability and improved CO_2 over N_2 selectivity.

Lo et al. [126] used waste polyethylene terephthalate (PET) bottle material in place of terephthalic acid as a precursor for the synthesis of five variants of nanostructured trivalent MOFs using different reagents. Among these, two MOF samples named MIL-53 and MIL-101 were investigated for CO_2 adsorption. BET surface areas obtained for these samples were 1022 m^2g^{-1} and 2939 m^2g^{-1} respectively. Under static conditions per gram of MIL-53 and MIL-101 respectively adsorbed 2.84 mmol and 3.11 mmol of CO_2 at 20 °C and 1 atm.

Arenillas et al. [59] utilized waste soft-drink bottles made of PET to prepare carbon adsorbents. The raw material was chemically activated with KOH and co-carbonized with three different compounds namely acridine, urea, and carbazole at 500 °C. Dynamic CO_2 uptake measurements were performed on weight gain basis using a thermogravimetric analyzer and highest uptake of 1.09 mmol g^{-1} was reported at 25 °C. The samples were desorbed at 100 °C by switching over to pure nitrogen in place of CO_2 gas.

2.2.6.3 Carbon nanotubes

Another recognizable carbon nanostructure which is gaining consistent attention towards CO_2 capture by adsorption is carbon nanotube (CNT) [127]. This may be credited to its significantly large surface area and pore volume per unit mass and low density. Besides, they also possess distinct chemical as well as thermal stability. These CNT sorbents may be single-walled CNTs or multi-walled (MWCNTs) depending upon the graphene sheet which may be in the form of continuous cylinder with hexagonal units or rolled multiple times. CNTs are usually modified with different amine solutions for improving their surface properties. The first CNT was synthesized by Iijima in 1991 by arcing between graphite electrodes [128]. However, commonly employed techniques for its synthesis are chemical vapor deposition and electrospinning [129].

Su et al. [130] functionalized commercial CNTs with 3-aminopropyltriethoxysilane and studied the cyclic CO_2 adsorption behavior and related physical as well as chemical properties. The investigations revealed fast CO_2 adsorption kinetics of modified CNTs. Also, the developed samples showed remarkable stability over 100 adsorption-desorption cycles. CO_2 uptake as high as 2.24 mmol g^{-1} was achieved at 25 ^oC with CO_2 inlet concentration of 15%. Also, the adsorption capacity showed an increase from 1.94 to 2.45 mmol g^{-1} by enhancing the amount of water vapor from 0 to 2.2%.

A non-toxic, biodegradable adsorbent was prepared by grafting ethylenediamine to a long-chain polymer polysuccinimide to form polyaspartamide which covered the MWCNTs and improved its surface properties by multiple times thus achieving higher CO_2 capture capacity [131]. The modified MWCNTs exhibited maximum CO_2 adsorption capacity of 1.59 mmol g^{-1} which was about four and a half times higher than that of unadorned MWCNT.

Deng et al [132] synthesized architecturally designed porous adsorbent by wrapping polyethyleneimine (PI) on CNT along with the insertion of purine as a spacer to enhance the CO_2 capture performance. The modified CNT showed high CO_2 uptake of about 3.87 mmol g^{-1} at 50 ^oC. Further, the adsorbents were desorbed at 100 ^oC in pure nitrogen flow and its cyclic adsorption capacity was assessed over 50 sorption cycles.

Comparative analysis of various precursors used for CO_2 capture; along with their operating conditions have been summarized in Table 2.1.

2.3 Summary of Literature review

The comprehensive review of literature indicates that numerous solid adsorbents have been developed for capturing CO_2 which mainly include zeolites, mesoporous silicas, and hybrid crystalline solids such as MOFs, covalent organic frameworks, and activated carbons (ACs). Among these, ACs synthesized from waste materials have been widely focused and employed, owing to their cost-effectiveness, easy availability, chemical stability, and remarkable surface properties. Besides, moisture removal is not required for these materials and they are easily regenerable. ACs can be prepared from various carbonaceous sources, such as coal, fly ash, sunflower seed shells, sugarcane bagasse, lotus waste, coconut shell, wood, polymers, etc. Recently, synthesis of adsorbents from waste plastics has gained attention of the researchers as it helps to solve two global environment problems - plastic waste disposal and CO_2 capture. However, there is a need to work more on physical and chemical activation of carbon precursor obtained from waste plastics in order to achieve well-developed pore structures and subsequently enhance CO_2 capture capacity. Also, most of the studies reveal that the CO_2 adsorption performance has been evaluated under static conditions within temperature range of 0-30 °C. The static method is a batch process in which the adsorbent remains in contact with the same batch of adsorbate (gas mixture) for a very long time (infinite time, being a slow process) so that all the adsorbent sites are fully exposed to the adsorbate and the equilibrium is achieved. Whereas the dynamic method is a continuous process in which the adsorbent comes

in contact with the adsorbate for a short time only and the equilibrium is never achieved. That is why; the adsorption capacity measured by dynamic process is always lower than that of static process. But, in industrial practice only dynamic process is supposed to be used to get a reasonably high rate and therefore, it is pertinent to dynamically measure the CO_2 uptakes of developed adsorbents at higher temperature range as they can portray true image as per relevance of CO_2 capture from flue gas stream whose emission temperature lies in the range of 40-100 °C.

Table 2.1 Literature review

Precursor	**Modifier**	**Adsorption Temp(^{0}C)**	**Pressure, P_{CO2}(bar)**	**Adsorption capacity (mmol g^{-1})**	**Method**	**Regeneration Temp. (^{0}C)**	**Reference**
MCM-41	amine	25	1	0.67	TGA	70	[78]
β-25 zeolite	amine	35	1	4.7	Fixed bed	60	[84]
Type-T zeolite	-	15	1	4.01	Fixed bed	145	[86]
LTA zeolite	amine	60	1	2.3	Dynamic TGA	150	[88]
Sugarcane Bagasse	KOH	25	1	4.8	Static	110	[113]
Recycled PET	KOH	25	1	1.09	Dynamic TGA	100	[59]
Norit R2030CO2	-	25	1	1.9	Fixed bed	100	[109]
Carpet wastes	KOH	30	1	3.13	Dynamic TGA	100	[133]
Peanut shells	KOH	25	0.15	1.54	Static	25 (vaccum)	[67]
MF/MCM-41	CO_2	30	1	0.64	Fixed bed	200	[134]
Epoxy /MCM-41	CO_2	30	1	0.91	TGA	200	[135]
Epoxy /MCM-41	CO_2	30	1	0.65	Fixed bed	200	[136]
SBA-15	PEI	75	1	3.09	Static	120	[80]
Waste wool	KOH	0 25	1	3.7 2.78	TGA	--	[115]
Chitosan	PEH	100	1	3.72	Static	100	[79]
CNT	Purine	50	1	3.87	Dynamic TGA	100	[132]
PVC	amine	25	1	0.50	TGA	75, 2h	[137]
Hydrotalcite	PEI	50	1	1.72	TGA	150	[93]
Hydromagnesite	-	200	1	1.73	Fixed bed	400	[98]

Chapter 3 – Materials and Experimental Methods

3.1 Materials

PET waste used for the study was collected from household waste and food courts of the institute campus containing disposable water and cold drink bottles.

Potassium hydroxide (KOH) pellets and potassium carbonate (K_2CO_3) powder required for chemical activation were purchased from Shantilal Dharamshi Fine Chemicals Ltd., India. Analytical grades were chosen for both the reagents.

Grade-1 purity (99.999%) helium gas, high purity nitrogen gas (99.995%) and carbon dioxide gas (99.99%) used for experimentation were obtained from M/s Sigma Gases and Services, Ltd., India.

3.1.1 Adsorbent development

For adsorbent preparation, waste PET bottles were carbonized in a tubular furnace under an atmosphere of inert nitrogen for 2 h under isothermal conditions. Thereafter, the carbonized material was activated with two different chemicals (KOH and K_2CO_3).

3.2 Adsorbent characterization techniques

3.2.1 Surface area and pore size distribution

N_2 sorption isotherms were obtained at −196 °C using BELSORP Max sorption analyzer by Bel, Japan, Inc. Prior to this, carbon samples were outgassed at approximately 200 °C for almost 12 h to make it completely free of inherent moisture and entrapped gases. The surface area of every sample was determined by means of BET (Brunauer-Emmet-Teller) equation. Total pore volume estimation was made from the amount of N_2 adsorbed at P/P_0 ratio of 0.99. Pore size distributions (PSDs) were obtained from Barrett-Joyner-Halenda (BJH) method and Non-Localized Density Functional Theory (NLDFT) method was used for analysis of micro-pore distribution.

3.2.2 X-ray diffraction (XRD)

The diffraction patterns of the carbon adsorbent samples were examined through a X'Pert PRO diffractometer (Make PANalytical, Netherlands) under *Cu-Ka* radiation and wide scanning angle in the 2θ measurement range of 10° to 80° to determine their phase compositions. Aluminium sample holders were used for holding carbon powder samples. Instrument

functioned at recommended settings of 45 kV for voltage and 40 mA for current.

3.2.3 High resolution transmission electron microscopy (HRTEM)

To assess the shape and particle size of samples, high-resolution images were obtained using HRTEM. The micrographs were recorded on JEOL transmission electron microscope (Model JEM-2100, Japan) operating under an accelerating voltage of 200 kV. Prior to analysis, carbon adsorbent was dispersed in toluene and then carefully placed on copper grid coated with carbon.

3.2.4 Scanning electron microscopy (SEM)

A scanning electron microscope (Model JEOL JSM-6510 LV) operating at 20 kV voltage was used to obtain micrographs of activated samples and comprehend surface morphology. At the start, the sample was sputter coated with gold to an approximate thickness of 50 micrometer to prevent problems related to sample charging and obtain high resolution images.

3.2.5 Thermogravimetric analysis (TGA)

To investigate the thermal stability of carbon adsorbents, each sample was subjected to thermogravimetric measurements performed on thermal analyser (Model/Make TA Q500, USA). For analysis, nearly 20 mg of powdered sample was carefully placed in the platinum pan with the help of spatula and heated from 30 ˚C to 900 ˚C giving a step increment of 10 ˚C min^{-1}. Pure nitrogen was made to flow in the system at a rate of 50 ml min^{-1} throughout experimentation.

3.2.6 Elemental (CHNS)

Elemental contents (%) of carbon, oxygen, and hydrogen present in the prepared carbons were determined by using Thermo Scientific elemental analyzer (Model FLASH 2000). Amount of oxygen present was determined by difference.

3.2.7 Fourier transform infrared (FTIR) spectroscopy

FTIR spectra were collected on a FTIR spectrophotometer, PerkinElmer Spectrum (USA) 100 series for mid IR range, between a wave number range of about 4000-400 cm^{-1} (2.5-25 μm) and resolution of 4 cm^{-1}.

3.2.8 X-ray photoelectron spectroscopy (XPS)

Chemical composition of the upper most layers of the samples was determined by using a surface sensitive and high performance X-ray photoelectron spectroscopy technique. The analysis was accomplished on XPS, Omicron ESCA combined with Kratos Axis Ultra delay line detector for higher sensitivity and resolution. The source of X-ray used was monochromated Al-K_α with 15 kV potential at the anode. The survey scan and high resolution scan were captured respectively at 50 eV and 20eV pass energy. Emission current of about 10 mA and the pressure of about 0.2×10^{-8} torr were retained in the analysis chamber. Reconstruction of O1s and C1s peaks was performed by XPS peak 4.1software. After subtracting the Shirley background, the curve-fitting was performed assuming a Gaussian peak.

3.2.9 Temperature programmed desorption (TPD)

The surface chemistry of the optimum sample was analyzed by temperature-programmed desorption (TPD) using Micromeritics' chemisorption analyzer (Autochem II 2920) coupled with a katharometer detector also known as thermal conductivity detector. Initially, the powdered sample was pretreated at 200 °C under helium flow and then the temperature of the cell was lowered to 30 °C to start adsorption. During adsorption, CO_2 gas was made to flow and it was followed by desorption under helium flow by heating up to 300 °C.

3.3 Performance evaluation of carbon adsorbents

3.3.1 Experimental setup for fixed-bed adsorption study

Experimental setup consisting of fixed bed adsorption column, a gas mixer and online gas chromatograph (GC) was used for carrying out dynamic CO_2 adsorption and desorption studies on developed carbon adsorbents. The adsorption column was made of stainless steel with an inner diameter of 9.39 mm and height of 300 mm as shown in Fig. 3.1. Type K thermocouple was positioned in middle of the column to measure the temperature of the bed. A thin layer of evenly spread glass wool was carefully placed on both the ends of the adsorption column to avoid loss of adsorbent. Two gas mass flow controllers (MFCs) by Bronkhorst (Ruurlo, Netherlands) individually regulated the flow rate of CO_2 and N_2 to attain a desired CO_2 concentration for typical run. Then both the gas streams were mixed in a gas mixer and subsequently sent to the adsorption column. The amount of CO_2 adsorbed was analyzed by an online gas chromatograph (Agilent 7890A) with a TCD (thermal conductivity detector) and a

monitor. Helium supported as a carrier gas (mobile phase) in GC and injection temperature was set at 180 °C.

3.3.2 Dynamic CO_2 adsorption/desorption measurements

The samples were pretreated in an oven at 200 °C for 12 h for removal of moisture before carrying out the adsorption-desorption studies on carbon adsorbents. For performing the adsorption experiment, adsorbent sample (~2g) evenly mixed with inert glass beads (~6 g) was placed in the column flushed with dry nitrogen gas at the rate of 50 ml per minute. Later, the temperature was elevated from 30°C to 200 °C and held for 2 h to ensure complete elimination of trapped gases. Thereafter, the temperature was lowered to the desired adsorption temperature. Then, N_2/CO_2 mixture was passed at 80 ml min^{-1} flow rate till saturation limit to carry out the adsorption. Afterward, the sample was desorbed by elevating column temperature to 200 °C in the presence of pure N_2 flowing at 50 ml min^{-1}. The complete cycle (adsorption/desorption) was performed for five times to examine the regeneration potential of the adsorbent samples.

The amount of CO_2 adsorbed by the adsorbents at any time is represented as q_t in milli mol per gram (mmol g^{-1}), is determined by means of Eq. (1) [138, 139].

$$q_t = \frac{1}{m_a}\int_0^t Q_v\,(C_o - C)dt \tag{3.1}$$

Where, Q_v is the volumetric flow rate of gas in ml min^{-1}, m_a represents the mass of the adsorbent sample in g, C_o and C are concentrations of CO_2 at inlet and exit respectively in mmol ml^{-1} and t indicates the time taken for adsorption in minutes.

3.4 Adsorption kinetics study

The extent of coverage by the adsorbate molecules on the surface of adsorbents, adsorption dynamics, and performance of adsorbents may be estimated by consideration of the kinetics of adsorption. It also helps in gaining deep understanding of the underlying fundamental mechanisms. To examine the kinetics of CO_2 adsorption on PET waste based adsorbents, five models for kinetics study namely pseudo first order, pseudo second order, Elovich, Avrami, and fractional order were considered.

3.4.1 Pseudo first order kinetic model

In 1898, Lagergren suggested a kinetic model which assumes that the rate of adsorption is directly related to the number of free dynamic sites available on the adsorbent's surface. It was named as pseudo first order model. This model is most frequently used for liquid-solid and gas-solid systems.

Pseudo first order model is stated as [140]:

$$q_t = q_e\left(1 - \exp\left(-k_1 t\right)\right) \tag{3.2}$$

Where, q_e and q_t respectively represent the amount of adsorbate adsorbed (mmol g^{-1}) at equilibrium conditions and at particular time t. k_1 represents the rate constant in min^{-1} for pseudo first order model.

3.4.2 Pseudo second order kinetic model

In 1995, Ho [141, 142] came up with another model named pseudo second order kinetic model which assumed that the uptake capacity is directly proportional to the available free sites on the surface of the adsorbent.

The expression for pseudo-second order is given as:

$$\frac{dq_t}{dt} = k_2\left(q_e - q_t\right)^2 \tag{3.3}$$

Where, k_2 represents the rate constant for pseudo second order equation and its units are g mol^{-1} min^{-1}. Integration of the above equation within limits t = 0 to t and q_t = 0 to q_t followed by rearrangement leads to following equation:

$$q_t = \frac{k_2\, q_e^2\, t}{1 + k_2\, q_e\, t} \tag{3.4}$$

3.4.3 Elovich kinetic model

Elovich model works on the principle that the amount of gas adsorbed on the adsorbent's surface falls exponentially with increase in the volume of adsorbate gas. It was originated in 1934 when Zeldowitsch [143] observed an exponential fall in carbon monoxide adsorption rate on MnO_2 (manganese dioxide) when amount of CO adsorbed increased. The rate equation for Elovich model can be presented as:

$$\frac{dq_t}{dt} = \alpha(e^{-b\,q_t}) \tag{3.5}$$

Where, q_t (mmol g^{-1}) is the amount of adsorbate gas adsorbed at time t; α and b respectively are constants representing the initial adsorption rate and surface coverage. The units of α and b are expressed in mmol per gram per second and gram per mmol respectively. Integrating the equation 3.5 between boundaries t = 0 to t and q_t = 0 to q_t, results in following equation:

$$q_t = \frac{\ln(\alpha b)}{b} + \frac{\ln(t)}{b} \tag{3.6}$$

3.4.4 Avrami kinetic model

Avrami model [144] assumes random nucleation sites on the adsorbent surface and accounts for chemical as well as physical adsorption for the prediction of CO_2 uptake. Equation expressing this model may be given as below:

$$q_t = q_e\left(1 - e^{\left(-k_a\,t^n\right)}\right) \tag{3.7}$$

Where, k_a is the Avrami constant expressed in min^{-1}.

3.4.5 Fractional order model

This model assumes direct proportionality of adsorption rate with n^{th} and m^{th} power of driving force for adsorption and time required, respectively.

The rate equation for fractional order can be depicted as [145]:

$$\frac{dq_t}{dt} = k_n(G)^n t^{m-1} \tag{3.8}$$

Where, $G = (q_e - q_t)$ is the driving force for adsorption, k_n is the rate constant for fractional order and m, n represent the fractional model constants

Integration of the above equation within the above mentioned limits gives following equation:

$$(q_e - q_t) = \frac{1}{[((n-1)k_n/m)t^m + (1/q_e^{n-1})]^{1/n-1}} \tag{3.9}$$

3.4.6 Error calculation

The kinetic modeling helps to predict the CO_2 loading on adsorbents. However, the adequacy and uncertainty related to kinetic models is judged by deviation of predicted results from experimentally generated ones i.e. relative error (E) and coefficient of linear regression coefficient ($0<R^2<1$). To evaluate the best-fit adsorption kinetic model, relative error percentage (E (%)) was calculated by the following expression.

$$E\ (\%) = \sqrt{\frac{\sum[(q_{t(exp)} - q_{t(pred)})/q_{t(exp)}]^2}{N-1}} \times 100 \qquad (3.10)$$

Where, $q_{t(exp)}$ is the experimentally determined CO_2 loading, $q_{t(pred)}$ refers to model predicted CO_2 uptake and N represents the number of experimental data points.

3.5 Adsorption isotherm models

Adsorption isotherm study helps to predict the sorption mechanism and get some knowledge about the surface characteristics of the porous adsorbent and its attraction towards the adsorbate. In a typical isotherm, the amount of adsorbate loading is plotted as a function of equilibrium concentration or partial pressure at a constant temperature. Therefore the experimentally obtained data was analyzed using Freundlich, Langmuir, and Temkin adsorption isotherm models to assess the equilibrium CO_2 loading.

3.5.1 Freundlich isotherm model

Freundlich gave a relation on empirical basis, relating the amount adsorbed per unit weight of adsorbent and its partial pressure at fixed temperature which is applicable for non-ideal as well as multilayer sorption on non-homogeneous surfaces.
It can be shown as [146]:

$$q_e = K_F P^{1/n} \qquad (3.11)$$

Further, the logarithmic form of equation is given as:

$$\log q_e = \log K_F + \frac{1}{n} \log P \qquad (3.12)$$

where, n and K_F are the Freundlich coefficients which correspond to slope and intercept of $\log(q_e)$ versus $\log(P)$ plot and these are respectively related to intensity and capacity of adsorption.

3.5.2 Langmuir isotherm model

Langmuir, came up with a simple adsorption isotherm model which correlates amount of adsorbate adsorbed to the adsorbate partial pressure. Also, it assumes that adsorbate molecules occupy the single layer on adsorbent's surface and these molecules do not interact with each other.

Langmuir isotherm equation can be presented as [147]:

$$q_e = \frac{q_m \ K_L \ P}{1 + K_L \ P} \tag{3.13}$$

Where, q_e (mmol g^{-1}) refers to the adsorbate adsorbed at equilibrium and q_m (mmol g^{-1}) stands for the maximum adsorption of adsorbate in forming the monolayer. K_L is the Langmuir constant and is represented in atm^{-1}.

3.5.3 Temkin isotherm model

Temkin isotherm equation is formulated on the basis of even distribution of binding energies and assumes a linear fall in heat of adsorption with the surface coverage. Temkin model is expressed by following equation [148]:

$$q_e = B \ ln(K_T P) \tag{3.14}$$

Where, B (J mol^{-1}) is the isotherm constant and K_T (atm^{-1}) is the binding constant for Temkin model.

3.6 Selectivity

Another important parameter which assesses the competitive nature of a particular component over other components in a gas mixture towards adsorption is selectivity. Since the concentration of CO_2 is substantially less than N_2 in the flue gas, therefore its removal is rather challenging which can be overcome by high CO_2 over N_2 selectivity. Theoretically, CO_2/N_2 selectivity can be evaluated with the following relation. Further, it can be compared with the adsorbed amounts measured from breakthrough curves.

$$S_{CO_2} = \frac{X_{CO_2} / X_{N_2}}{Y_{CO_2} / Y_{N_2}} \tag{3.15}$$

In the relation, symbol X_{CO_2} indicates the mole fraction of CO_2 adsorbed by solid phase and Y_{CO_2} represents the mole ratio of CO_2 in the gas phase. Similarly, X_{N_2} *and* Y_{N_2} signify the mole fractions in solid and gas phase respectively for N_2.

3.7 Thermodynamic investigation

3.7.1 Thermodynamic properties

For an efficient design of an adsorption system thorough knowledge of thermodynamic properties is desirable. However, adsorption thermodynamics concentrates around few important properties like isosteric heat of adsorption, Gibbs free energy change, enthalpy and entropy change. Gibbs function at standard conditions, ΔG^0 (in J $(mol)^{-1}$) is given below:

$$\Delta G^0 = -R_g T \ln\left(K_{eq}\right) \tag{3.16}$$

Where, K_{eq} represents the equilibrium constant obtained from Freundlich model at temperature T [149].

Further, for evaluating the enthalpy and entropy change, van't Hoff equation is applied. This equation correlates adsorption equilibrium constant with adsorption temperature and can be represented by the following expression [149].

$$\ln\left(K_{eq}\right) = -\frac{\Delta H^\circ}{R_g}\frac{1}{T} + \frac{\Delta S^\circ}{R_g} \tag{3.17}$$

Where, ΔH^0 is the molar adsorption enthalpy and ΔS^0 is the entropy change under standard conditions. From the slope of $\ln(K_{eq})$ and $1/T$ plot, the value of ΔH° can be obtained and intercept will provide the value for ΔS^0 [150].

Isosteric heat of adsorption, Q_{st} is considered as an indicator of interactive strength between the adsorbate and solid adsorbent. It measures the amount of heat generated during process of adsorption and therefore gives an idea of energy required for regeneration of the adsorbent. Q_{st} at constant loading q_e can be estimated from the Clausius–Clapeyron equation in kJ mol^{-1} [151].

$$Q_{st} = -R\left[\frac{\partial\, ln\ P}{\partial\left(\frac{1}{T}\right)}\right]_{q_e} \tag{3.18}$$

Where, P and T indicate the pressure and temperature respectively, and q_e is the amount of adsorbate adsorbed.

3.7.2 Heat duty for regeneration

The regeneration heat duty of the adsorbent (Q_r) can be calculated from a simple equation as mentioned below:

$$Q_r = Q_d + Q_{sen} \tag{3.19}$$

Where, Q_{sen} represents the sensible heat i.e. the amount of heat added to raise the adsorbent's temperature to desorption temperature and Q_d is the heat required for desorption which is assumed to be almost same as Q_{st} i.e. the heat released during adsorption. Units for both the terms are depicted as kJ mol^{-1}. Sensible heat can be determined from following equation:

$$Q_{sen} = \frac{C_p * (T_d - T_a)}{Adsorption\ capacity} \tag{3.20}$$

Where, C_p represents the specific heat capacity in J $(g)^{-1}$ $(K)^{-1}$ and T_d and T_a indicate the desorption and adsorption temperature respectively.

3.8 Software used

XPS spectra were analyzed through highly featured software named XPS peak 4.1. Application software Origin Pro 8 was utilized for fitting of different kinetic as well as isotherm models with the experimentally generated data through non-linear regression.

Adsorption column breakthrough profiles were modeled and simulated in MATLAB environment using MATLAB R2015a software.

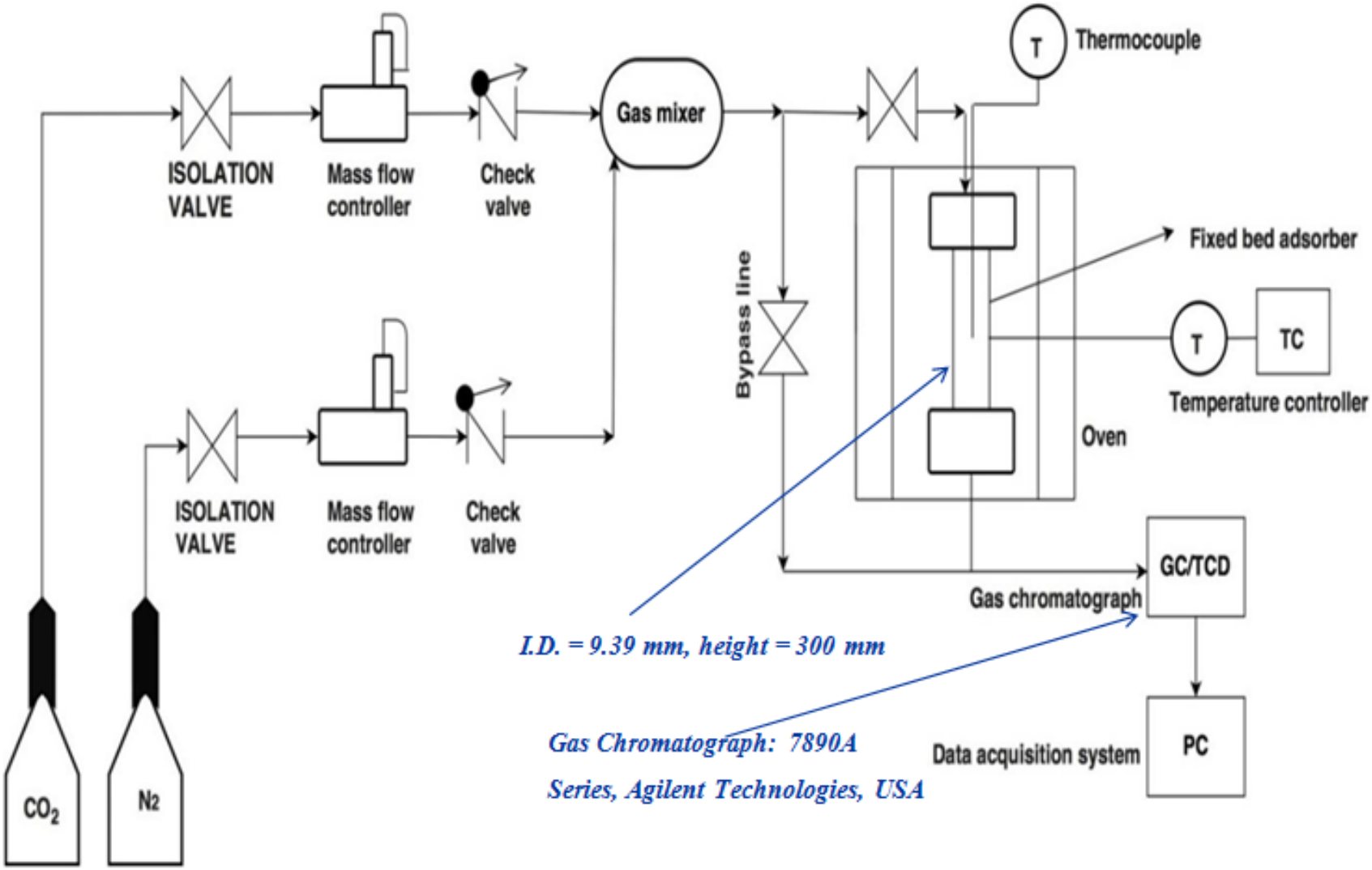

Fig. 3.1 Schematic representation of the experimental setup for dynamic adsorption study

Chapter 4 – Polyethylene Terephthalate (PET) Based Porous Carbon Adsorbents

4.1 Adsorbent preparation

4.1.1 Carbonization of polyethylene terephthalate waste

Initially, waste PET bottles were properly washed and then manually squashed. Then, they were hacked into smaller pieces and approximately 20–22 g of material was loaded into the ceramic boat for carbonization at different temperatures (500–800 °C) in a tubular furnace under an atmosphere of inert nitrogen maintaining heating rate of 10 °C min^{-1} for almost 2 h under isothermal conditions. The sample which was carbonized at 700 °C produced highest CO_2 uptake as compared to other samples, hence it was considered as reference sample for further investigations and named as B-700. Thereafter, the carbonized material was cooled and ground to fine size and then activated with two different chemicals using KOH and K_2CO_3.

4.1.2 Chemical activation of carbonized PET material

For chemical activation of samples, the selected activating agent was thoroughly mixed with the char with varying mass ratios of activating agent to carbon (1 to 4). The obtained mixtures were dried in an oven for 12 h at 105 ºC.

4.1.3 Preparation of chemically activated adsorbents

Initially, the activation was performed with KOH. The KOH activated sample was dried overnight and then carbonized in quartz tubular furnace in N_2 atmosphere (flow rate 50-60 ml per min). To attain the temperature of 500 ºC, heating rate of 10 ºC per minute was maintained in the furnace. The process was repeated for three other temperatures specifically 600, 700 and 800 ºC and the sample loaded in furnace was kept for 2 h under isothermal conditions. Later the samples were properly washed with 1 M HCl and then repeatedly with distilled water to eliminate excess chlorides and KOH. The activated samples were again dried in an oven at 120 ºC prior to usage in study. Finally, the samples were named as Act-m-n where ‘m’ described the mass ratio of KOH to carbon and ‘n’ denoted the activation temperature. All notations of the prepared carbon adsorbents along with their activation conditions are summed up in Table 4.1.

The schematic diagrams for the preparation of carbon adsorbents and activated samples are depicted in Fig. 4.1 (a) and Fig. 4.2 (b) respectively.

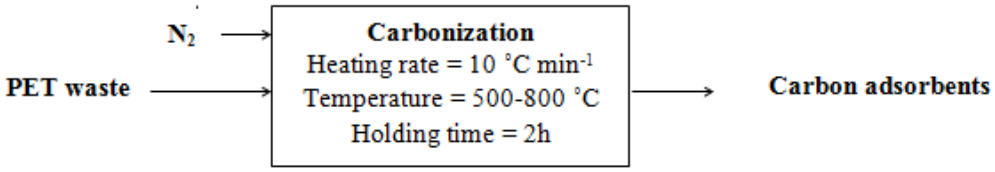

Fig. 4.1 (a) Schematic of the preparation of the carbon adsorbents from PET waste

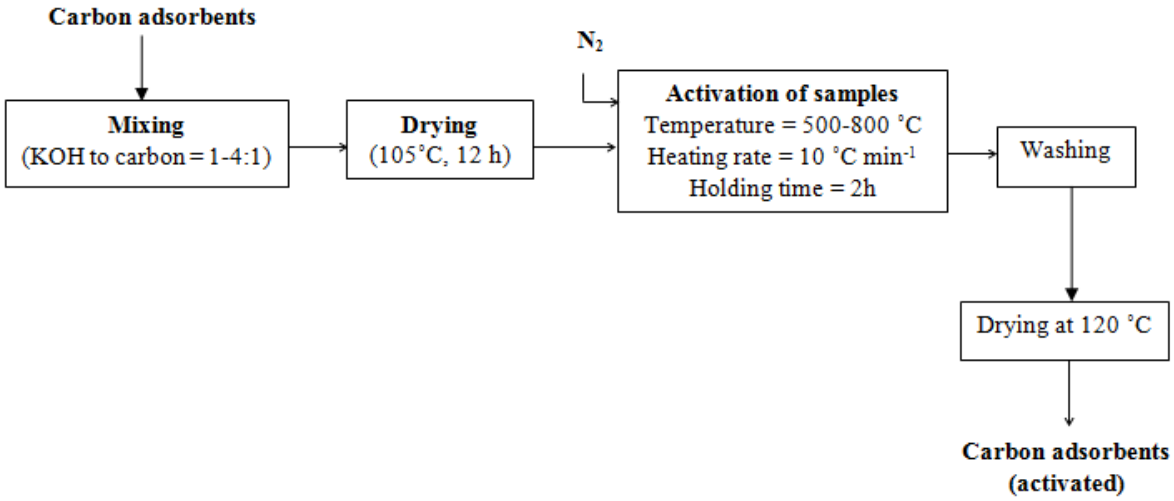

Fig. 4.1(b) Schematic of chemical activation process of carbon adsorbent(s)

Table 4.1 Carbon adsorbent samples[@] and their activation conditions

Sample representation	KOH to carbon (mass ratio)	Activation temperature (°C)
B-700	-	-
Act-1-700	1	700
Act-2-700	2	700
Act-3-700	3	700
Act-4-700	4	700
Act-3-500	3	500
Act-3-600	3	600
Act-3-800	3	800

@ carbonized at 700 °C

4.2 Characterization

4.2.1 Surface area and pore size distribution

Nitrogen adsorption and desorption isotherms of directly carbonized sample B-700 and KOH activated adsorbent samples are shown in Fig. 4.2(a).

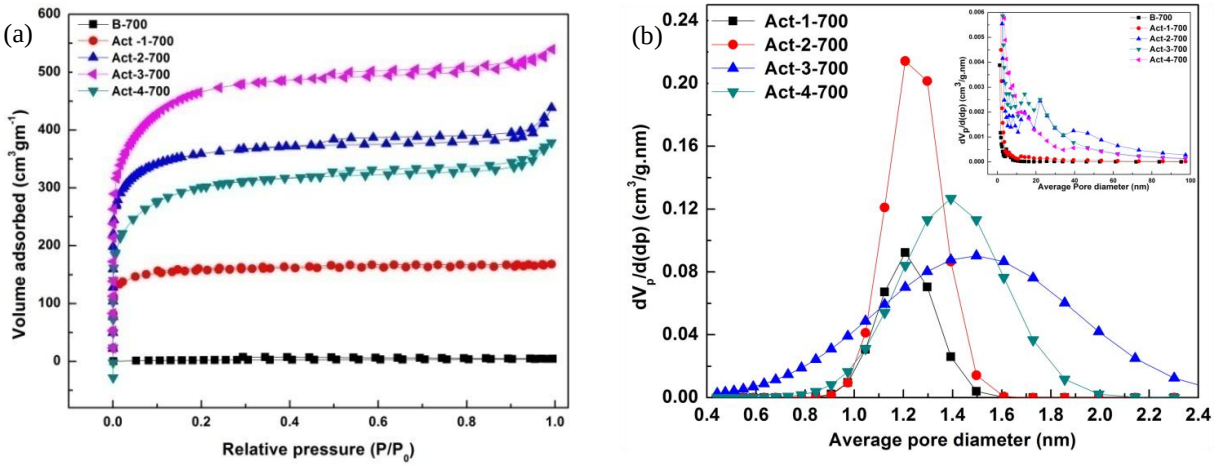

Fig. 4.2 (a) N_2 adsorption and desorption (at 77K) isotherms measured for carbon samples and (b) Pore size distribution of samples by NLDFT method (inset: BJH plot)

It is quite noticeable from the isotherms that volume of N_2 absorbed is minimal in B-700

indicating lack of porosity in the sample. Whereas, the chemically activated (at 700°C) samples show the predominance of micropores as illustrated from the shape of isotherms (typical Type 1) as described by IUPAC classifications for microporous materials. Also, existence of H4 hysteresis loop inside relative pressure (P/P_o) range of 0.45 to 0.90 indicate the presence of slit-like mesopores along with micropores [152]. This behavior may be due to the catalytic action of KOH which enhanced the rate of gasification reaction (equations 4.1 to 4.2). Further, the intermediates like K_2CO_3 and K_2O either decomposed or reacted at dynamic sites present in carbon (equation 4.4 and 4.5) which led to generation of plentiful micropores [153].

$$4KOH + C \rightarrow 4K + CO_2 + 2H_2O \quad (4.1)$$

$$2KOH \rightarrow K_2O + H_2O \quad (4.2)$$

$$K_2O + CO_2 \rightarrow K_2CO_3 \quad (4.3)$$

$$K_2CO_3 + 2C \rightarrow 2K + 3CO \quad (4.4)$$

$$K_2O + C \rightarrow 2K + CO \quad (4.5)$$

Table 4.2 depicts substantial improvement in surface area values of activated samples in comparison to that of a directly carbonized sample (B-700). Further, KOH to carbon mass ratio also affected surface area and pore volume. These parameters improved with KOH to carbon mass ratio upto 3 and decreased with further increase in mass ratio which may be attributed due to collapsing of pores. Highest surface area of 1690 $m^2\ g^{-1}$ was obtained for Act-3-700 and volume occupied by micropores and mesopores was recorded to be 0.78 $cm^3\ g^{-1}$ and 0.05 $cm^3\ g^{-1}$, respectively. Pore size distributions (PSDs) of the adsorbent samples are presented in Fig. 4.2(b). PSDs clearly show the dominance of micropores in all the activated samples which are totally absent in directly carbonized sample (B-700). High micropore surface suggests exposure of higher number of active sites for maximum number of interactions with the incoming gas molecules which would result in greater mass transport of CO_2. Also, the kinetic diameter of CO_2 (3.30 Å) is smaller than that of N_2 (3.64 Å), therefore it has a higher tendency to penetrate the pores and get trapped. The NLDFT method was employed for micropore analysis of samples and BJH pore size for mesopores (shown in Fig. 4.2(b) inset). Pores can be classified in two main types: (1) ultrafine micropores (<1 nm), and micropores (1 to 2 nm), (2) small mesopores (2 to 10

nm) and the optimum sample possesses ultramicroporosity which is beneficial for trapping CO_2 gas [154, 155]. Hence, the results show that activation conditions affect textural properties and best values are obtained at optimal temperature and mass ratio of activating agent to precursor [155]. The size of the pores fall within the range of 1 to 2 nm, which is considered a fine array for diminutive molecule adsorption.

4.2.2 Elemental (CHN) analysis

Table 4.2 Textural properties and elemental analysis of the activated adsorbents

Textural properties of adsorbents, from N_2 adsorption isotherms at -196^oC					Composition of elements (wt %)		
Carbon sample	BET area, S_{BET} ($m^2 g^{-1}$)	Total pore volume, V_p ($cm^3 g^{-1}$)	Mesopore volume, V_{me} ($cm^3 g^{-1}$)	Micropore volume, V_{mi} ($cm^3 g^{-1}$)	C	H	O*
B-700	9.27	0.01	-	-	86.0	2.27	11.7
Act-1-700	591	0.26	0.01	0.25	80.4	0.63	19.0
Act-2-700	1320	0.67	0.07	0.60	68.1	0.57	31.3
Act-3-700	1690	0.83	0.05	0.78	65.1	0.57	34.3
Act-4-700	1280	0.66	0.07	0.59	69.6	0.48	29.9

*calculated by difference

Elemental analysis of carbon adsorbents confirms the enhancement of oxygen content with KOH activation as apparent from Table 4.2. It can be seen that with enhancement in KOH to carbon mass ratio up to 3 the oxygen content increased from 19.0 to 34.3 % owing to inclusion of oxygen during activation, making Act-3-700 more basic for capturing acidic gases. Carbon content (%) decreased with increase in impregnation ratio and its percentage was smallest for Act-3-700 (65.1%) which might be due to removal of C-C bonds in comparison to oxygen functionalities. The increase in oxygen content indicates that oxygen molecules are added in the adsorbent due to activation process. Similar observations were made by Tiwari et al. [139]. From these results, it can be concluded that Act-3-700 has been activated properly and has developed highest surface area making it more suitable for CO_2 capturing. B-700 shows presence of very small amount of oxygen which reduces its affinity towards CO_2 due to more acidic nature than other samples.

4.2.3 X-ray diffraction (XRD) analysis

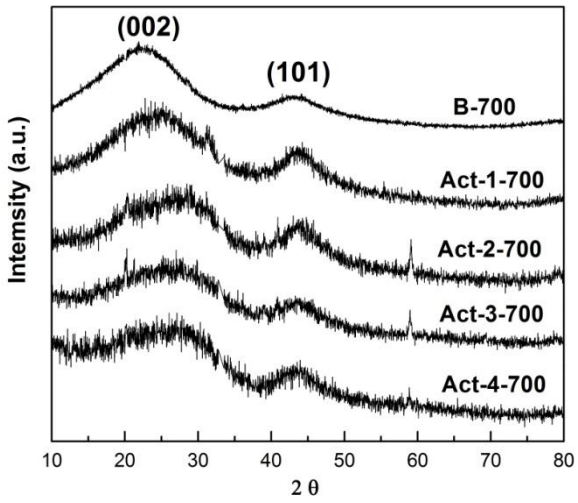

Fig. 4.3 XRD patterns of carbon adsorbents

Fig. 4.3 illustrates the XRD patterns of carbon adsorbent carbonized at optimum temperature of 700°C without activation and carbonizates activated at different impregnation ratios. Noticeable decrease in peak intensities is observed in XRD patterns of all KOH activated samples. Also, peak broadening is observed at 2θ range between 22-23^{o} and a small hump is visible in the 2θ span of 43-45^{o} in all the samples. Former values of 2θ may be indexed as (0 0 2) for diffraction planes present in graphitic carbon and later is attributed to the overlapping of (1 0 0) and (1 0 1) diffraction peaks indicating disordered structure and low crystallinity of the samples [156, 157]. Also, KOH activated samples with KOH:carbon mass ratio of 2, 3 and 4 indicate presence of an intense and sharp peak at 2 θ= 59° of graphitic carbon which is not visible in B-700 and Act-1-700, suggesting that former samples possess more graphitic pore walls and higher crystallinity than non/less activated ones which have more amorphous pore walls [158]. The interlayer spacing was calculated using Scherrer's formula as 2.703 A° for the optimum sample. The difference in structure between the activated carbons and graphite are reflected through visible enlargement and irregular comparative intensities of the (0 0 2) and (1 0 1) diffractions [159]. Hence, it can be deduced that KOH activation results in the formation of disordered and arbitrarily oriented graphitic carbon layers which subsequently lead to generation of high specific surface areas favorable for CO_2 adsorption [152, 160].

4.2.4 High resolution transmission electron microscopy (HRTEM)

HRTEM was used for examining the particle morphology of the prepared carbons. Fig. 4.4 shows the HRTEM micrographs of the directly carbonized sample and other samples prepared by chemical activation.

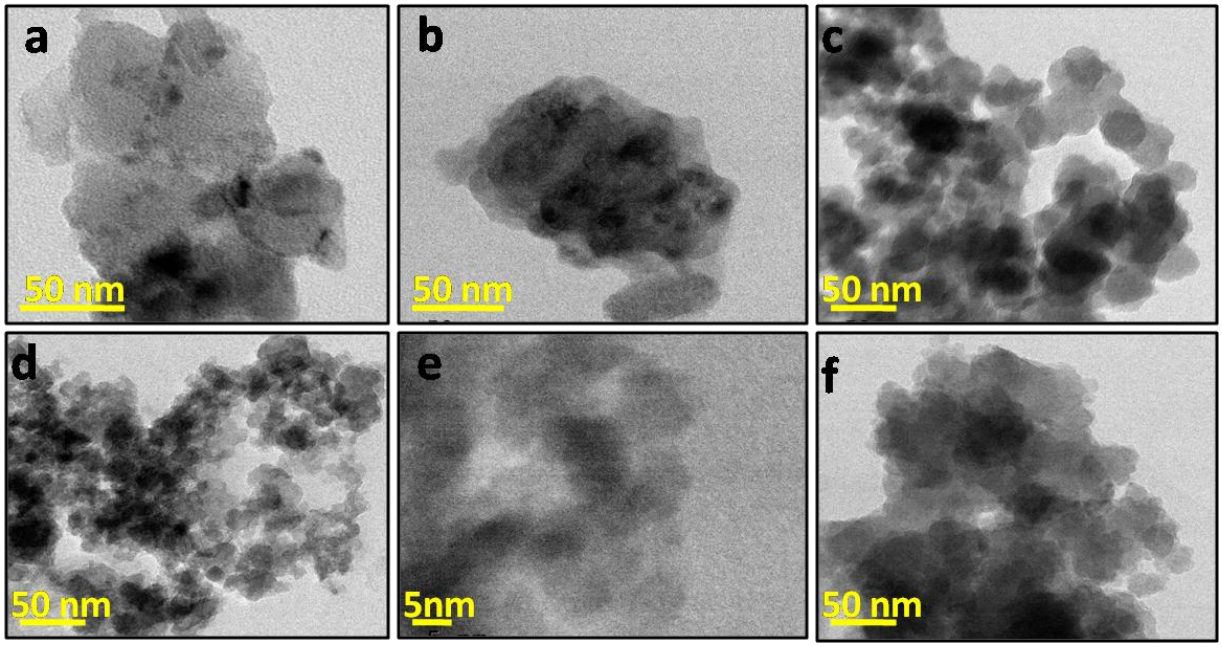

Fig. 4.4 HRTEM images of directly carbonized sample along with activated carbons **(a)** B-700, **(b)** Act-1-700 **(c)** Act-2-700 **(d)** Act-3-700 and **(e)** Act-3-700 at higher magnification **(f)** Act-4-700

Particle size of all the activated samples lies in nano range varying between 20 to 50 nm. However, Fig 4.4 (d and e) show the porous structure of Act-3-700 illustrating the pores with size less than 5nm. Also, these images elucidate the microstructure of the spherical units of Act-3-700.

4.2.5 Scanning electron microscopy (SEM)

Fig. 4.5(a) shows the structural morphology of the sample (B-700) prepared by the carbonization process and SEM micrographs of the chemically activated adsorbent samples can be seen in Fig. 4.5[(b)-(e)].

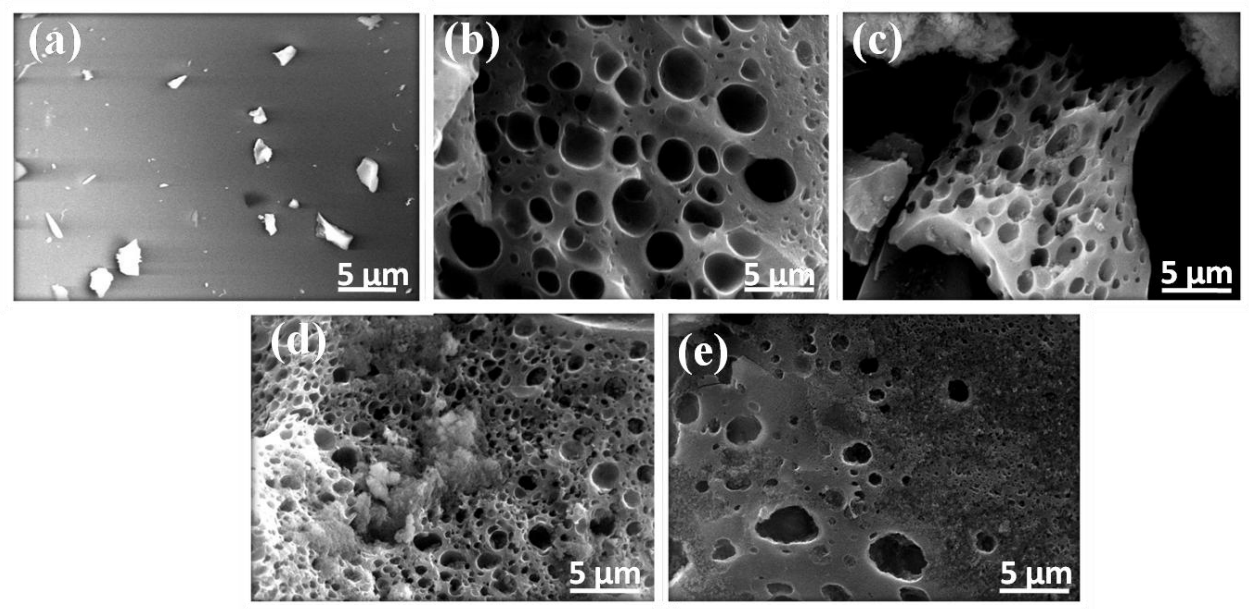

Fig. 4.5 Scanning electron micrographs of (a) B-700, (b) Act-1-700, (c) Act-2-700, (d) Act-3-700, (e) Act-4-700

It is seen that the adsorbent prepared through direct carbonization (B-700) consists of a minimal number of pores whereas chemically activated carbons appear as agglomerates consisting of small grains with voids which can offer admittance to the porosity. The best porous structure can be seen in sample Act-3-700 and this is also in agreement with a proper N_2 adsorption/desorption isotherm. Such morphology indicates that effect of KOH activation is uniformly spread over the surface of the substrate. This porous structure development is mainly due to release of excess gases (CO and CO_2) during activation process and HCl treatment carried prior to activation process for removal of potassium. Development of porosity makes adsorbent feasible for capturing and retaining maximum amount of CO_2 molecules. Hence this can be inferred that KOH activation process helped in better development of pores. On the basis of SEM and HRTEM results, it can be established that all the activated adsorbents from PET possess porosity required for adsorption of CO_2.

4.2.6 FTIR analysis

FTIR analysis was used to detect the binding sites involved in the adsorption process. FTIR spectra of samples recorded prior to and after KOH activation are shown in Fig. 4.6.

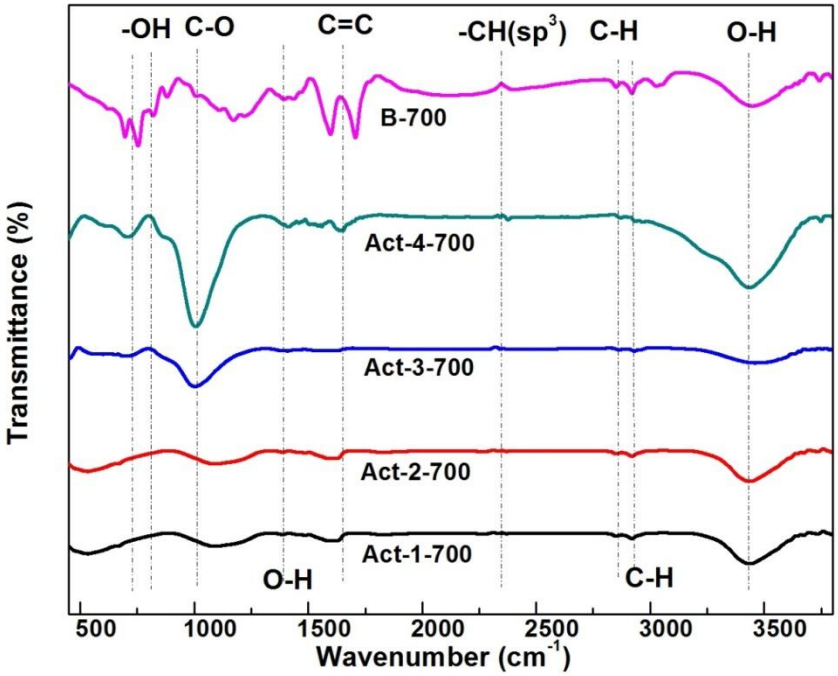

Fig. 4.6 FTIR spectra of directly carbonized (B-700) and KOH activated samples

All the samples illustrate the peaks of analogous functional groups but with diverse intensities. It can be seen that directly carbonized sample i.e. B-700 exhibits broader peaks with overlapping bands indicating its composite structure. Three prominent peaks occurring at 3440 cm^{-1}, 1620 cm^{-1}, and 1079 cm^{-1} noticed in all the samples. Here, peak near 3440 cm^{-1} is attributed to vibration caused by O-H stretching by virtue of adsorbed water or hydroxyl functional groups [161]. Band in range of 1620-1640 cm^{-1} is due to stretching of carboxylate ion (COO-) and ester carbonyl groups [162]. A peak at ~1079 cm^{-1} is a distinguishing feature of C-O-C stretch in aromatic ethers, thus confirming the existence of oxygen [152]. Additionally, few less distinct peaks occurring at ca. 2900, 2300, 1440, 780 and 680 cm^{-1} corresponding to C-H aliphatic stretching indicative of increasing unsaturation [26, 163, 164], C-H sp^3 stretching [165], bending vibrations of O-H groups of alcohols [166], out of plane bending of C-H groups in benzene derivatives [167], out of plane bending of -OH group present in alcohols [168], respectively were seen. Band intensities at ca. ~3400 cm^{-1} and ~1000 cm^{-1} signify presence of oxygenated functional groups which enhance the Lewis basic character of the activated samples and thus facilitate capture of acidic CO_2 [152]. Though the intensity of these two peaks is maximum for Act-4-700 but the XPS study (Table 4.4) confirms the presence of basic oxygen moieties (O2 and O3) in higher amount (~70 %) in Act-3-700 than Act-4-700 (~47%) leading to higher CO_2 capture capacity.

4.2.7 X-ray photoelectron spectroscopy (XPS) analysis

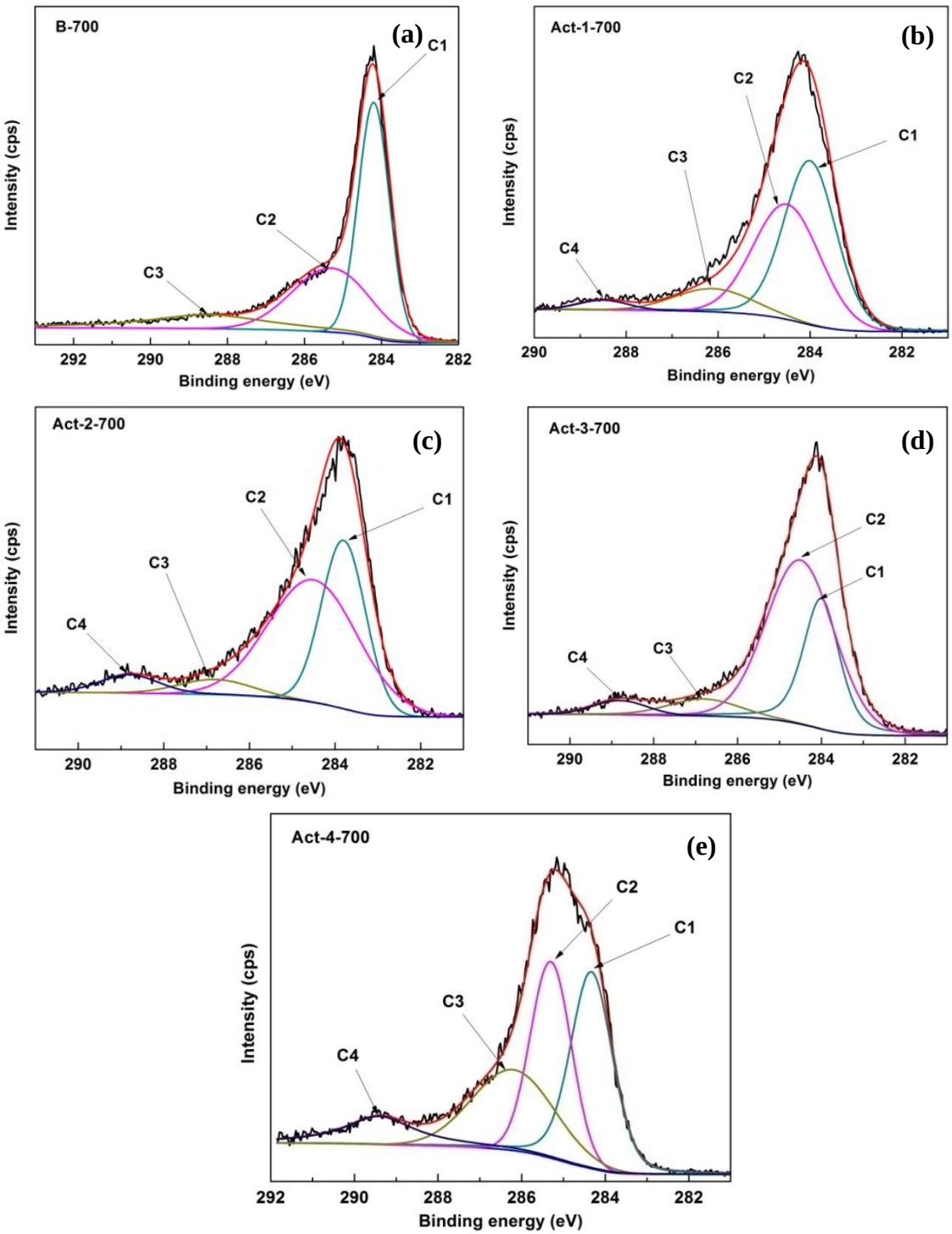

Fig. 4.7 High resolution XPS spectra of C1s region for (a) B-700 and (b) Act-1-700 (c) Act-2-700 (d) Act-3-700 (e) Act-4-700

Fig. 4.7 shows the de-convolution of C1s spectra of different samples for optimum fitting into four peaks where C1 (BE = 284.0–284.3 eV) represents sp^2 and sp^3 atoms of carbon [169], C2 (BE = 285.3–285.7 eV) corresponds to C-O bond of alcoholic, phenolic, ether or imine groups, C3 (BE = 286.8–287.4 eV) represents carbonyl or quinone groups and C4 (BE = 288.5–289.2 eV) represents carboxyl or ester group [170]. With the rise in KOH to carbon mass ratios the content of graphitic carbon drops while the oxygenated carbon (C2+C3+C4) increases demonstrating progression of the reaction between carbon and KOH as shown in Table 4.3 [171].

Table 4.3 XPS results of C1s spectra

Fraction of functional groups in Cls spectra (%)					
Sample		Graphite (C1)	Phenol – ether(C2)	Carbonyl-quinine(C3)	Carboxyl-ester(C4)
B-700	BE	284.3	285.7	-	288.5
	FWHM	0.96	2.35	-	3.73
	A %	49.97	32.99	-	17.03
Act-1-700	BE	284.0	284.5	286.1	288.5
	FWHM	1.34	1.71	2	1.29
	A %	47.68	40.30	9.44	2.57
Act-2-700	BE	283.8	284.5	286.8	288.8
	FWHM	1.21	2.5	2	1.61
	A %	35.75	53.32	5.27	5.63
Act-3-700	BE	284.0	284.5	286.8	288.8
	FWHM	1.01	1.91	1.99	1.5
	A %	29.50	59.94	6.62	3.92
Act-4-700	BE	284.2	285.3	286.2	289.4
	FWHM	1.18	1.15	2.32	2
	A %	33.97	30.08	27.86	11.08

Deconvolution of O1s XPS spectra of various carbon samples into four prominent peaks at binding energies beginning at 530.7 eV (O1), and then followed by 531.65 eV (O2), 532.73 eV (O3) and 533.7 eV (O4) consecutively are shown in Fig. 4.8.

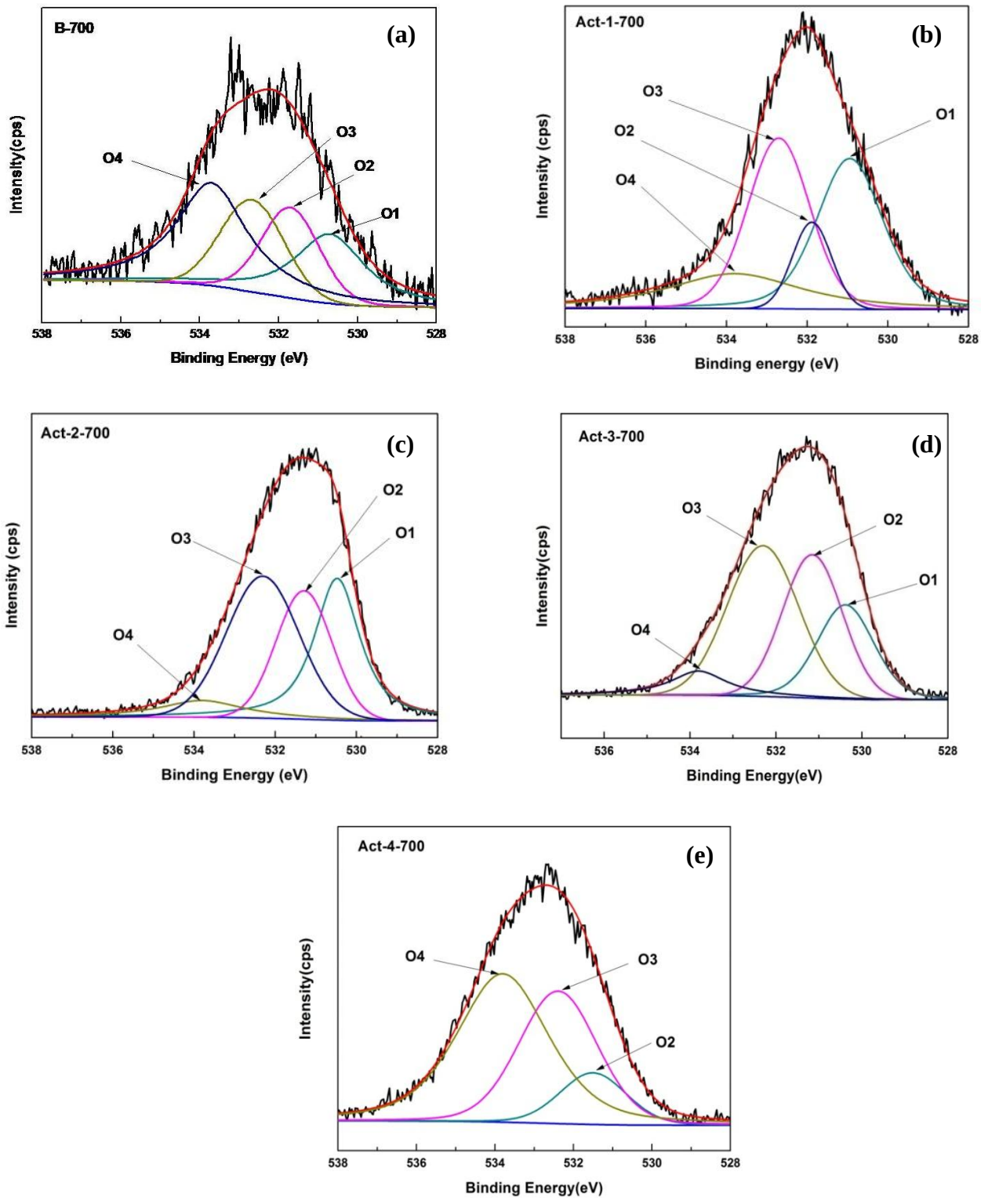

Fig. 4.8 High resolution XPS spectra of O1s region for (a) B-700 and (b) Act-1-700 (c) Act-2-700 (d) Act-3-700 (e) Act-4-700

Peak O1 is related to ketone group, O2 represents carbonyl [172], O3 pertains to hydroxyl group and O4 indicates existence of carboxylic group [173]. Values of area % confirm the presence of higher O2 and O3 oxygen moieties in Act-3-700 as indicated in Table 4.4, which is a characteristic feature of more basic samples leading to higher affinity towards acidic gas CO_2 [174].

Table 4.4 XPS results of O1s spectra

The fraction of functional groups in Ols spectra (%)					
Sample		Ketone(O1)	Carbonyl(O2)	Hydroxyl(O3)	Carboxyl(O4)
B-700	BE	530.7	531.65	532.73	533.7
	FWHM	2.11	1.73	1.89	2.14
	A %	23.84	19.03	20.06	37.05
Act-1-700	BE	530.93	531.87	532.7	533.7
	FWHM	1.93	1.14	1.81	3.94
	A %	35.22	10.39	34.40	19.96
Act-2-700	BE	530.4	531.28	532.30	533.8
	FWHM	1.33	1.62	2.1	2.45
	A %	31.28	24.95	36.49	7.26
Act-3-700	BE	530.37	531.14	532.29	533.79
	FWHM	1.55	1.64	1.95	1.55
	A %	21.47	31.54	39.52	7.45
Act-4-700	BE	-	531.49	532.38	533.79
	FWHM	-	1.99	2.35	2.75
	A %	-	11.63	35.47	52.89

4.2.8 Thermal analysis

TG and DTG curves of raw PET, carbonized PET and activated carbon adsorbents are shown in Figs. 4.9 and Fig. 4.10 respectively.

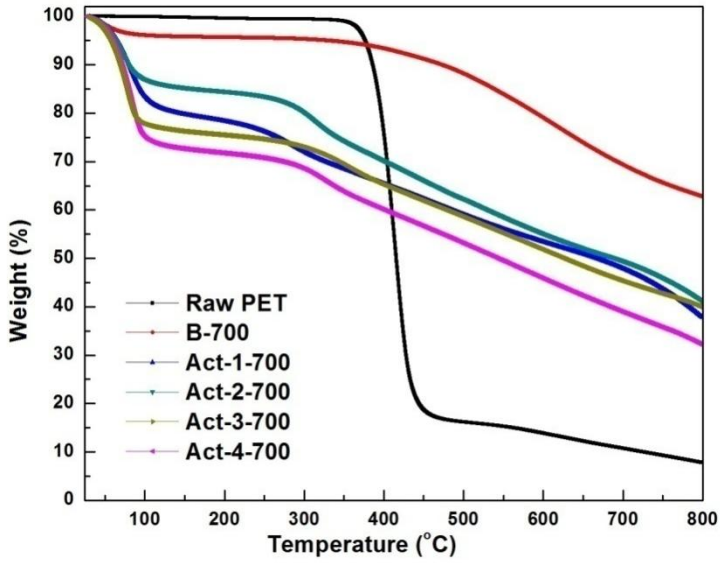

Fig. 4.9 Thermogravimetric (TG) curves of raw PET and carbon adsorbents

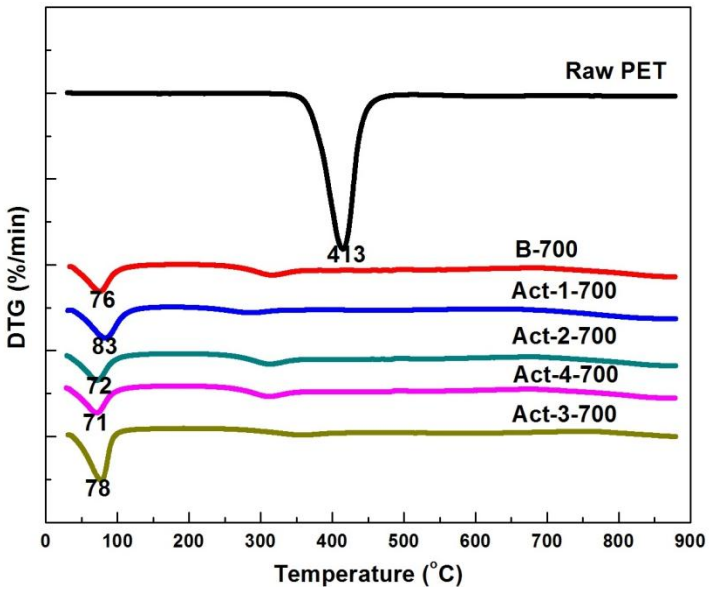

Fig. 4.10 Derivative thermogravimetric (DTG) curves of raw PET and carbon adsorbents

Raw PET decomposed at ca. 400 °C showing a substantial weight loss of about 95%. However, for other samples changes in weight are observed in two distinct regions. Weight loss in the initial region (up to 100 °C) is mainly due to the removal of moisture; whereas, drop in weight with temperature increase from 300-800 °C is probably due to the evolution of CO and CO_2 as a result of thermal decomposition of oxygen moieties (especially carbonyl and carboxylate groups) present in the adsorbent samples. The weight loss order observed in the 300-800 °C range is: Act-4-700 (76.3%) > Act-1-700 (74.83%) > Act-2-700 (71%) > Act-3-700 (67.2%) > B-700 (41.8%). Among the activated samples minimum weight loss by Act-3-700 suggests good integration between the carbon surface and oxygen functional groups formed due to KOH activation and hence supporting to exhibit the highest thermal stability by the optimum sample.

DTG curve for raw PET very distinctly indicates the absence of moisture as no peak for mass loss is observed till the temperature of 100 °C. However, it shows a substantial mass loss at 413 °C suggesting thermal instability at this temperature. DTG curves for all other carbon adsorbents show mainly one prominent peak which lies in the range of 71-83 °C. This may be ascribed to release of moisture adsorbed by the samples.

4. 3 CO_2 adsorption performance

4.3.1 Preliminary analysis using TGA

In order to observe the effect of various activation parameters on CO_2 adsorption capacity at preliminary stage, dynamic CO_2 uptake of prepared porous adsorbents was evaluated thermogravimetrically. A thermogravimetric analyzer (model TA Q500, TA instruments, USA) was used to carry out the dynamic CO_2 adsorption-desorption measurements of the carbon adsorbents. Before adsorption, the sample was pretreated in an oven at 200 °C for 12 h. Around 18-20 mg of the completely dried sample was kept in the thermogravimetric platinum pan and temperature of assembly was raised to 200 °C. It was retained at this temperature for 2 h under a steady flow of 50 $ml.min^{-1}$ N_2 gas for eliminating wetness and previously adsorbed gases. Thereafter, the furnace temperature was lowered to bring down the temperature of assembly to the desired temperature of adsorption and detained at this temperature for 10 min. Then, 100% CO_2 gas was made to pass in place of N_2 gas at the same flow rate. CO_2 uptake capacities were obtained by recording the variation in weight with time. After the adsorbent sample got

saturated, column was purged with N_2 gas for desorption at 200 °C. The process was repeated at various conditions for examining the effect of activation parameters on CO_2 uptake. Since this method involves adsorption on weight gain basis, it generally results in higher adsorption capacity due to adsorption of other gases. Therefore, for precise results dynamic adsorption was performed in fixed bed column coupled with gas chromatograph (GC) for CO_2 concentration monitoring. CO_2 uptake of prepared porous adsorbents was evaluated at a particular CO_2 concentration (12.5%) and constant temperature (30 °C).

4.3.1.1 Effect of activation time

To study the effect of variation in activation time from 1 h to 2.5 h, dynamic CO_2 uptake capacities of obtained samples were initially evaluated thermogravimetrically (labelled TGA) and then through fixed bed column coupled with gas chramatograph (labelled GC). The variation in CO_2 uptake with time is depicted in Fig. 4.11. Both the methods showed an improvement in adsorption capacity when the activation time was enhanced from 1 to 1.5 h, and thereafter the adsorption became sluggish till 2 h time. Further, increase in time up to 2.5 h caused decrease in adsorption capacity. Therefore, 2 h is the optimum time for adsorbent activation.

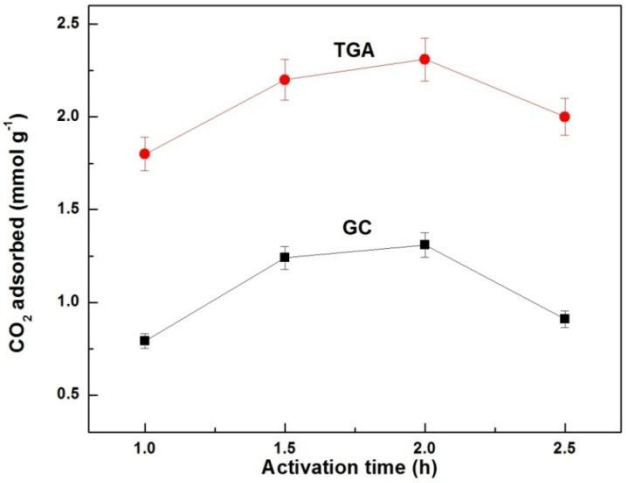

Fig. 4.11 Effect of activation time on CO_2 uptake capacity of porous adsorbents evaluated thermogravimetrically with 100% CO_2 and in fixed bed with 12.5% CO_2 at 30 °C

4.3.1.2 Effect of KOH to carbon ratio

Further, four different samples were prepared by varying KOH to carbon mass ratios (1-4). The carbon samples were activated in tubular furnace at 700 ˚C for 2 h and it was found that thermogravimetric CO_2 uptake showed good improvement with enhancement in KOH to carbon mass ratio up to 3 and declined further when ratio was raised to 4 as depicted in Fig. 4.12. This may be attributed to proper activation of Act-3-700 which is also confirmed from higher oxygen content and higher surface area (Table 4.2) of this sample resulting in higher adsorption capacity. This could be also due to cleavage of more C-C bonds than oxygen functional group. However, the decrease in adsorption capacity of the adsorbent sample Act-4-700 is probably due to deterioration of its textural properties, pore blockage caused by higher KOH:carbon mass ratio and more contribution of carboxyl (O4) functional group imparting acidic nature to sample which was confirmed from XPS results. Similar trend was observed for CO_2 uptake evaluated in fixed bed column but with lower values. Consequently, KOH to carbon mass ratio of 3 was finally selected for further study.

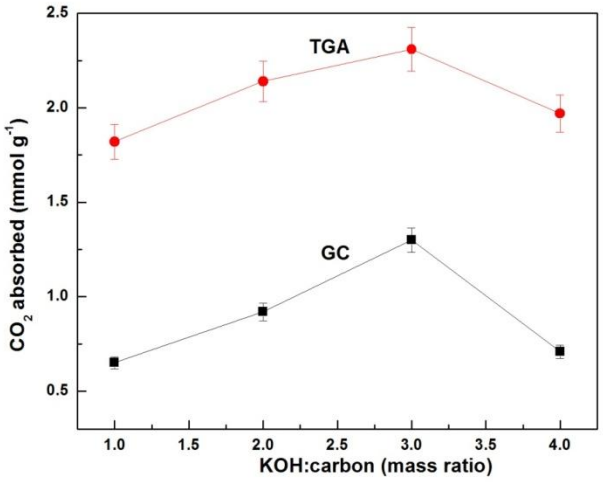

Fig. 4.12 Effect of KOH:carbon mass ratio on CO_2 uptake capacity of porous adsorbents evaluated thermogravimetrically with 100% CO_2 and in fixed bed with 12.5% CO_2 at 30 °C

4.3.1.3 Effect of activation temperature

Fixing KOH to carbon mass ratio of 3, adsorbent samples were prepared at different activation temperatures (500 to 800 ˚C) and activated for 2 h. The CO_2 uptake capacities of prepared

samples were determined thermogravimetrically and in fixed bed column. The results are shown in Fig. 4.13. The amount of CO_2 adsorbed increased as the temperature of activation was raised to 700 ˚C and slowed down when the temperature was further increased to 800 ˚C. Actually, the reaction between KOH and carbon atoms does not proceed to completion at lower temperatures, thereby resulting in lesser number of micropores leading to reduced CO_2 adsorption capacity at lower temperatures. However, their potential to generate more pores increases with rise in temperature but still higher temperatures (> 700 ˚C) might be responsible for collapsing of pores and hence lowered CO_2 adsorption capacity.

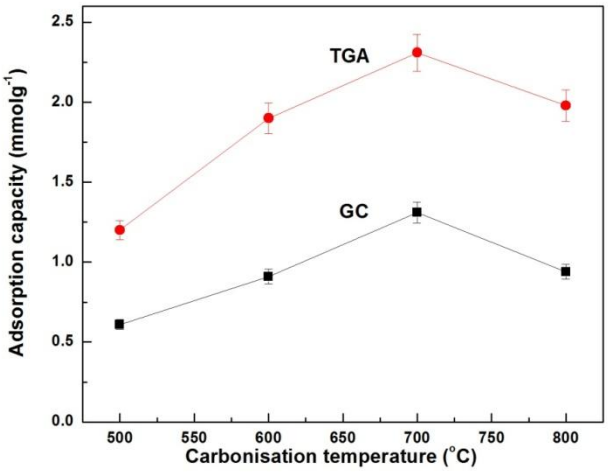

Fig. 4.13 Effect of activation temperature on CO_2 uptake capacity of porous adsorbents evaluated thermogravimetrically with 100% CO_2 and in fixed bed with 12.5% CO_2 at 30 °C

Therefore, the optimum conditions considered for adsorbent development were activation temperature of 700 ˚C, KOH to carbon mass ratio 3 and 2 h activation time. Thus, Act-3-700 was considered as most favorable sample for further study.

4.3.1.4 Effect of activating agent

In order to investigate the effect of another activating agent, fresh adsorbent sample was prepared by activating B-700 (carbonized PET waste at 700 °C) with potassium carbonate (K_2CO_3) following same procedure as mentioned in sections 4.1.2 and 4.1.3. Four samples were prepared by activating in variable K_2CO_3:carbon mass ratios (1-4) but at constant activation

temperature of 700 °C for 2 hours. The samples were named as KCA-a-b, where 'a' symbolized the mass ratio of K_2CO_3:carbon and 'b' represented the temperature set for activation.

Characterization of K_2CO_3 activated samples

The N_2 sorption isotherms of directly carbonized sample and K_2CO_3 activated samples are depicted in Fig. 4.14(a). Results indicate insignificant adsorption of nitrogen by the base sample suggesting non-porous nature of sample. The shape of isotherms for all the chemically activated samples follows typical Type 1 isotherm which confirms the presence of micropores.

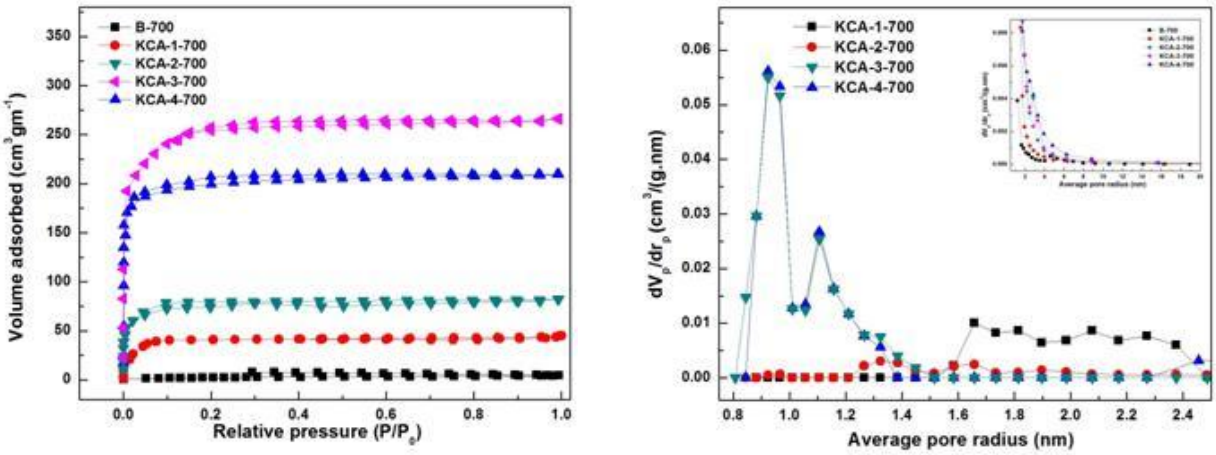

Fig. 4.14 (a) N_2 adsorption and desorption (at 77K) isotherms measured for carbon samples and (b) Micropore distribution of samples (inset: BJH pore size distribution)

The surface and textural properties of K_2CO_3 activated samples are displayed in Table 4.5. It can be observed that with increase in K_2CO_3:carbon mass ratio upto 3 there was an increase in pore volume which decreased with further increase in mass ratio. This may be attributed to widening of pores during activation causing increase in micropore volume and eventually total pore volume. Under inert atmosphere, K_2CO_3 gets reduced by carbon to produce metallic potassium and carbon monoxide (Equation 4.4) which causes loss in weight and increase in specific surface area [175]. However, the pores get collapsed at higher K_2CO_3:carbon mass ratio. Similar trends in surface area and pore volume were observed for KOH activation also. KCA-3-700 exhibited highest surface area and maximum micropore volume of 658.6 $m^2\ g^{-1}$ and 0.26 $cm^3\ g^{-1}$ respectively. Pore size distributions of K_2CO_3 activated samples are presented in Fig. 4.14(b). PSDs clearly show the presence of micropores in the range of 0.8-2.4 nm in all the activated

samples while micropore volume was almost confined in narrower range of 0.8-1.5 nm for KCA-3-700 which exhibited highest CO_2 adsorption capacity. The NLDFT method was applied for analysis of micropores and BJH method for obtaining PSD (shown in Fig. 4.14(b) inset).

Table 4.5 Textural properties of K_2CO_3 activated adsorbents from N_2 adsorption isotherms

Carbon sample	BET area, S_{BET} ($m^2 .g^{-1}$)	Total pore volume, V_p ($cm^3 .g^{-1}$)	Mesopore volume, V_{me} ($cm^3 .g^{-1}$)	Micropore volume, V_{mi} ($cm^3 .g^{-1}$)
KCA-1-700	54.8	0.12	0.05	0.07
KCA-2-700	186.7	0.18	0.04	0.14
KCA-3-700	658.6	0.32	0.06	0.26
KCA-4-700	592.3	0.29	0.07	0.22

SEM analysis was performed to examine the change in surface texture before and after activation. Fig. 4.15(a) depicts the SEM image of the sample B-700 and micrographs of adsorbent samples prepared by K_2CO_3 activation can be seen in Fig. 4.15[(b)-(e)].

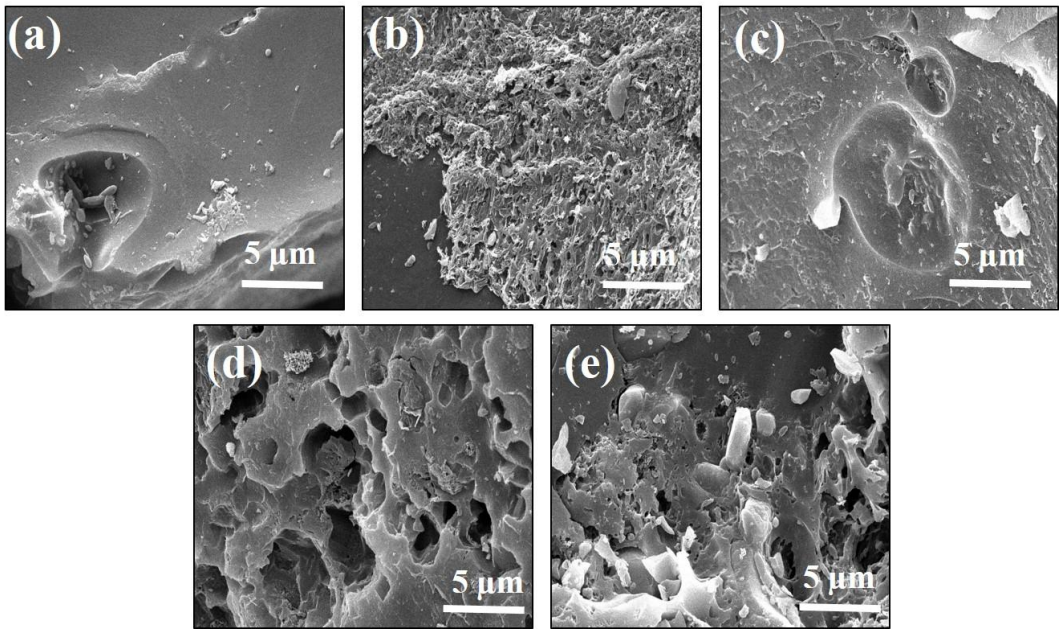

Fig. 4.15 Scanning electron micrographs of (a) B-700, (b) KCA-1-700, (c) KCA-2-700, (d) KCA-3-700, (e) KCA-4-700

As apparent from micrographs, adsorbent prepared by direct carbonization (B-700) possesses almost non-porous surface. However, all the adsorbent samples activated with different K_2CO_3 to

carbon ratio show improvement in porosity, with KCA-3-700 showing the finest pore structure. During activation and carbonization, K_2CO_3 decomposes to form potassium oxide (K_2O) which reacts with active carbon to release gases like CO and CO_2. Similar, behavior was observed with KOH activated samples also. However, the pores were finer in KOH activated samples in comparison to K_2CO_3 activated samples.

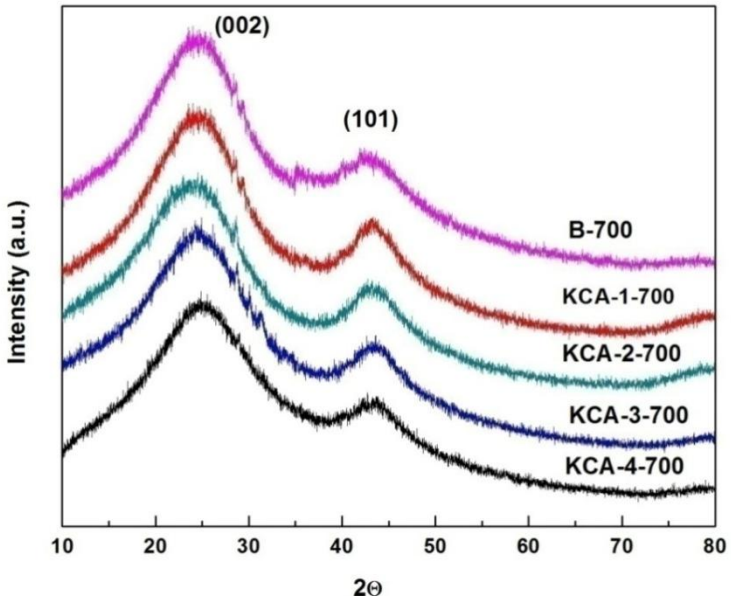

Fig. 4.16 XRD patterns of K_2CO_3 activated adsorbent samples

Fig. 4.16 illustrates the X-ray micrographs of the reference sample (directly carbonized sample) and activated samples prepared with different K_2CO_3:carbon mass ratios. No intense peak was observed for any of the sample, clearly indicating amorphous nature of the adsorbent samples. The peak intensities diminished with increase in K_2CO_3. Broadening of peak is observed in 2θ range of 25-27^o followed by a small hump between 43-45^o in all the samples. For the similar reasons as explained in section 4.2.3, the values of 2θ in former region are indexed as (0 0 2) and (1 0 1) in later region. These values point towards the disordered structure and poorly crystalline nature of the samples. Hence, it can be concluded that K_2CO_3 activation also contributes in generation of high surface area due to uneven and randomly oriented carbon layers favorable for gas adsorption.

Elemental analysis of the K_2CO_3 activated samples was performed to find out the content of elements present in the samples as shown in Table 4.6. From the results it can be interpreted that

with increase in K_2CO_3 to carbon mass ratio up to 3, carbon content (%) decreased from 78.1 to 75.3% due to removal of C-C bonds and the oxygen content increased from 20.9 to 26.5 % due to addition of oxygen during activation, thus making KCA-3-700 more basic which is beneficial for capturing acidic gases. However, the increase in oxygen content was about 34.3% for KOH activated samples which is much higher than K_2CO_3 activated samples indicating higher basicity of former samples.

Table 4.6 Elemental analysis of K_2CO_3 activated adsorbent samples

Carbon sample	Content of elements (wt %)		
	C	H	O*
KCA-1-700	78.1	1.03	20.9
KCA-2-700	77.8	0.77	21.4
KCA-3-700	72.5	0.98	26.5
KCA-4-700	75.3	1.19	23.5

*by difference

The characterization results show that KOH activated samples possess improved porosity, higher oxygen content, and better textural properties than K_2CO_3 activated samples which strongly point towards the their higher probability to capture CO_2.

4.3.2 Dynamic CO_2 adsorption-desorption measurements

4.3.2.1 Effect of activating agent:carbon ratio

Figs. 4.17 (a) and (b) demonstrate the breakthrough curves for adsorbent samples activated with different KOH:carbon and K_2CO_3:carbon mass ratios respectively at 30 °C and 12.5% CO_2. A breakthrough curve can be plotted by recording the exit concentration of the adsorbate with respect to time. In the start of the adsorption process, most of the adsorbate gets adsorbed in the bed, indicating zero concentration at the exit. Gradually, the mass transfer zone travels further till the whole bed gets saturated. At this point, the adsorbate oozes out of the bed and its concentration (C) starts increasing till it equalizes inlet concentration (C_o). The exit concentration is recorded for plotting breakthrough curves.

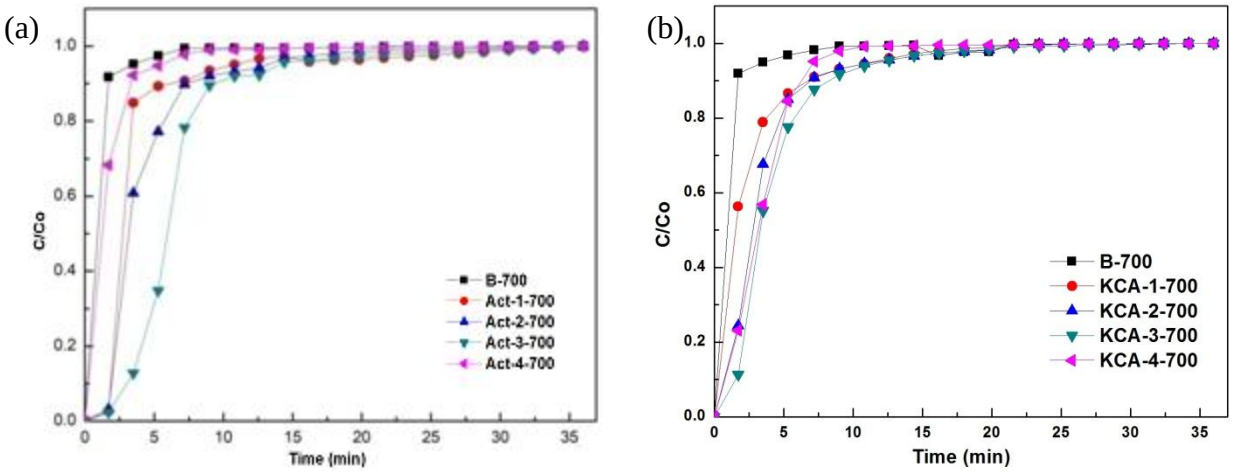

Fig. 4.17 Breakthrough curves of (a) KOH activated adsorbents (b) K_2CO_3 activated adsorbents

It can be observed in the figures that during the initial stage, CO_2 was not detected in the exit stream for both the activated samples, indicating complete adsorption of gas. But after some time, concentration of CO_2 in the outlet started increasing and correspondingly C/C_o ratio too, suggesting progression of mass transfer zone towards the bed outlet. This progression was comparatively faster in KOH activated samples than K_2CO_3 activated samples as evident from shorter breakpoint time (t_b =1.6 min) and higher dynamic adsorption capacities, elucidating better textural properties and surface properties of KOH activated samples (S_{BET} = 1690 m^2g^{-1} and V_{mi} = 0.78 cm^3 g^{-1}). In Fig. 4.17(a), the breakthrough curve for Act-3-700 appeared broader in comparison to curves of the other samples. This clearly suggests faster penetration of CO_2 in the adsorbent bed thereby exhibiting maximum adsorption capacity (1.31 mmol g^{-1}). Also, similar trend was seen in Fig 4.17(b) where KCA-3-700 (t_b = 1.8 min) displayed broadest curve and subsequently showed highest CO_2 uptake of 0.89 mmol per gram of adsorbent. The reason for this behavior may be due to inferior surface textural features of the sample (S_{BET} = 658.6 m^2g^{-1} and V_{mi} = 0.26 cm^3 g^{-1}). Therefore the bed packed with Act-3-700 saturated earlier resulting in shorter breakthrough time than KCA-3-700. B-700 with negligible porosity showed the steepest curve with least breakpoint time of CO_2 in the bed, thereby resulting in minimum adsorption capacity.

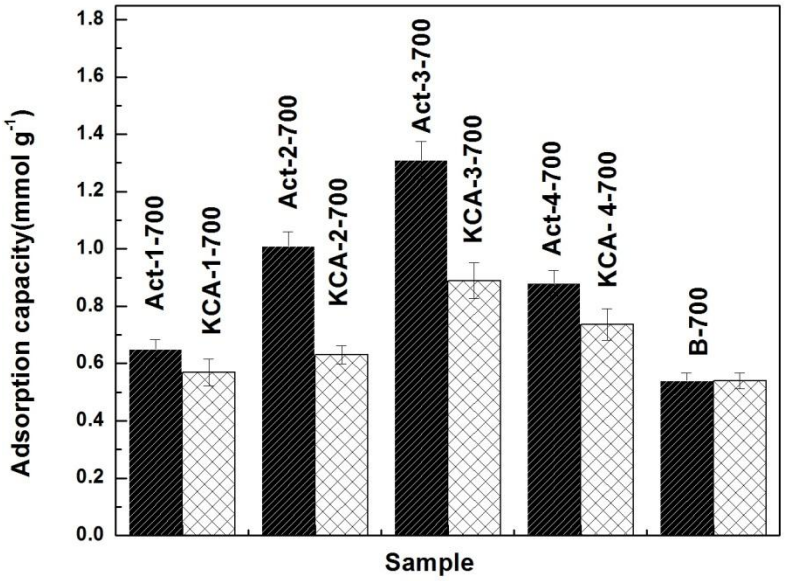

Fig. 4.18 CO_2 uptake by carbon adsorbents at 30 °C and 12.5% CO_2

Further, the equilibrium CO_2 adsorption capacities of KOH and K_2CO_3 activated samples with different impregnation ratios at 30 °C and 12.5% CO_2 concentration are shown in Fig. 4.18. It was observed that CO_2 uptakes of K_2CO_3 activated samples followed similar trend as observed with KOH activated carbon samples. CO_2 adsorption capacity increased with increase in K_2CO_3 to carbon mass ratio up to 3 and dropped with further increase in mass ratio. Highest CO_2 uptake of 1.31 mmol g^{-1} and 0.89 mmol g^{-1} was exhibited by Act-3-700 and KCA-3-700 respectively. Similar effect of activating agents on CO_2 capture capacity has been reported in literature [176, 177]. Higher CO_2 uptakes obtained at all ratios of KOH activation may be attributed to its well-built porous structure as established from SEM & TEM results. Also, the XPS analysis confirmed the existence of oxygen moieties which enhance basicity in the adsorbent, thereby increasing its attraction towards acidic CO_2 gas. Pevida et al. [178] also reported similar results. Further, KCA-3-700 showed lower adsorption capacity due to inferior textural properties and lesser oxygen content as observed from BET and elemental analysis. Therefore, it can be concluded that CO_2 capture capacity is greatly influenced by presence of basic functionalities and textural properties.

4.3.2.2 Effect of adsorption temperature

At 5% CO_2 concentration

CO_2 breakthrough curves for Act-3-700 and KCA-3-700 plotted at different adsorption temperatures (30, 50, 75, and 100 °C) at 5% CO_2 concentration are shown in Fig. 4.19 (a) and (b) respectively.

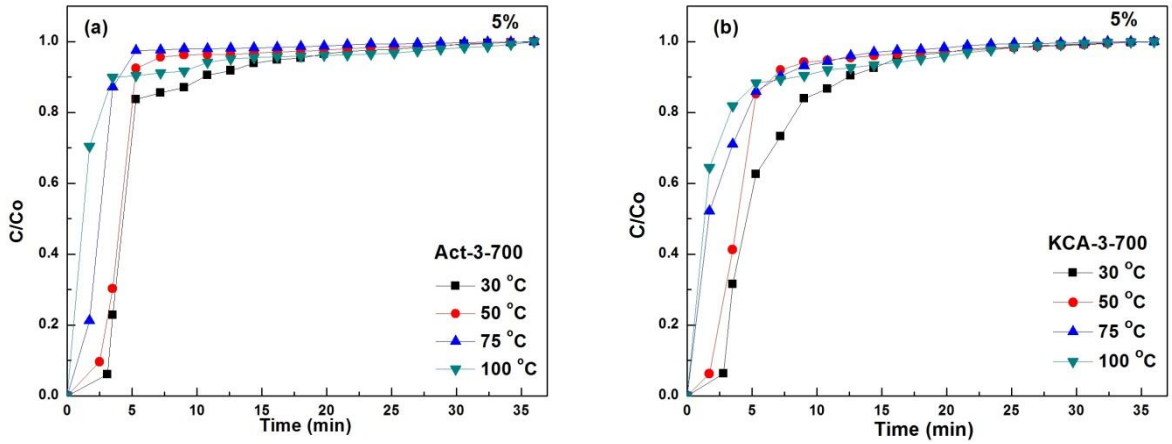

Fig. 4.19 CO_2 breakthrough curves for (a) Act-3-700 and (b) KCA-3-700 at 5% CO_2 and different temperatures

It is recognized that with increase in temperature from 30-100 °C, adsorbents got saturated earlier and thereby showing a decline in CO_2 adsorption capacity from 0.55 to 0.28 mmol g^{-1} and 0.36 to 0.17 mmol g^{-1} for KOH and K_2CO_3 activated samples respectively. At all temperatures, initially no CO_2 was spotted at the outlet of the fixed bed column owing to adsorption of CO_2 molecules on the surface and pore sites of the adsorbent. The exit of CO_2 gas from the column followed the order as 100 °C > 75 °C > 50 °C > 30 °C. This tendency might be due to breakpoint time stretch caused due to fall in temperature, which consequently enhanced the adsorption capacity at lower temperatures. Also, this behavior is an indicative of physisorption nature of the adsorption process. Similar observations have been reported in literature [139, 179].

At 7.5% CO_2 concentration

Breakthrough behavior of Act-3-700 and KCA-3-700 were observed at 7.5% CO_2 concentration and different temperatures (Fig. 4.20(a) and (b)). The corresponding equilibrium CO_2 adsorption

capacities are given in Tables 4.7 and 4.8. From the figure, it can be interpreted that when the adsorption temperature increased from 30-100 °C there was an appreciable decrease in CO_2 adsorption capacity. The CO_2 uptake decreased from 0.81 to 0.34 mmol g^{-1} for KOH and 0.57 to 0.22 mmol g^{-1} for K_2CO_3 activated samples respectively.

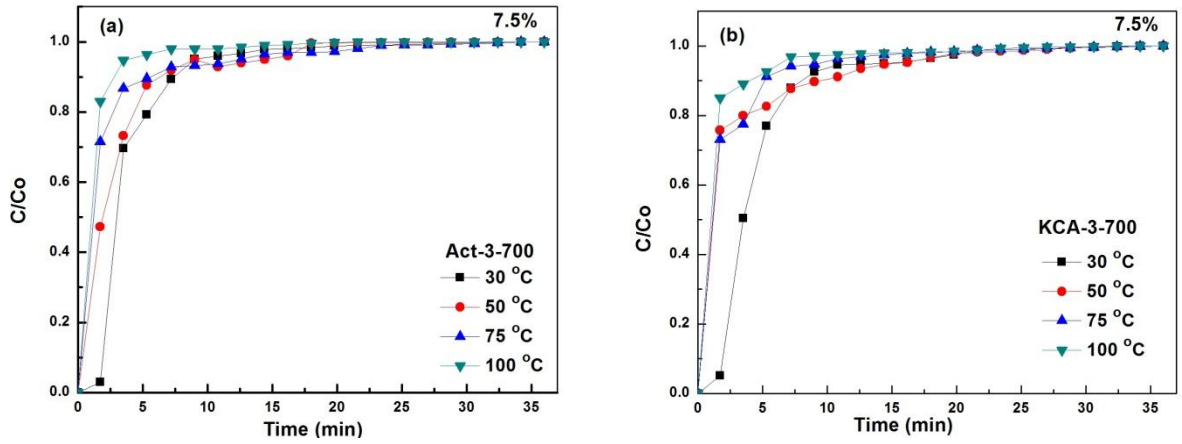

Fig. 4.20 CO_2 breakthrough curves for (a) Act-3-700 and (b) KCA-3-700 at 7.5% CO_2 and different temperatures

At 10% CO_2 concentration

Fig. 4.21(a) and (b) depict the CO_2 breakthrough curves for Act-3-700 and KCA-3-700 at 10% CO_2 concentration and different temperatures. KOH and K_2CO_3 activated samples exhibited highest CO_2 adsorption capacities of 1.1 and 0.77 mmol g^{-1} respectively at 30 °C. Least CO_2 uptakes were obtained at 100°C for both the samples. Dynamic CO_2 uptakes for Act-3-700 and KCA-3-700 at 10% CO_2 and variable temperatures are summarized in Tables 4.7 and 4.8.

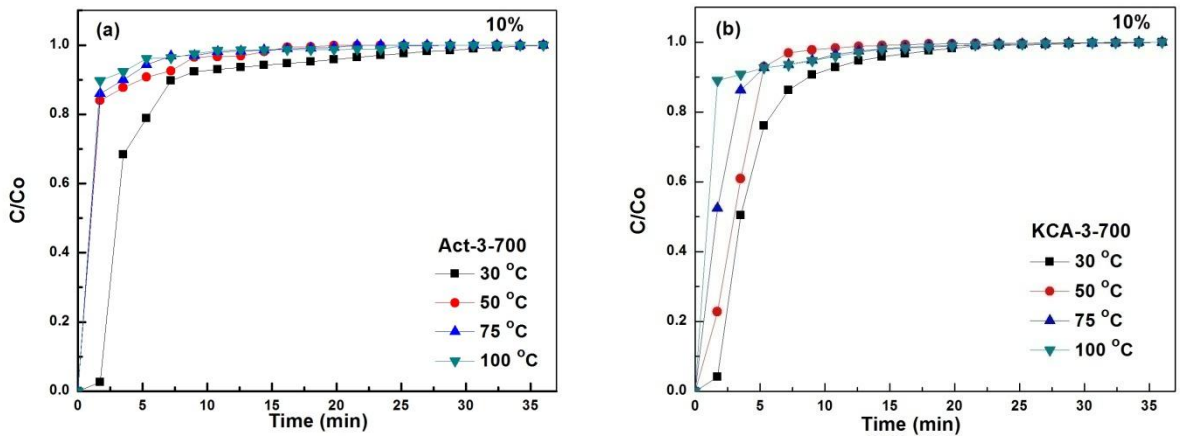

Fig. 4.21 CO_2 breakthrough curves for (a) Act-3-700 and (b) KCA-3-700 at 10% CO_2 and different temperatures

At 12.5% CO_2 concentration

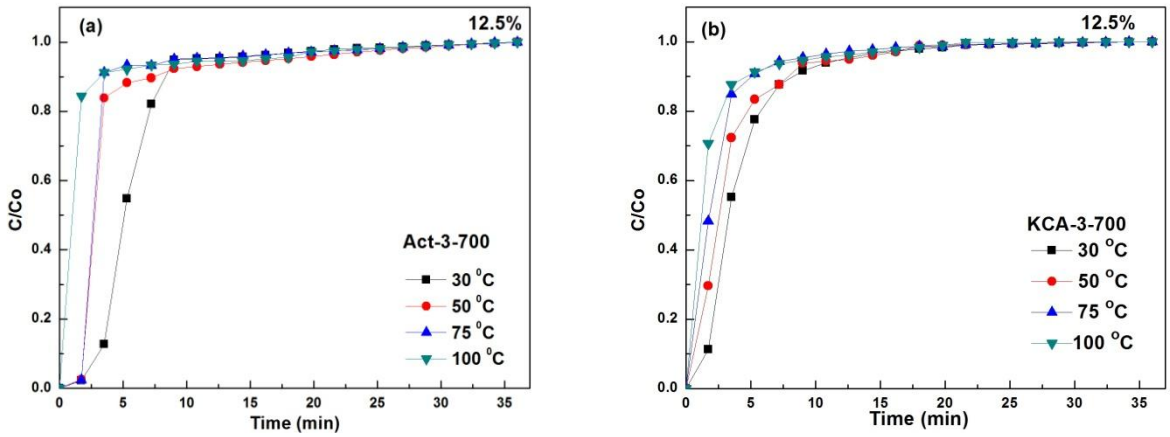

Fig. 4.22 CO_2 breakthrough curves for (a) Act-3-700 and (b) KCA-3-700 at 12.5% CO_2 and different temperatures

The CO_2 breakthrough curves for Act-3-700 and KCA-3-700 at highest evaluated CO_2 concentration (12.5%) are represented in Fig. 4.22(a) and (b) at different temperatures. The CO_2 adsorption capacity trend can be seen in Tables 4.7 and 4.8 for KOH and K_2CO_3 activated samples respectively. It can be observed that CO_2 uptake decreased from 1.31-0.58 mmol g^{-1} and 0.89-0.45 mmol g^{-1} respectively for Act-3-700 and KCA-3-700 with variation in temperature from 30-100 °C at 12.5% CO_2 concentration. This declining pattern indicates the physisorption nature of adsorbents. Actually, as the temperature rises, molecules acquire more kinetic energy

and hence move faster and collide more frequently. Hence, higher number of CO_2 molecules is able to overcome the activation barrier leading to instability of adsorbate gas on surface of the adsorbent. Thus the desorption rate is enhanced which results in reduced CO_2 uptake.

Table 4.7 CO_2 uptake on Act-3-700 with variation in CO_2 concentration and adsorption temperature

Temperature (°C)	CO_2 adsorption capacity (mmol g^{-1}) at			
	5%	7.5%	10%	12.5%
30	0.55	0.81	1.1	1.31
50	0.45	0.57	0.75	1.01
75	0.35	0.48	0.60	0.78
100	0.28	0.34	0.40	0.58

Table 4.8 CO_2 uptake on KCA-3-700 with variation in CO_2 concentration and adsorption temperature

Temperature (°C)	CO_2 adsorption capacity (mmol g^{-1}) at			
	5%	7.5%	10%	12.5%
30	0.36	0.57	0.77	0.89
50	0.25	0.37	0.53	0.72
75	0.20	0.30	0.41	0.54
100	0.17	0.22	0.30	0.45

4.3.2.3 Effect of feed concentration

Further, the effect of feed concentration on CO_2 uptake of Act-3-700 and KCA-3-700 was investigated at 30 °C (adsorption temperature) and results obtained for feed concentrations of 5, 7.5%, 10% and 12.5% are depicted in Fig. 4.23.

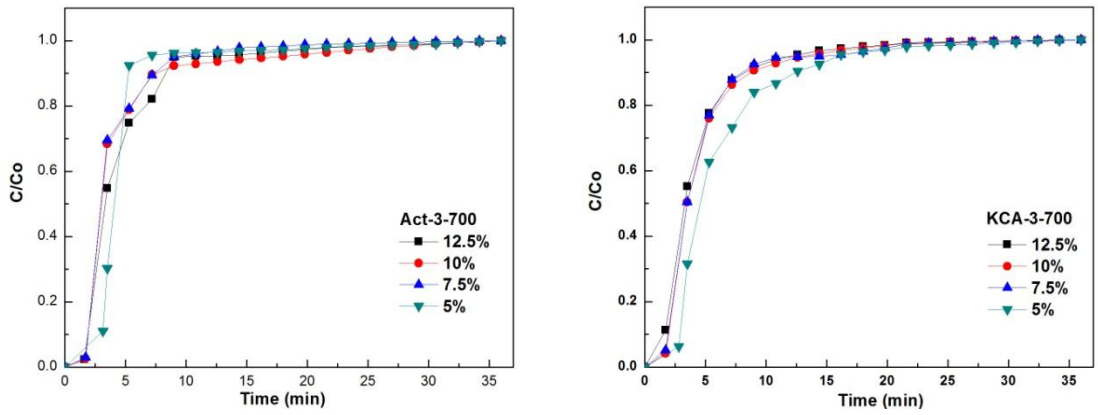

Fig. 4.23 CO_2 breakthrough curves for (a) Act-3-700 and (b) KCA-3-700 at different CO_2 concentrations and 30 °C

It is notable that increase in feed concentration caused a shift in breakpoint to a lesser time indicating early saturation of bed. Highest breakthrough time was obtained for 5% CO_2 concentration (t_b = 3.15 min), and least for 12.5% CO_2 concentration (t_b = 1.6 min) for Act-3-700. On the other hand, with KCA-3-700, breakpoint time appeared at 2.8 min for 5% CO_2 concentration and 1.77 min for 12.5% CO_2 concentration. Also, it was noticeable that increase in concentration from 5% to 12.5% caused an increase in CO_2 uptake from 0.55 to 1.31 and from 0.36 to 0.89 mmol g^{-1} for Act-3-700 and KCA-3-700 respectively. This may be due to more availability of adsorbate molecules per gram of adsorbent at higher concentrations which caused faster saturation of bed resulting in higher CO_2 uptake. Alike inferences were also reported by Tiwari et al. [139] with different adsorbents.

With the variation in two main parameters namely adsorption temperature and CO_2 concentration, noticeable change in CO_2 adsorption capacity of both the activated samples Act-3-700 and KCA-3-700 was observed which is shown in Fig. 4.24. At a particular adsorption temperature of 30 °C, the increase in CO_2 concentration from 5% to 12.5% caused increase in adsorption capacity from 0.55 to 1.31 mmol g^{-1} and from 0.36 to 0.89 mmol g^{-1} respectively, for KOH and K_2CO_3 activated samples. This may be explained due to availability of more adsorbate molecules per unit of active sites available for CO_2 adsorption at higher carbon dioxide concentration. Further, at lower temperatures the CO_2 molecules get adsorbed by virtue of van der Waal forces (physical adsorption), but rise in temperature of the adsorbent bed (30 to 100 °C)

boosted energy (internal) of the adsorbent molecules which brought about the release of CO_2 gas from the surface causing early desorption and subsequently lower adsorption capacity.

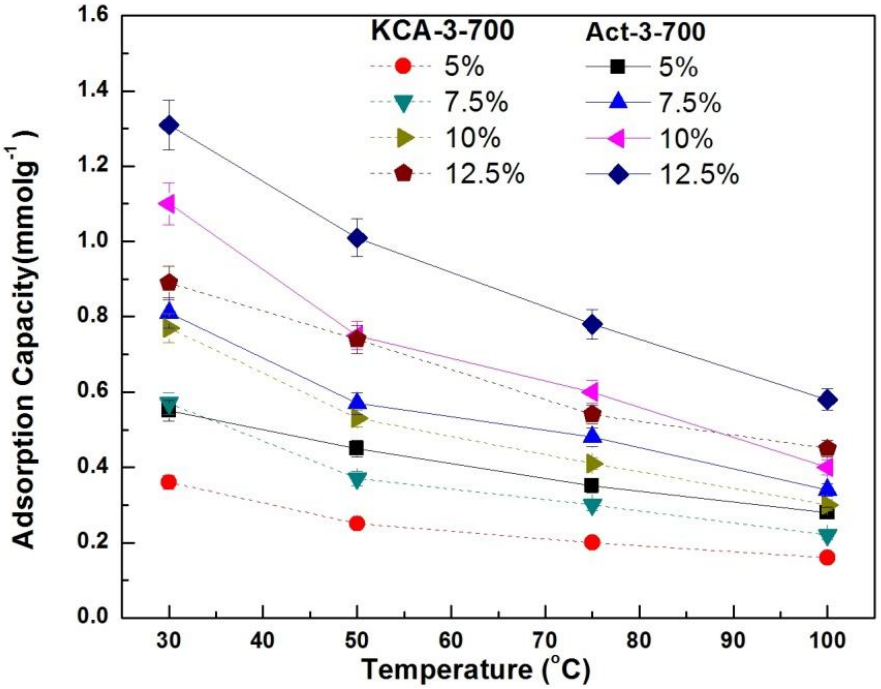

Fig. 4.24 Comparison of CO_2 uptake on Act-3-700 and KCA-3-700 at different adsorption temperatures and CO_2 concentrations

On the whole, the use of KOH as an activation agent increased the BET surface area and microporosity of the samples which resulted in the enhancement of CO_2 adsorption capacity due to availability of more active sites for greater interactions with the incoming gas molecules. Also, inference of the above results clearly show that the performance of KOH activated samples is better in comparison to that of K_2CO_3 activated adsorbents. Therefore, the further studies were conducted with the adsorbent activated with KOH.

4.3.3 Adsorbate selectivity and adsorbent regenerability

4.3.3.1 Adsorbate (CO_2) selectivity

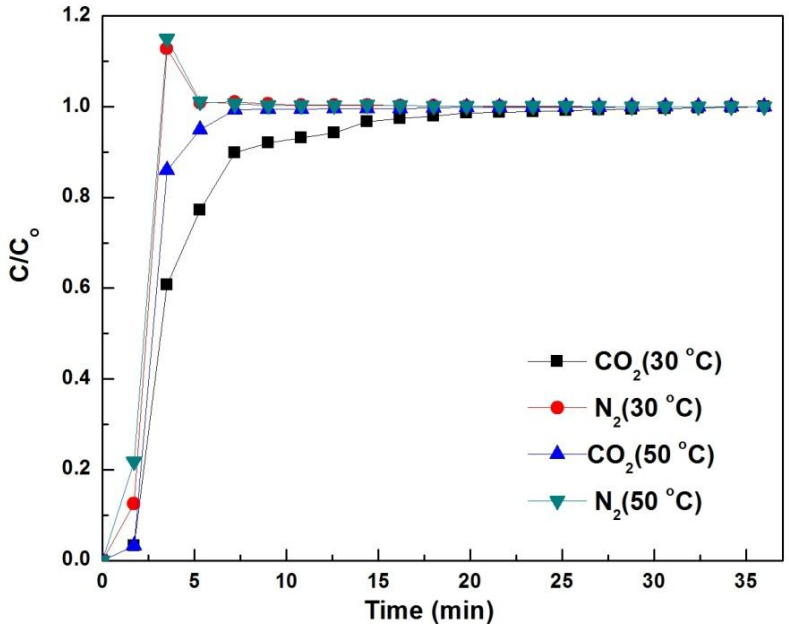

Fig. 4.25 Selectivity of CO_2/N_2 on Act-3-700 for 12.5% CO_2 at 30 °C and 50 °C

Breakthrough curves of CO_2/N_2 for 12.5% CO_2 at 30 °C and 50 °C are shown in Fig. 4.25. A hump in the breakthrough curve for N_2 is quite visible at C/C_0 >1 which indicates the competitive behavior of the adsorption process. Because of higher N_2 concentration, it has tendency for higher occupancy in vacant sites in initial stage but later on it gets replaced with CO_2, indicating adsorbent's greater selectivity towards CO_2. Furthermore, N_2 is spotted at the exit in comparison to CO_2 indicating lower affinity of adsorbent towards N_2. Goel et al. [180] also reported similar trends.

4.3.3.2 Cyclic adsorption/desorption study

Regenerabilty of adsorbents plays a significant role in selection of an adsorbent for industrial applications [20]. Therefore, to substantiate adsorbent's (Act-3-700) regenerability, multiple adsorption and desorption cycles were performed. Prior to adsorption, the temperature of the fixed bed column was raised to 200 °C and held for 2 h with pure N_2 flow for removal of moisture and subsequently dropped down to desired adsorption temperature. Then, a simulated flue gas mixture of CO_2 (concentration varying from 5 to 12.5%) and N_2 at 80 ml min^{-1} was

passed in column to perform adsorption. After completion of adsorption, the sample was desorbed at 200 °C under inert gas (N_2) flow. The same procedure was then repeated over five cycles. The activated carbon adsorbent showed complete regenerablility and CO_2 gas also easily desorbed from adsorbent as visible in Fig. 4.26(a). Further, stable performance of adsorbents was assured through a steady adsorption capacity over five adsorption-desorption cycles at different temperatures (Fig. 4.26(b)).

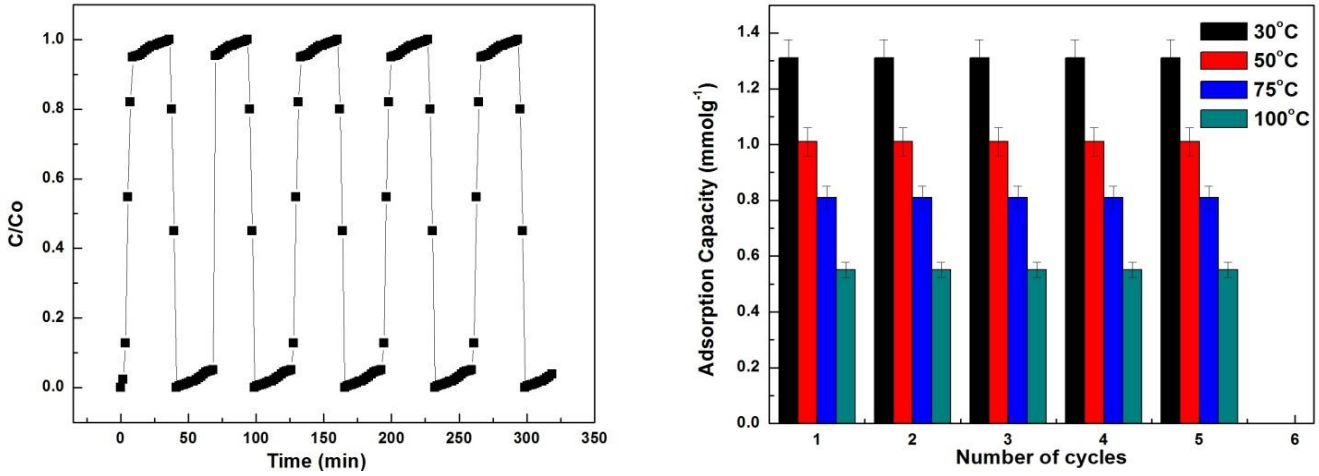

Fig. 4.26 (a) Adsorption and regeneration cycles for Act-3-700 at 30 °C with 12.5% CO_2 (b) Multi-cycle CO_2 uptake at different temperatures with 12.5% CO_2

4.4 Temperature programmed desorption

The objective of plotting TPD profile was to illustrate the vigorous heterogeneity of the carbon surface adsorption behavior. Fig. 4.27 demonstrates the desorption profile of Act-3-700 adsorbent. Quite an expansive peak in the range of 75-150 °C was viewed with the highest signal at 103 °C and then with a further increase in temperature the CO_2 signal descended with a tail touching value of 300 °C. In TPD-CO_2 study, the peaks that appear below 200 °C are usually considered weak, between 200-400 °C are medium, between 400-600 °C as strong and higher than 600 °C may be regarded as very strong basic sites [181]. The peak lying between 100 and 200° C is believed to be due to weak basicity related to weakly adsorbed CO_2 on the surface of the adsorbent [182].

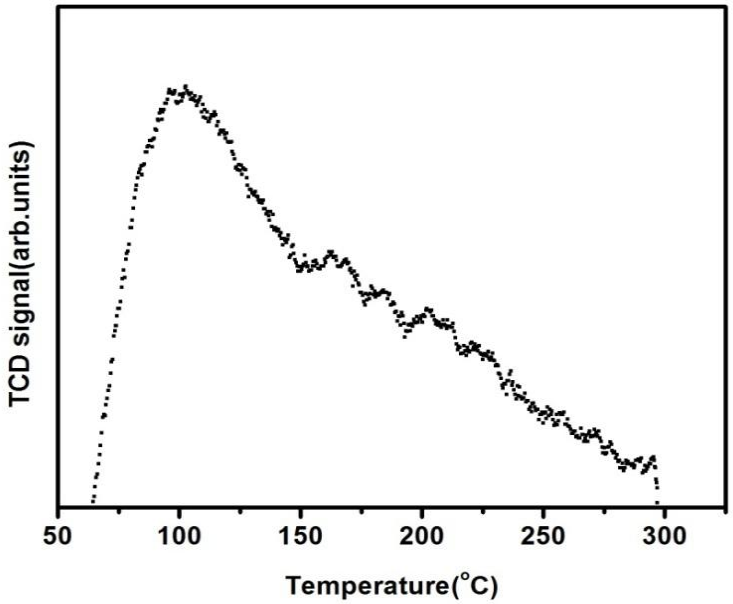

Fig. 4.27 Temperature programmed desorption profile of CO_2 from Act-3-700

In our work, the peak at 103 °C points towards the removal of CO_2 molecules bound with the surface of the adsorbent with weak physical forces. However, at higher temperatures (beyond 200 °C) CO_2 signal became faint with an extending tail indicating the contribution of chemisorption behavior due to the presence of medium basic groups. In a similar work, Gunathilake and Jaroniec [183] also reported high CO_2 uptake (2.61 $mmolg^{-1}$) at ambient conditions. Besides, the value of average isosteric heat (-12.08 kJ mol^{-1}) supports the physisorption of CO_2 on the adsorbent [184]. On the whole, it can be deduced that CO_2 got adsorbed predominantly by physisorption.

Comparative analysis has been carried out for adsorption capacities of carbon adsorbents obtained in the current work with that reported in literature at diverse operating conditions and shown in Table 4.9. The analysis shows that many research groups have worked on preparation of carbon adsorbents from PET wastes using various activating agents. However, KOH is widely accepted resulting in higher CO_2 uptakes. Also, most of the CO_2 capture capacities are evaluated either thermogravimetrically or under static conditions. In the former method adsorption is measured on weight gain basis which may involve higher component of error due to adsorption of other gases, hence it is a suitable method for preliminary studies only. Later method uses volumetric adsorption instrument for measurement of adsorption capacities of a known volume of

sample under static conditions which are at all times higher in comparison to those obtained under dynamic conditions [33]. But, in the present work performance evaluation of the synthesized carbon adsorbents from PET wastes has been carried out using a fixed bed column under dynamic conditions, which is more realistic for capture of flue gases from fossil-fuel based power plants.

Table 4.9 Comparison of CO_2 adsorption capacities from various studies

Carbon source	Activator	Activation temp. (°C)	Time (h)	N_2 flow rate (ml min^{-1})	Max. surface area (m^2g^{-1})	Temp./Pressure	Conditions	CO_2 uptake ($mmolg^{-1}$)	Reference
PET waste	KOH	700	2	60	1690	30°C, 1bar	Dynamic (FB)	1.31	This study
PET waste	KOH	700	2	60	1690	50°C, 1bar	Dynamic (FB)	1.01	This study
PET waste	CO_2	925	2	-	2176	25°C, 4bar	Static	4.04	[185]
Melamine Formaldehyde	CO_2	700	2	60	~193	30 °C, 1bar	Dynamic (FB)	0.64	[134]
HMMM	CO_2	700	2	60	463	30 °C, 1bar	Dynamic (FB)	0.676	[179]
Waste CDs	KOH	700	1	1800	2710	25 °C, 1bar	Static	3.3	[60]
PET wastes	KOH	800	1	50	1338	30°C, 5bar	Static	~5.3	[186]
PET/Dolomite	-	850	1	100	331	20 °C, 1bar	Dynamic (FB)	0.215	[187]
Palm stone	H_3PO_4	450	1	80	1889	0 °C, 1bar	Static	3.1	[188]
Bamboo	KOH	600	1.5	-	1846	25 °C, 1bar	Static	4.5	[68]
Carpet Waste	KOH	800	1	100	1910	25 °C, 1bar	Dynamic (TGA)	1.9	[104]
PET/carbazole	KOH	500	0.5	20	418	30,100 °C, 1bar	Dynamic (TGA)	1.09,0.27	[59]

FB= fixed bed

4.5 Kinetic Study

The kinetics of CO_2 uptake on chemically activated carbon prepared from PET wastes at different temperatures was modeled using five kinetic models, namely, pseudo-first-order, pseudo-second-order, Elovich model, fractional-order and Avrami model. Predicted uptakes by different kinetic models, at different temperatures for 12.5% CO_2 in the feed are depicted in Fig. 4.28.

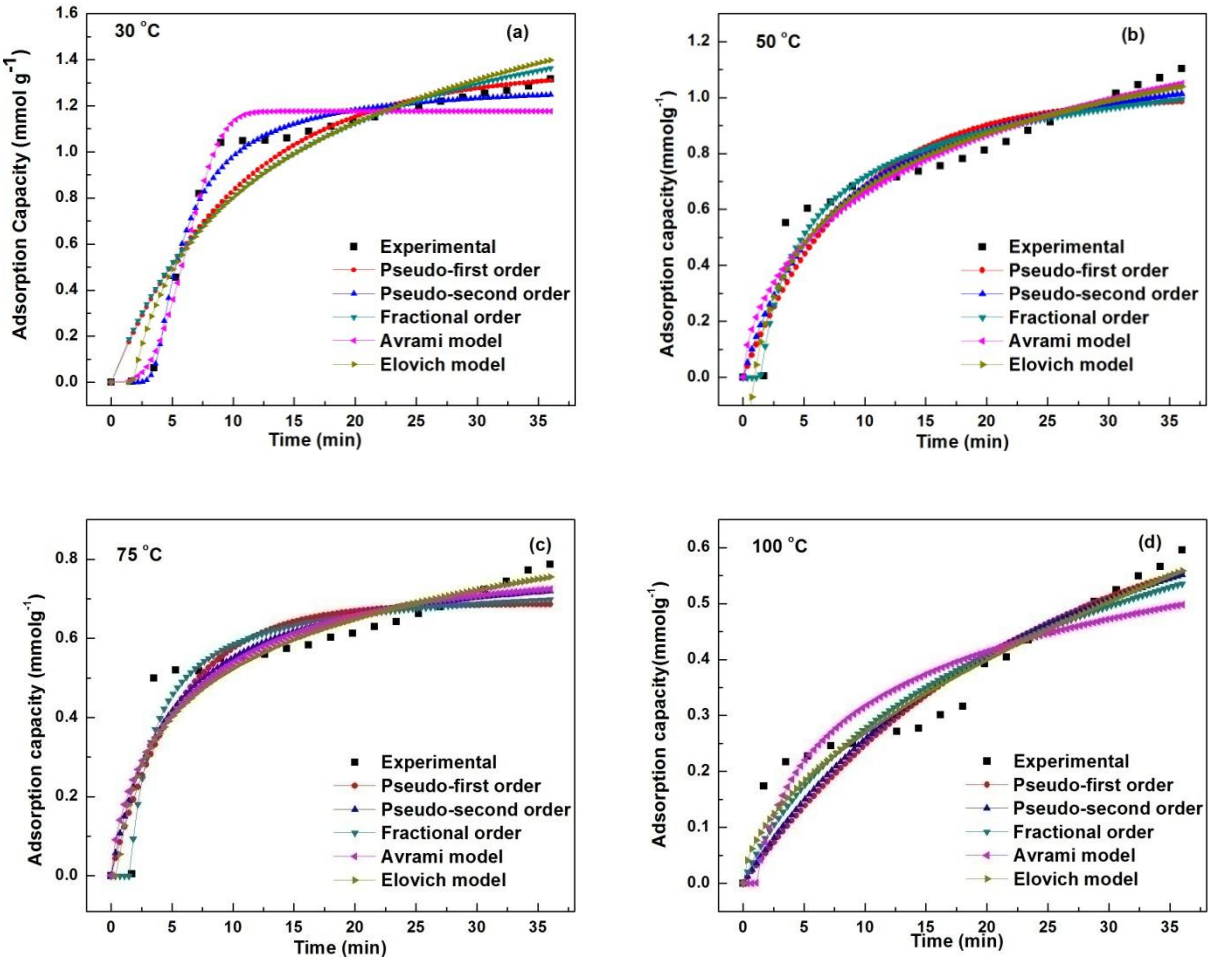

Fig. 4.28 Comparison of model predicted and experimental results of CO_2 uptake kinetics on Act-3-700 at 12.5% CO_2

Table 4.10 Model equations and kinetic parameters for CO_2 uptake on Act-3-700

Model		Temperature (°C)			
		30	50	75	100
Pseudo 1st order	k_1 (min^{-1})	0.095	0.1035	0.165	0.0432
$q_t = q_e(1-\exp(-k_1 t))$	q_e (mmol g^{-1})	1.35	1.02	0.694	0.604
	R^2	0.924	0.895	0.852	0.878
	Error %	2.50	2.32	3.02	2.24
Pseudo-second order	k_2 (g $mmol^{-1}$ min^{-1})	0.0413	0.084	0.226	0.36
$q_t = \frac{k_2 q_e^2 t}{1+k_2 q_e t}$	q_e (mmol g^{-1})	1.85	1.2	0.83	0.64
	R^2	0.911	0.919	0.882	0.885
	Error %	6.23	5.32	7.36	4.23
Fractional order	k_n (g^{m-1} $mmol^{1-m}$ min^{-1})	1.81	1.42	1.01	0.8
$q_t = q_e - \frac{1}{[((n-1)k_n/m)t^m + (1/q_e^{n-1})]^{1/n-1}}$	q_e (mmol g^{-1})	1.39	1.16	0.985	0.65
	n	14.2	13.51	13.01	12.30
	m	9.80	7.61	6.52	5.49
	R^2	0.992	0.991	0.988	0.979
	Error %	1.23	1.02	2.06	1.94
Avrami Model	k_n (min^{-1})	0.002	0.153	0.237	0.01
$q_t = q_e(1-\exp(-k_a t^n))$	q_e (mmol g^{-1})	1.44	1.17	0.82	0.53
	n	3.25	0.566	0.632	0.56
	R^2	0.978	0.922	0.865	0.936
	Error %	1.69	2.39	9.68	3.89
Elovich Model	α (mmol $g^{-1}s^{-1}$)	0.4314	0.284	0.179	0.138
$q_t = \frac{\ln(\alpha b)}{b} + \frac{\ln(t)}{b}$	b (g $mmol^{-1}$)	1.59	3.78	7.25	10.39
	R^2	0.908	0.940	0.8843	0.842
	Error %	3.6	4.5	1.9	1.65

It was observed that initially the CO_2 adsorption rate was higher due to the availability of ample unoccupied sites and gradually the adsorption process slowed down as it approached equilibrium due to resistance caused by a decrease in vacant sites for CO_2 capture. The model equations and kinetic parameters obtained for different models are presented in Table 4.10. Pseudo-first and second models over-estimated in the initial region and under-estimated in the intermediate region of the adsorption process with the regression coefficient (R^2) value lying in the range of 0.85-0.91. Further, Elovich model also depicted an inferior fit with experimental data ($0.87< R^2 < 0.91$). Avrami model showed closer fitting with experimental data in comparison to the earlier three models with R^2 values within 0.85-0.97. However, fractional-order model displayed a superior fit along with complete data and hence best explained the overall kinetics of the system. This was confirmed from the highest R^2 value and least error percentage. Adsorption rate constant (k_n) was found to decrease with increase in adsorption temperature because of exothermic nature of adsorption process. At higher temperatures, adsorption rate may become faster but lesser amount of CO_2 is adsorbed due to faster desorption of CO_2 from carbon surface. Kinetic model parameters *n* and *m* exhibit the effect of driving force and diffusion resistance respectively. Values of n and m decreased with increase in adsorption temperature and were found to be highest at 30 °C suggesting utmost driving force at this temperature and highest rate of adsorption process respectively, due to least diffusional resistance at this temperature.

4.6 Isotherm Study

To gain a proper understanding of the CO_2 equilibrium uptake on the prepared adsorbents three isotherm models namely Langmuir, Temkin, and Freundlich models have been considered. The adsorption capacities obtained from these models were fitted on experimentally calculated CO_2 uptakes by Act-3-700 at different adsorption temperatures are plotted as a function of CO_2 partial pressure and shown in Fig. 4.29.

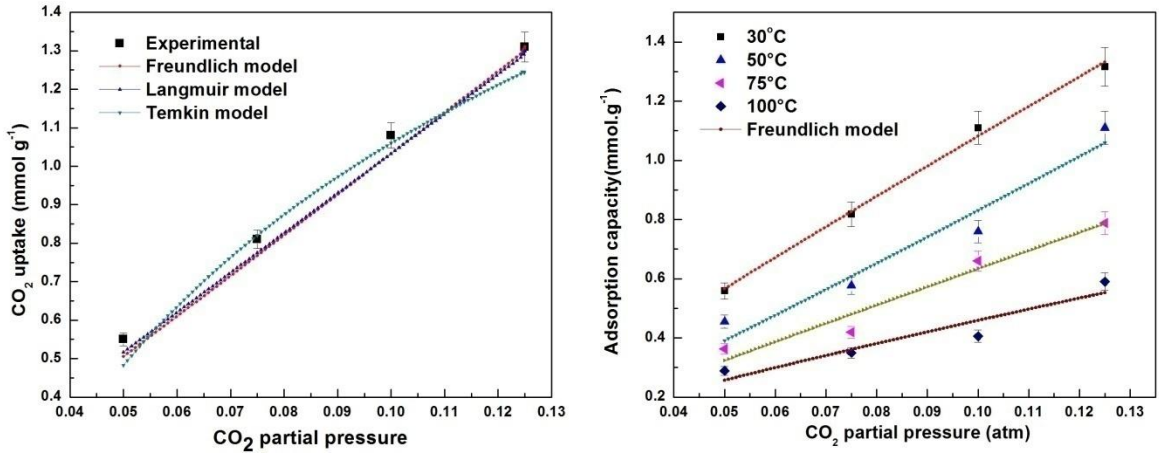

Fig. 4.29 Comparison of CO_2 uptake on Act-3-700 (a) Isotherm model predicted and experimental results at 30 ^oC (b) Freundlich isotherm model prediction and experimental results at different temperatures

Parameters obtained from fitting of these three models are depicted in Table 4.11. On the basis of the values obtained for correlation coefficient R^2, Freundlich isotherm best described the adsorption process, suggesting heterogeneity due to which several layers of adsorbate molecules are formed on the surface of the adsorbent (multilayer adsorption) which is an indicative of physical adsorption. The decrease in values of Freundlich constant (K_F) with increase in temperature indicates the exothermic characteristic of adsorption process. Value of n more than 1, suggests good adsorption conditions and also indicate higher CO_2 adsorption at lower temperatures [189].

Table 4.11 Adsorption isotherm parameters

Langmuir isotherm $q_e = \frac{q_m K_L P}{1 + K_L P}$			
T (°C)	K_L (atm^{-1})	q_m (mmol g^{-1})	R^2
30	0.865	13.5	0.995
50	0.889	9.8	0.977
75	0.205	2.44	0.956
100	1.72	3.14	0.885
Freundlich isotherm $q_t = K_F P^{1/n}$			
T (°C)	K_F (mmol $g^{-1}atm^{-1/n}$)	n	R^2
30	9.28	1.07	0.995
50	10.16	0.92	0.979
75	5.87	1.03	0.988
100	3.14	1.19	0.967
Temkin isotherm $q_e = B\ln(K_T P)$			
T (°C)	K_T (atm^{-1})	B (kJ mol^{-1})	R^2
30	37.82	0.83	0.982
50	35.51	0.67	0.906
75	38.46	0.48	0.913
100	47.43	0.29	0.884

4.7 Thermodynamic investigation

4.7.1 Thermodynamic properties

Thermodynamic properties were evaluated for CO_2 adsorption process on Act-3-700 at different temperatures of adsorption from equations 3.16 and 3.17 and values are mentioned in Table 4.12. The values of ΔG° obtained at all temperatures were lower than zero and negative. This suggests that the adsorption process was feasible and spontaneous too. Further, the slope of plot between ($ln\ K_{eq}$) and ($1/T$) from van't Hoff equation provided the value of ΔH° which was also negative

confirming the release of heat during adsorption. Positive value of entropy change confirmed the spontaneous nature of the process.

Table 4.12 Thermodynamic properties of Act-3-700 for CO_2 adsorption

Thermodynamic parameter	Temperature of adsorption (°C)			
	30	50	75	100
$\Delta G°$ (kJ mol^{-1})	-6.06	-5.28	-5.29	-3.65
$\Delta H°$ (kJ mol^{-1})	-15.19			
$\Delta S°$ (kJ $mol^{-1}K^{-1}$)	0.026			

Isosteric heat of adsorption (Q_{st}) on Act-3-700 at specific loadings was evaluated using Clausius-Clapeyron equation [190] and is shown in Fig. 4.30. The Q_{st} value varied from -7.77 to -17.33 kJ mol^{-1}, which is emblematic for physisorption [191]. The calculated average value of Q_{st} is 12.08 kJ mol^{-1} which is lower than the average value for isosteric heat on activated carbon reported in literature (18-20 kJ mol^{-1}) [192] and therefore physisorption is favored. Unsystematic trend obtained by Q_{st} value points towards the heterogeneous nature of adsorbent surface. Besides, it also provides an indication of weakly adsorbed molecules by virtue of van der Waals forces and therefore can be desorbed with much ease.

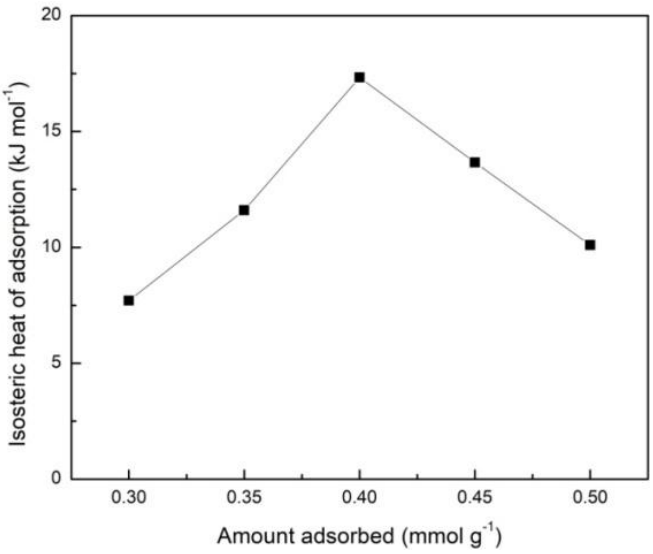

Fig. 4.30 Isosteric heat of adsorption of CO_2 on Act-3-700 at different CO_2 loadings

4.7.2 Heat duty for regeneration

For calculating the regeneration heat duty or energy required for desorbing CO_2, a complete adsorption-desorption cycle was performed using optimized sample Act-3-700. Simulated flue gas with 87.5% N_2 and 12.5% CO_2 was fed to the fixed bed column. Adsorption run was initiated at a temperature of 30 °C and continued till saturation limit of adsorbent. Thereafter, column was purged with dry N_2 gas and temperature was raised to 200 °C for regeneration of bed. CO_2 uptake obtained for Act-3-700 was 1.31 mmol g^{-1}. Further, the sensible heat was calculated from equation 3.20. The value of specific heat capacity for Act-3-700 was taken from literature and considered to be 1.44 J (g. °C)$^{-1}$ [193]. The calculations for regeneration heat duty are shown below:

Temperature of adsorption, T_a = 30 ˚C

Temperature of desorption, T_d = 200 ˚C

Difference in temperature, (T_d - T_a) = 170 ˚C.

Amount of CO_2 adsorbed on Act-3-700 = 1.31 mmol CO_2 per g adsorbent

= 1.31*(10^{-3}) * 44 = 0.0576 kg CO_2 per kg adsorbent

So, sensible heat needed for raising the temperature of adsorbent bed by 170 ˚C = (1.44×170)/ (0.00131) J $(mol)^{-1}$ CO_2 = 186.87 kJ $(mol)^{-1}$ CO_2.

Generally, 75% heat recovery is assumed in context of gaseous stream [194, 195] which suggests that the net sensible heat requirement for the process is 25% of the theoretically calculated sensible heat.

Thus, net sensible heat is equal to (0.25 × 186.6) k J $(mol)^{-1}$ CO_2 = 46.71 kJ $(mol)^{-1}$ CO_2.

Also, from equation 3.19, Q_{st} obtained for adsorption process is 12.08 kJ per mole CO_2

Therefore,

Total heat energy input for the process= (46.71 + 12.08) kJ $(mol)^{-1}$ CO_2 = 58.79 kJ $(mol)^{-1}$ CO_2

= (58.79/44) MJ $(kg)^{-1}$ CO_2 = 1.34 MJ kg^{-1} CO_2

Assuming amount of carbon dioxide generated from burning of coal (bituminous) for producing energy is 205.3 lbs (million Btu)$^{-1}$ = 8.84×10^{-2} kg per MJ of energy, the carbon dioxide generated for meeting the energy demand for regeneration in the present experiment is calculated accordingly.

Energy required for desorbing 1.31 mmol g^{-1} of CO_2 adsorbed on Act-3-700 = 1.34 × 0.0576

= 0.07718 MJ

If coal has been burnt for producing 0.07718 MJ of energy for regeneration of the adsorbent, then the amount of CO_2 generated would be (8.84×10^{-2}) × (0.07718) kg CO_2 = 0.00682 kg CO_2.

This corresponds to (0.00682/0.0576) x 100 = ~11.84% energy penalty.

Chapter 5 – Modeling and Simulation of Fixed Bed Adsorption

To explain the dynamics of the adsorption process, modeling and simulation of a fixed bed adsorption process is required [196, 197]. A pragmatic design of an adsorption column requires repeated experimentation either on lab or pilot scale and this tends to consume a lot of time and money [198]. Therefore, for understanding the behavior of newly developed adsorbents without performing several experiments, mathematical modeling and simulation on a fixed-bed column that takes into consideration all related transport phenomena is required [199]. Further, the breakthrough behavior of a desired component in the bulk gas can be predicted at all positions in the packed column. The flow diagram for development of mathematical model for adsorption process for CO_2 capture is shown in Fig. 5.1.

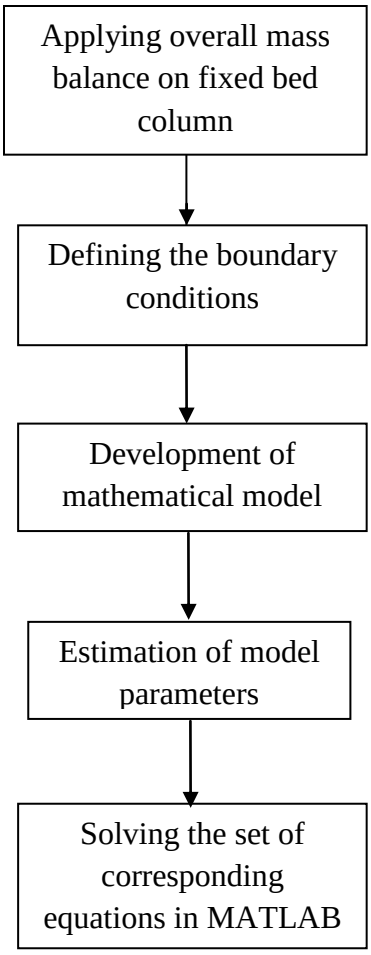

Fig. 5.1 Schematic flow diagram of modeling of the adsorption process

5.1 Model development

To develop a model for gas-solid adsorption in a column, the adsorption phenomenon can be accomplished through four basic steps; to begin with (i) mass transfer of gaseous phase via convection and molecular diffusion, (ii) mass transfer between gas phase and the adsorbent's outer surface i.e. film diffusion (iii) mass transfer within the particles by means of pore and surface diffusion (intraparticle mass transfer), and (iv) the adsorption-desorption equilibrium. Fig. 5.2 depicts the various regions and mode of mass transfer on a thin slice of adsorbent.

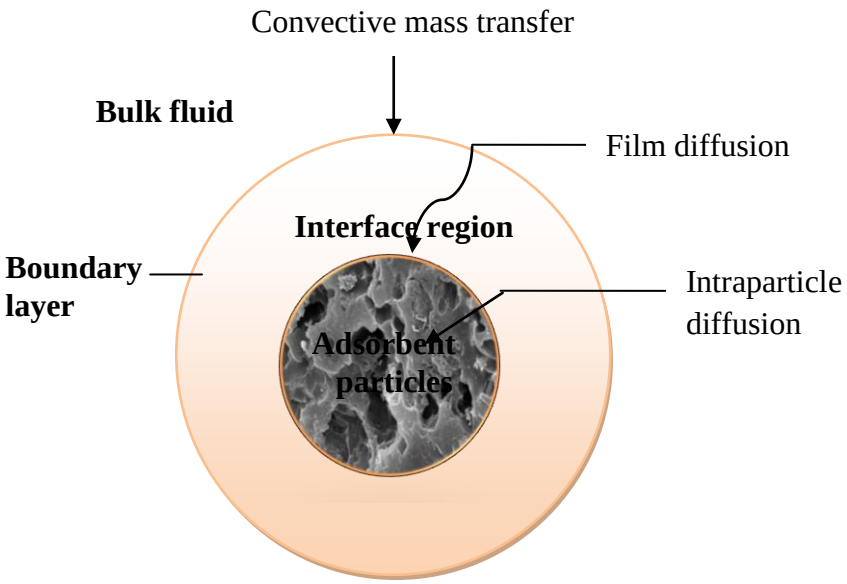

Fig. 5.2 Basic regions and steps of adsorption process

Before applying the mass balance on the packed bed, the following widely used assumptions are made:

a. The gas phase is in plug flow with axial dispersion and concentration is assumed uniform radially. Hence, the one-dimensional model is appropriate to explain the dynamics [200].
b. The isothermal operation is assumed.
c. The gas phase is assumed to behave ideally [201].
d. The adsorbent particles are spherical in shape.
e. Axial dispersion in the gas phase is considered and the mass transfer from gas phase to solid phase is represented by a linear driving force model [202].

f. The pressure gradient across the bed is negligible.

g. Constant velocity is considered along the length of the adsorber column.

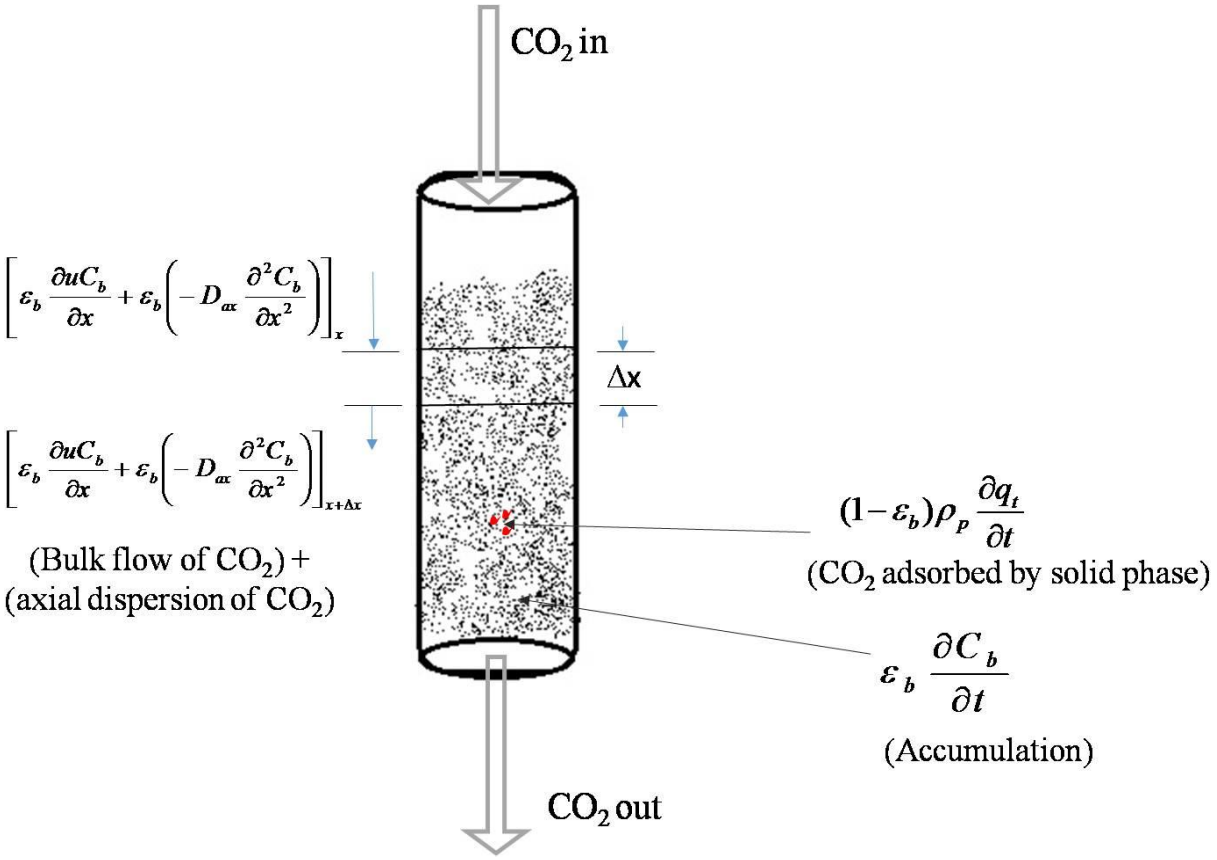

Fig. 5.3 Schematic representation of mass conservation balance for CO_2 over a thin slice of porous bed

In order to derive the equation for the unsteady mass balance of CO_2 gas along the bed, we consider a thin slice of the bed of thickness Δx at a distance x from the inlet of feed to the bed as shown in Fig. 5.3. Let A be the cross-sectional area of the bed. For a thin slice of the porous bed of particles, the mass conservation equation for CO_2 can be written as follows:

CO_2 entering due to dispersion – CO_2 exiting by dispersion + CO_2 entering by bulk flow – CO_2 exiting by bulk flow – CO_2 transferred to solid phase = accumulation of CO_2

Or CO_2 entering due to (bulk flow + dispersion) – CO_2 exiting by (bulk flow + dispersion) = accumulation of CO_2 + CO_2 transferred to solid phase

Input rate of CO_2 gas to the slice by bulk flow (at x) = $\varepsilon_b \left(uC_b\right)\Big|_x$

Input rate of CO_2 gas to the slice by axial dispersion = $\varepsilon_b \left(-D_{ax}\dfrac{\partial C_b}{\partial x}\right)\Big|_x$

Output rate of CO_2 gas from the slice at x + Δx by bulk flow = $\varepsilon_b \left(uC_b\right)\Big|_{x+\Delta x}$

Output rate of CO_2 gas from the slice by axial dispersion = $\varepsilon_b \left(-D_{ax}\dfrac{\partial C_b}{\partial x}\right)\Big|_{x+\Delta x}$

Rate of transfer of CO_2 gas to the solid phase adsorbent = $(1-\varepsilon_b)\,\Delta x\left(q_{t+\Delta t}-q_t\right)$

Rate of accumulation of the adsorbate = $\varepsilon_b\ \Delta x\dfrac{\partial C_b}{\partial t}$

Inserting the terms, we have

$$A\varepsilon_b\Delta t\left(\frac{u}{\varepsilon_b}-D_{ax}\frac{\partial C_b}{\partial x}\right)_{x,t}-A\varepsilon_b\Delta t\left(\frac{uC_b}{\varepsilon_b}-D_{ax}\frac{\partial C_b}{\partial x}\right)_{x+\Delta x,t+\Delta t}=A\varepsilon_b\Delta x\left(C_b\big|_{t+\Delta t}-C_b\big|_t\right)_{x,t}+A(1-\varepsilon_b)\Delta x\left(q_{t+\Delta t}-q_t\right)$$

Dividing both sides by $A\varepsilon_b\Delta t$

$$\left(\frac{uC_b}{\varepsilon_b}-D_{ax}\frac{\partial C_b}{\partial x}\right)_{x,t}-\left(\frac{uC_b}{\varepsilon_b}-D_{ax}\frac{\partial C_b}{\partial x}\right)_{x+\Delta x,t+\Delta t}=\frac{\Delta x}{\Delta t}\left(C_b\big|_{t+\Delta t}-C_b\big|_t\right)_{x,t}+\left(\frac{(1-\varepsilon_b)}{\varepsilon_b}\right)\frac{\Delta x}{\Delta t}\left(q_{t+\Delta t}-q_t\right)$$

Dividing by Δx and taking limit $\Delta x\to 0$ and $\Delta t\to 0$

$$\lim_{\Delta x\to 0}\left(\frac{\left(\dfrac{uC_b}{\varepsilon_b}-D_{ax}\dfrac{\partial C_b}{\partial x}\right)_{x,t}-\left(\dfrac{uC_b}{\varepsilon_b}-D_{ax}\dfrac{\partial C_b}{\partial x}\right)_{x+\Delta x,t+\Delta t}}{\Delta x}\right)$$

$$=\lim_{\Delta t\to 0}\left(\frac{\varepsilon_b\left(C_b\big|_{t+\Delta t}-C_b\big|_t\right)_{x,t}+(1-\varepsilon_b)\left(q_{t+\Delta t}-q_t\right)}{\varepsilon_b\ \Delta t}\right)$$

$$\text{or } \lim_{\Delta x \to 0} \left(\frac{\Delta\left(D_{ax} \frac{\partial C_b}{\partial x} - \frac{u C_b}{\varepsilon_b} \right)}{\Delta x} \right) = \lim_{\Delta t \to 0} \left(\frac{\varepsilon_b \Delta C_b + (1-\varepsilon_b)\Delta q_t)}{\varepsilon_b \, \Delta t} \right)$$

On solving and rearranging the terms we get,

$$-D_{ax} \frac{\partial^2 C_b}{\partial x^2} + \frac{\partial u C_b}{\partial x} + \frac{\partial C_b}{\partial t} + \frac{(1-\varepsilon_b)}{\varepsilon_b} \frac{\partial q_t}{\partial t} = 0 \tag{5.1}$$

In the above equation, D_{ax} corresponds to the coefficient of axial dispersion of adsorbate molecules in the column (m^2 sec^{-1}), u represents interstitial velocity of the particles or the particle fluid velocity in the bed due to convection in $m.sec^{-1}$, ε_b indicates the bed voidage, C_b is the bulk phase concentration of CO_2 measured in $mol.m^{-3}$, and q_t ($mol.g^{-1}$) represents the total concentration of adsorbate molecules adsorbed onto the solid adsorbent.

The above equation is the mathematical equation for obtaining the unsteady state concentration distribution of CO_2 gas along the bed. Similar equations have been reported by Knox et al. [203].

The following initial and final conditions are considered:

$C_b(0,t) = C_{in}$ $\quad at\ x = 0,\ t = 0$ (5.2)

$C_b(x,0) = 0$ $\quad at\ \ 0 < x < L,\ t = 0$ (5.3)

$$D_{ax} \frac{\partial C}{\partial x} = -u\left(C_{in} - C_b\right) \quad at \quad x = 0,\ t > 0 \tag{5.4}$$

$$\frac{\partial C}{\partial x} = 0 \quad at \quad x = L,\ t \geq 0 \tag{5.5}$$

5.1.1 Linear Driving Force (LDF) model

When the gas molecules enter the adsorption column and come in contact with the adsorbent bed, their rate of diffusion is governed by the difference of adsorbate concentration in the bulk and its equilibrium concentration in the adsorbent bed. Further, these molecules penetrate into the porous structure and get adsorbed on the surface or walls of the pores. Based on the diffusion mechanism four different rate models have been proposed and investigated by researchers. First one is homogeneous surface diffusion model (HSDM), which assumes the occurrence of

adsorption on the surface of the internal pores, second is pore diffusion model (PDM) which presumes that the diffusion occurs in the sorbed phase and then adsorption occurs evenly along the walls of the pores. The third model is pore and surface diffusion model (PSDM) which accounts for simultaneous occurrence of the surface as well as pore diffusion in the pores and lastly linear driving force model (LDF) model.

However, the mathematical models HSDM, PDM and PSDM are rigorous in nature and computationally time-consuming. Therefore, with the purpose of reducing the complication involved in modeling, concentrated parameters model can be employed to particle or adsorbed phase. In this context, the linear driving force (LDF) is utilized. LDF model was originally proposed by Gleuckauf and Coates [204]. It is considered a practical tool to study the adsorption kinetics on heterogeneous solids, evaluate adsorbent fixed bed dynamics, correlate and predict mono and multicomponent gas adsorption, and to design adsorptive processes as well. Linear driving force model was much investigated for gas separation in 1980's and has been used to describe the dynamic and batch adsorption behavior, using different adsorbents and flow conditions.

The effective mass transfer rate given by LDF model is expressed in Eq. 5.6 [205]:

$$\frac{\partial q_t}{\partial t} = \frac{3k_f}{a_p \rho_P}\left(C_b - C_s\right) \tag{5.6}$$

Where, k_f is the effective mass transfer coefficient, m sec^{-1}; C_s and C_b represent the concentration of CO_2 in equilibrium with surface concentration and bulk phase respectively, and a_p denotes the radius of the adsorbent particle.

Adsorption Isotherm

The relation between the adsorbate (CO_2) and solid adsorbent concentration at the interface is well described by Freundlich isotherm as written below:

$$q_t = K_F P^{1/n} \tag{5.7}$$

The concentration C_i is related to partial pressure P_i by the following equation:

$$C_i = \frac{y_i P_i}{RT} \tag{5.8}$$

The above differential equations were solved numerically by reducing them to ordinary differential equations using the Method of Lines (MOL). In earlier studies, Hwang, Jun [206] used MOL for solving the governing equations for CO_2 adsorption on a bed of solids. The reduced equations were solved using an inbuilt solver named ode 15s of MATLAB. The results obtained were plotted and compared with the available experimental data.

Adsorption equilibrium of carbon dioxide on Act-3-700

In order to understand the fixed-bed dynamics of the adsorption of CO_2 from a mixture of $CO_2 - N_2$ on the synthesized adsorbents, it is important to investigate the adsorption equilibrium behavior of the individual components. The adsorption equilibrium of carbon dioxide on this activated carbon was studied and elaborated in section 4.6. Freundlich model best described adsorption process as confirmed from highest R^2 value (0.992) and least error percentage (1.23 %). Sorbent capacity calculated from experimental data (q_{exp}) at different temperatures and Freundlich isotherm model predicted CO_2 adsorption capacity (q_{pred}) from mass balance of breakthrough experiments is summarized in Table 5.1.

Table 5.1 Adsorbent capacity calculated from experimental data (q_{exp}) and Freundlich isotherm model predicted CO_2 adsorption capacity (q_{pred}) for 12.5% CO_2 at different temperatures

Experiment No.	T(°C)	q_{exp} (mmol g^{-1})	q_{pred} (mmol g^{-1})
1	30	1.31	1.32
2	50	1.01	1.05
3	75	0.78	0.77
4	100	0.58	0.55

5.1.2 Parameter estimation

Wilke equation was used for estimation of the viscosity of the gas mixture and Chapman–Enskog equation was used for the determination of molecular diffusivities [207]. Sherwood number required for determination of axial dispersion was calculated by using Wakao and Funazkri correlation [208] and mass transport parameters were calculated from correlations available in

the literature [209]. The values of various model parameters were calculated from widely accepted correlations and formulas as given in Table 5.2.

5.2 Simulation of fixed bed adsorption

In order to understand the kinetics of fixed bed adsorption column for prediction of breakthrough curves, we need to take the help of mathematical tools or computer-based software. The overall mass balance equation (eq. 5.1) applied on fixed-bed column in present study is a partial differential equation (PDE) as it consists of two independent variables: space (x) and time (t). Further, the adsorption equilibrium is favored by a non-linear isotherm i.e. Freundlich, therefore these coupled equations (5.1 to 5.7) were solved numerically by reducing them to ordinary differential equations using the Method of Lines (MOL). For this, an algorithm was formulated and executed into numerical computing software named MATLAB. The reduced equations were solved by an in-built solver ode 15 s of MATLAB. The results obtained were plotted and compared with the available experimental data. In earlier studies, Hwang et al. [206] and Chou and Chen [210] also used MOL for solving the governing equations for CO_2 adsorption on a bed of solids.

5.2.1 Method of lines

Method of lines is considered a well recognized numerical technique which has been successfully used for the analysis of boundary value problems in various areas of physics such as electromagnetic field, transmission lines, waveguide structures, and scattering problems [211, 212]. It is a special case of finite difference method but more accurate and computationally efficient. The fundamental approach of this technique involves discretization of a specified differential equation in either one or two dimensions and applying analytical solution in the other dimensions. The algorithm constructed by MOL is quite simple and condensed and therefore few discretization lines are required for computation; subsequently less time is required for computing. It also holds good numerical stability and easy convergence for variety of problems. Therefore, this method has an edge over analytical as well as finite difference method.

Basic steps involved in the application of MOL:

(i) Solution region is partitioned into layers.

(ii) The differential equation is discretized in one coordinate direction.

(iii) Partial differential equation is decoupled to ordinary differential equation.

(iv) Inverse transform is obtained and boundary conditions are introduced.

(v) Finally, the solution of the equations is obtained.

Table 5.2 Correlations and formulas used

Axial mass dispersion coefficient [213]

$$\frac{D_{ax}}{D_m} = 20 + 0.5Sc.\,Re\,, \quad Re = \frac{u\,d_p\rho_g}{\mu_g}, \quad Sc = \frac{\mu_g}{\rho_g D_m}, \; u = \frac{u_s}{\varepsilon_b}\,, \; u_s = \frac{v}{A_s}$$

External film mass transfer coefficient, *kf*

$$Sh = 2 + \left(1.1 \times (Re)^{\frac{3}{5}} \times (Sc)^{0.33}\right), \; k_f = \frac{Sh \times Dm}{d_p}$$

Molecular diffusivity [207, 214]

$$D_{m,i} = \frac{1-y_i}{\sum_{j=1}^{n}\frac{y_j}{D_{ij}}}, \quad D_m = \sum_{i=1}^{n} y_i D_{m,i}\,, \quad D_{ij} = \frac{0.0018583\sqrt{T^3\left(\frac{1}{M_i}+\frac{1}{M_j}\right)}}{P_t\sigma_{ij}^2\Omega_{ij}}$$

$$\Omega_{ij} = 1.06036\left(\frac{\varepsilon_{ij}}{\kappa T}\right)^{0.15610} + 0.19300\exp^{(-0.47635\frac{\kappa T}{\varepsilon_{ij}})} + \; 1.03587\exp^{(-1.52996\frac{\kappa T}{\varepsilon_{ij}})} + 1.76474\exp^{(-3.89411\frac{\kappa T}{\varepsilon_{ij}})}$$

$$\frac{\varepsilon_{ij}}{\kappa} = \frac{(\varepsilon_i\varepsilon_j)^{0.5}}{\kappa}, \qquad \sigma_{ij} = \frac{\sigma_i+\sigma_j}{2}$$

Gas viscosity and density

$$\mu_g = \sum_{i=1}^{n} \frac{y_i\mu_i}{\sum_{j=1}^{n} y_i\Phi_{ij}}$$

$$\Phi_{ij} = \frac{1}{\sqrt{8}}\left[1 + \left(1 + \frac{M_i}{M_j}\right)\right]^{-1/2}\left[1 + \sqrt{\frac{\mu_i}{\mu_j}}\left(\frac{M_i}{M_j}\right)^{-1/4}\right]^2$$

$$\mu_i = 2.6693 \times 10^{-5}\frac{\left(\sqrt{M_i T}\right)}{{\sigma_i}^2\Omega_\mu}$$

$$\Omega_\mu = 1.16145\left(\frac{\varepsilon_i}{KT}\right)^{0.14874} + 0.52487\exp^{(-0.7732\frac{KT}{\varepsilon_i})} + 0.16178\exp^{(-2.43787\frac{KT}{\varepsilon_i})}$$

$$\rho_g = \frac{P}{R_g T}\sum_{i=1}^{n} y_i M_i$$

5.3 Effect of operating parameters

The Fixed bed and operational parameters required for simulation of breakthrough curves were obtained using equations given in Table 5.2. These parameters have been summed up in Table 5.3.

Table 5.3 Fixed bed and operational parameters used for simulation

Parameter	Units	Value
Particle density (ρ_p)	$kg\ m^{-3}$	1600
Bulk density of solids (ρ_b)	$kg\ m^{-3}$	980
Voidage of bed (ε_b)	-	0.23
Mass transfer coefficient, external film (k_f)	$m\ sec^{-1}$	0.0513
Molecular Diffusivity	$m^2\ sec^{-1}$	1.53×10^{-5}
Gas phase axial dispersion (D_{ax})	$m^2\ sec^{-1}$	16.93×10^{-4}
Particle radius (a_p)	m	0.001
Bed length (l)	m	0.080
Packed bed diameter (d_b)	m	0.0093
Inlet feed concentration (C_{in})	$mol\ m^{-3}$	5.02
Mass of the adsorbent (m)	g	2
Total time of flow (t)	sec	2160

5.3.1 Effect of concentration

Table 5.4 Constitutive terms obtained for different concentrations of CO_2 in feed

Conc. (vol%)	ρ_g ($kg.m^{-3}$)	μ_g ($kg.\ m^{-1}.sec^{-1}$)	Re	Sc	Sh	D_{ax} ($m^2.sec^{-1}$)	k_f ($m.sec^{-1}$)
5	1.17	1.753×10^{-5}	11.18	0.976	6.64	16.93×10^{-4}	0.0509
7.5	1.18	1.747×10^{-5}	11.38	0.960	6.67	16.93×10^{-4}	0.0510
10	1.21	1.741×10^{-5}	11.57	0.943	6.69	16.93×10^{-4}	0.0512
12.5	1.22	1.735×10^{-5}	11.76	0.927	6.71	16.93×10^{-4}	0.0513

Constitutive terms required for breakthrough simulation at various concentrations are summarized in Table 5.4. The model for packed bed adsorption of CO_2 on the synthesized

adsorbent is validated with the experimental data for different concentrations of CO_2 in the feed. The model predicted breakthrough curves for CO_2 concentrations of 5%, 7.5%, 10%, and 12.5% are compared with experimental data generated at 30 ºC and atmospheric pressure (Fig. 5.4). It can be noticed that the model results are in conformance with the experimentally generated data. Also, it can be seen from Fig. 5.4 (a-d) that with increase in CO_2 concentration in the feed stream, the bed gets saturated early as compared to the saturation achieved at lower concentrations. This may be due to availability of more CO_2 molecules to the active sites on the adsorbent surface leading to higher adsorption capacity. However, there are some deviations in simulated results which may be due to simplified assumptions of transport phenomena.

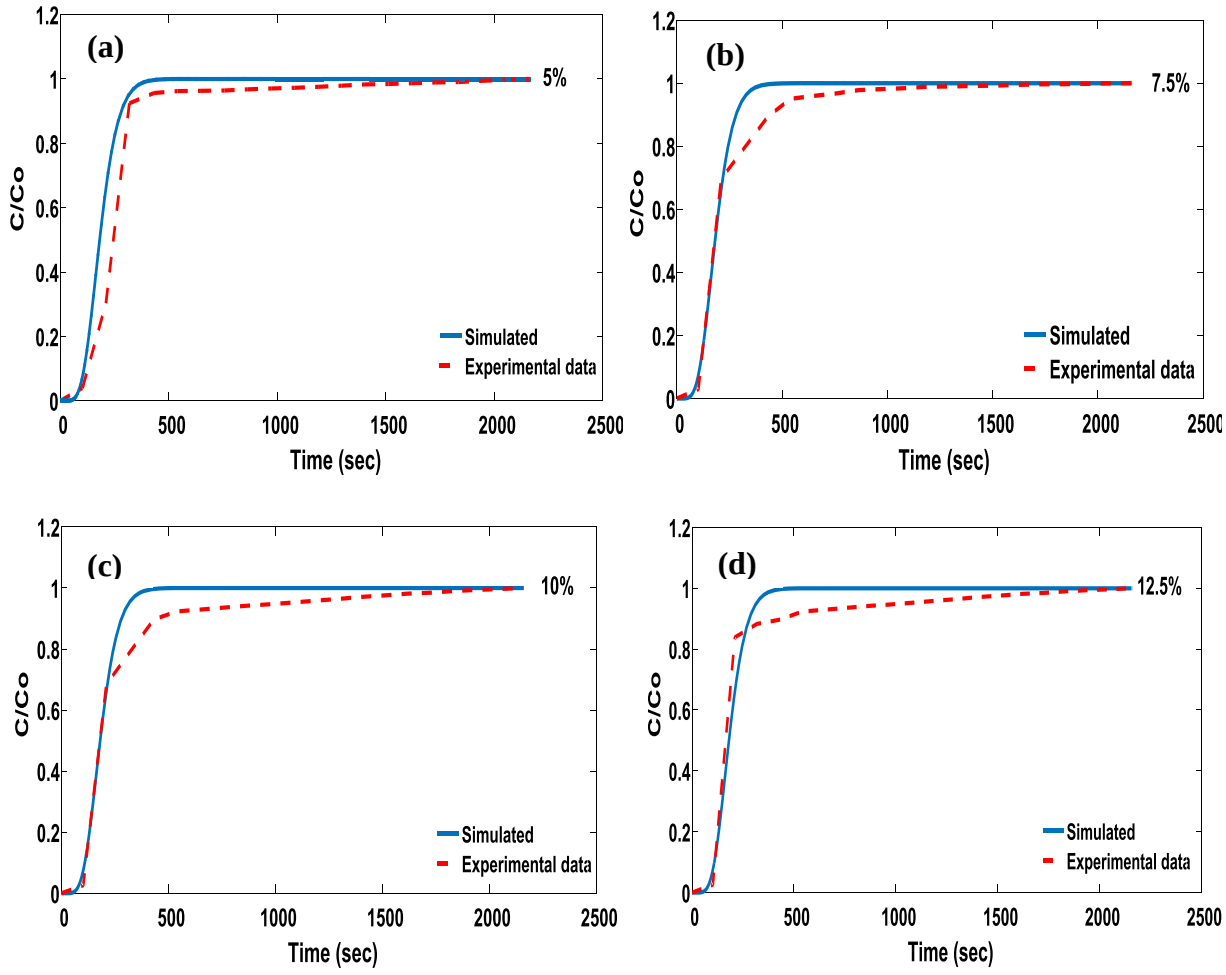

Fig. 5.4 Breakthrough curves at different concentrations (vol%) of CO_2 in feed (a) 5%, (b) 7.5%, (c) 10%, and (d) 12.5% of CO_2 at 30 ºC

5.3.2 Effect of temperature

Table 5.5 Constitutive terms obtained at different temperatures

T, °C	ρ_g ($kg.m^{-3}$)	μ_g ($kg.\ m.sec^{-1}$)	Re	Sc	Sh	D_{ax} ($m^2.sec^{-1}$	k_f ($m.sec^{-1}$)
30	1.22	1.73×10^{-5}	11.76	0.927	6.71	16.93×10^{-4}	0.0513
50	1.14	1.82×10^{-5}	10.51	0.923	6.39	18.57×10^{-4}	0.0550
75	1.064	1.92×10^{-5}	9.22	0.920	6.06	20.71×10^{-4}	0.0596
100	0.993	2.03×10^{-5}	8.173	0.917	5.77	22.99×10^{-4}	0.0642

Constitutive terms required for breakthrough simulation at various temperatures are summarized in Table 5.5. For these simulations the respective values of temperatures (30, 50, 75, 100 ºC) were substituted in the correlations in Table 5.2 for evaluating molecular diffusivity, axial dispersion and external film mass transfer coefficient and related dimensionless numbers like Reynolds number (Re), Schmidt number (Sc) and Sherwood number (Sh). The model results were compared with the experimental breakthrough curves obtained at different adsorption temperatures for CO_2 concentration of 12.5% (Fig. 5.5(a-d)).The model predicted results are in close conformity with the experimentally obtained data points at all temperatures. However, slight deviations of results from experiment data may be due to assumptions made before applying the macroscopic mass balance. Further, to compare the model predicted and experimentally generated data, parity plots were constructed for the breakthrough results obtained at different temperatures for 12.5% CO_2 concentration (Fig. 5.6). The regression analysis displayed good fitting of the model predicted and experimentally obtained results as confirmed the values of adjusted R^2 and error percentage (Table 5.6).

Table 5.6 Regression data obtained at different temperatures

Sr. No.	Adsorption temperature (ºC)	R^2	Error %
1	30	0.99077	1.971
2.	50	0.99822	0.872
3.	75	0.99411	1.57
4.	100	0.99776	0.988

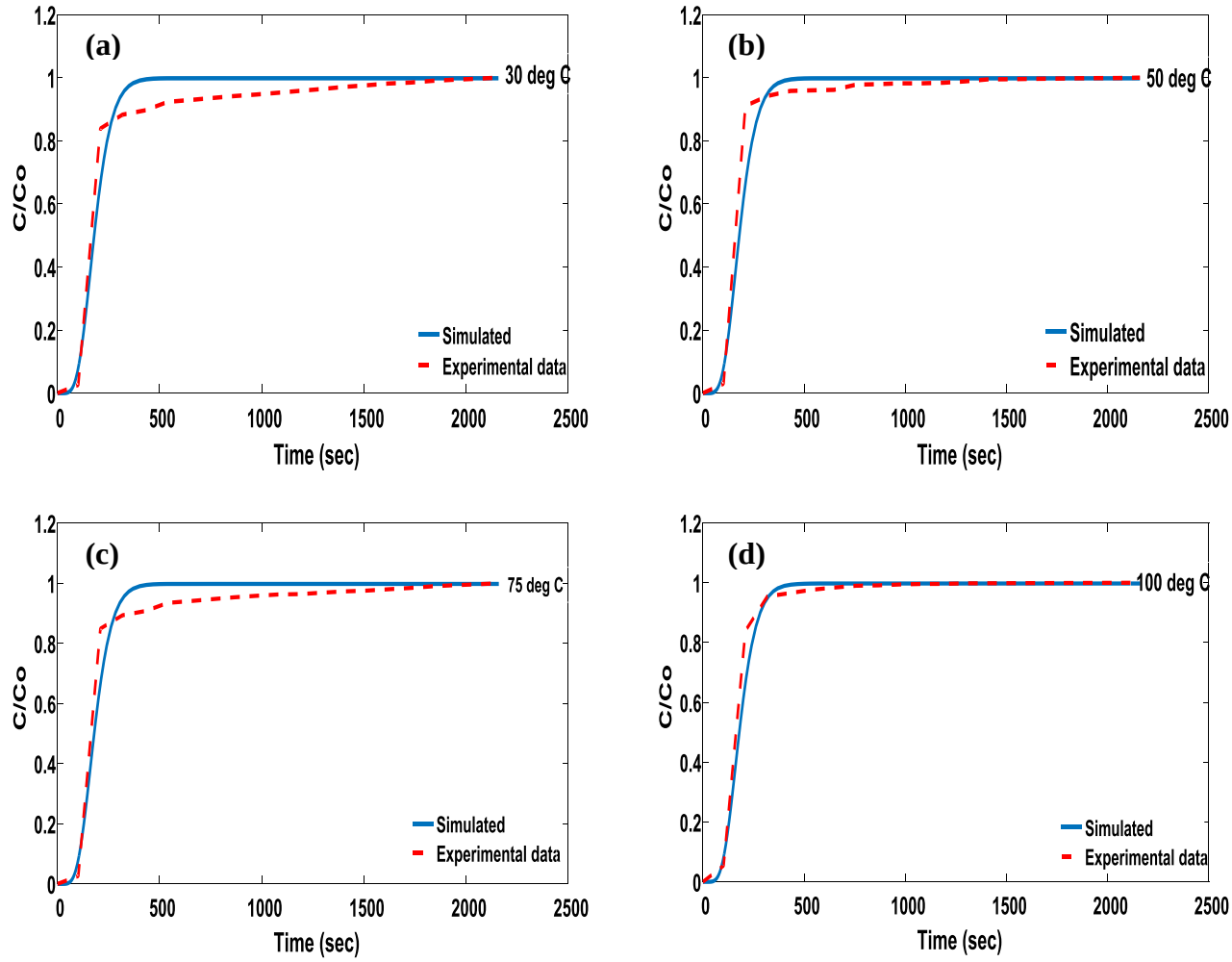

Fig. 5.5 Breakthrough curves at different temperatures (a) 30 °C, (b) 50 °C (c) 75 °C and (d) 100 °C for 12.5% CO_2 concentration

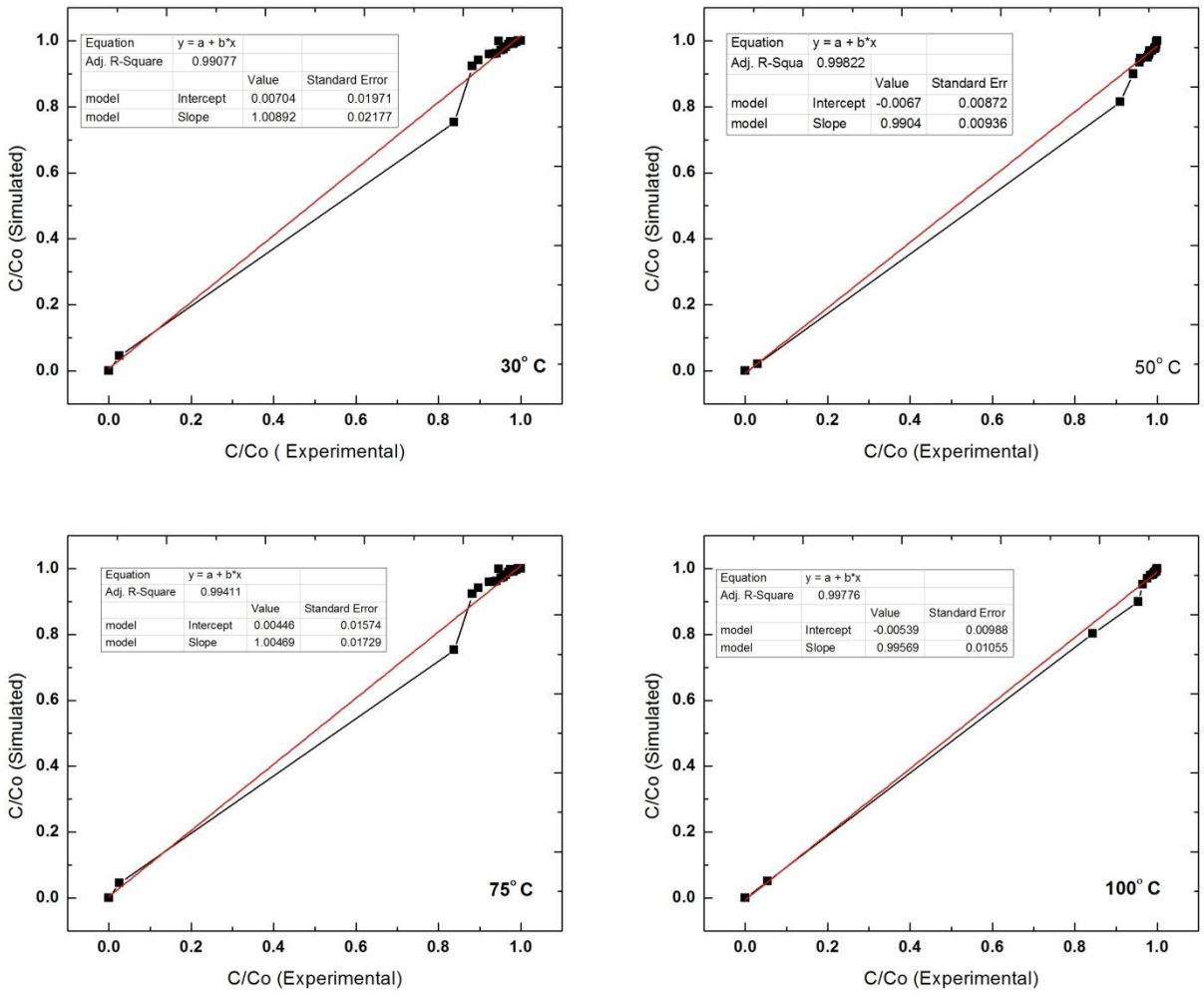

Fig. 5.6 Regression analysis of the model predicted and experimentally obtained results for Act-3-700 at different temperatures for 12.5% CO_2 concentration

Chapter 6 – Conclusions and Scope for Future Work

6.1 Conclusions

Porous carbon adsorbents with high surface area have been developed from PET wastes by carbonization and chemical activation with two different reagents (KOH and K_2CO_3) at different temperatures for efficient CO_2 adsorption. The prepared adsorbents exhibited considerable improvement in textural properties with rise in carbonization temperature and activating agent to carbon mass ratio. However, the performance of KOH activated samples was better than K_2CO_3 activated adsorbents. Therefore, the detailed studies were conducted with the adsorbent activated with KOH. The KOH activated adsorbents followed the CO_2 uptake in the sequence of Act-3-700 > Act-2-700 > Act-4-700 > Act-1-700 > B-700. The maximum adsorption capacity of 1.31 mmol g^{-1} is obtained for Act-3-700 at 30 °C and 12.5% CO_2 due to generation of higher microporosity and basic oxygen functionalities. The adsorbent shows good regenerability and stability over multiple adsorption-desorption cycles and is selective for CO_2 over N_2 for adsorption. Among the three attempted kinetic models, fractional-order best explained the kinetics of adsorption. Freundlich isotherm fit indicates the surface of adsorbent being heterogeneous and low values of isosteric heat shows physisorption behavior of the process. From thermodynamic investigations, negative values of Gibbs free energy change and enthalpy were obtained. These values respectively confirm the spontaneity and exothermicity of the adsorption process. The energy needed for desorbing 1 kg CO_2 from the activated adsorbent is found to be 1.34 MJ, which corresponds to 0.0576 kg CO_2 (~11.84% energy penalty).

The fixed bed model for CO_2 adsorption on the optimized adsorbent sample, using LDF approximation for mass transfer phenomena, satisfactorily described the experimental adsorption behavior. The model predicted breakthrough curves for different concentrations of CO_2 in feed (5%-12.5 vol%) and for different adsorption temperatures (30 -100 °C) matched closely with the experimental data.

6.2 Scope for future work

- Developing different carbon adsorbents from other waste plastics such as polyvinyl chloride (C_2H_3Cl), polycarbonate ($C_{16}H_{18}O_5$), polystyrene (C_8H_8), polyurethane foam ($C_{27}H_{36}N_2O_{10}$) etc. and evaluating their CO_2 capture potential.
- Investigating the influence of other impurities exiting from flue exhaust like oxides of sulphur (SO_x), oxides of nitrogen (NO_x), and moisture on CO_2 adsorption uptake, thus assessing the performance of the capture process in totality.
- Further investigations on the synthesized carbon adsorbents at ambient temperature and high pressures can be carried for assessing the improvement in their CO_2 capture capacity.

References

[1] Mukherjee A, Okolie JA, Abdelrasoul A, Niu C, Dalai AK. Review of post-combustion carbon dioxide capture technologies using activated carbon. *Journal of Environmental Science*s. 2019;83:46-63.

[2] Alonso A, Moral-Vico J, Markeb AA, Busquets-Fité M, Komilis D, Puntes V, et al. Critical review of existing nanomaterial adsorbents to capture carbon dioxide and methane. *Science of the Total Environment.* 2017;595:51-62.

[3] Siqueira RM, Freitas GR, Peixoto HR, do Nascimento JF, Musse APS, Torres AE, et al. Carbon dioxide capture by pressure swing adsorption. *Energy Procedia*. 2017;114:2182-92

[4] Kumar P, Aslam M, Singh N, Mittal S, Bansal A, Jha MK, et al. Characterization, activity and process optimization with a biomass-based thermal power plant's fly ash as a potential catalyst for biodiesel production. *RSC Advances*. 2015;5:9946-54.

[5] Change IC. Synthesis Report. Cambridge University Press, NY. USA. 2001.

[6] Azmi A, Aziz M. Mesoporous adsorbent for CO_2 capture application under mild condition: A review. *Journal of Environmental Chemical Engineering*. 2019;7:1-13.

[7] Yaumi A, Bakar MA, Hameed B. Reusable nitrogen-doped mesoporous carbon adsorbent for carbon dioxide adsorption in fixed-bed. *Energy*. 2017;138:776-84.

[8] D'Alessandro DM, Smit B, Long JR. Carbon dioxide capture: prospects for new materials. *Angewandte Chemie International Edition*. 2010;49:6058-82.

[9] IPCC, 2014: Climate Change 2014: Mitigation of climate change. Contribution of Working Group III to the Fifth Assessment Report of the Intergovernmental Panel on Climate Change. in: O. Edenhofer, R. Pichs-Madruga, Y. Sokona, E. Farahani, S. Kadner, K. Seyboth, A. Adler, I. Baum, S. Brunner, P. Eickemeier, B. Kriemann, J. Savolainen, S. Schlömer, C. von Stechow, T. Zwickel, J.C. Minx (Eds.) Cambridge, United Kingdom and New York, NY, USA, 2014.

[10] Al Mesfer MK, Danish M, Fahmy YM, Rashid MM. Post-combustion CO_2 capture with activated carbons using fixed bed adsorption. *Heat and Mass Transfer*. 2018;54:2715-24.

[11] CO2.earth. https://www.CO2.earth/. 2019 (accessed 10 January 2020)

[12] Yang H, Xu Z, Fan M, Gupta R, Slimane RB, Bland AE, et al. Progress in carbon dioxide separation and capture: A review. *Journal of Environmental Sciences*. 2008;20:14-27.

[13] Steeneveldt R, Berger B, Torp T. CO_2 capture and storage: closing the knowing–doing gap. *Chemical Engineering Research and Design*. 2006;84:739-63.

[14] Aeshala LM, Uppaluri R, Verma A. Electrochemical conversion of CO_2 to fuels: tuning of the reaction zone using suitable functional groups in a solid polymer electrolyte. *Physical Chemistry Chemical Physics.* 2014;16:17588-94.

[15] Akash A, Rao AB, Chandel MK. Relevance of carbon capture & sequestration in India's energy mix to achieve the reduction in emission intensity by 2030 as per INDCs. *Energy Procedia*. 2017;114:7492-503.

[16] Bennaceur K, Gielen D, Kerr T, Tam C. CO_2 Capture and Storage: A Key Carbon Abatement Option: OECD publishing Paris. 2008.

[17] Bui M, Adjiman CS, Bardow A, Anthony EJ, Boston A, Brown S, et al. Carbon capture and storage (CCS): The way forward. *Energy and Environment Science*. 2018;11:1062-176.

[18] *https://www.globalccsinstitute.com* (accessed 20 January 2020)

[19] Olajire AA. CO_2 capture and separation technologies for end-of-pipe applications - A review. *Energy*. 2010;35:2610-28.

[20] Rashidi NA, Yusup S. An overview of activated carbons utilization for the post-combustion carbon dioxide capture. *Journal of CO_2 Utilization*. 2016;13:1-16.
[21] Irons R, Sekkapan G, Panesar R, Gibbins J, Lucquiard M. CO_2 capture ready plants. IEA Greenhouse Gas Programme. 2007.
[22] Figueroa JD, Fout T, Plasynski S, McIlvried H, Srivastava RD. Advances in CO_2 capture technology-the US Department of Energy's Carbon Sequestration Program. *International Journal of Greenhouse Gas Control*. 2008;2:9-20.
[23] Sánchez J, Maroño M, Cillero D, Montenegro L, Ruiz E. Laboratory-and bench-scale studies of a sweet water-gas-shift catalyst for H_2 and CO_2 production in pre-combustion CO_2 capture. *Fuel*. 2013;114:191-8.
[24] Wall T, Stanger R, Liu Y. Gas cleaning challenges for coal-fired oxy-fuel technology with carbon capture and storage. *Fuel*. 2013;108:85-90.
[25] Rubin ES, Mantripragada H, Marks A, Versteeg P, Kitchin J. The outlook for improved carbon capture technology. *Progress in Energy and Combustion Science*. 2012;38:630-71.
[26] Al-Qodah Z, Shawabkah R. Production and characterization of granular activated carbon from activated sludge. *Brazilian Journal of Chemical Engineering.* 2009;26:127-36.
[27] Drage T, Smith K, Pevida C, Arenillas A, Snape C. Development of adsorbent technologies for post-combustion CO_2 capture. *Energy Procedia.* 2009;1:881-4.
[28] Zhang Z, Cai J, Chen F, Li H, Zhang W, Qi W. Progress in enhancement of CO_2 absorption by nanofluids: A mini review of mechanisms and current status. *Renewable Energy.* 2018;118:527-35.
[29] Rezakazemi M, Heydari I, Zhang Z. Hybrid systems: combining membrane and absorption technologies leads to more efficient acid gases (CO_2 and H_2S) removal from natural gas. *Journal of CO_2 utilization*. 2017;18:362-9.
[30] Nanda S, Reddy SN, Mitra SK, Kozinski JA. The progressive routes for carbon capture and sequestration. *Energy Science & Engineering.* 2016;4:99-122.
[31] Jajesniak P, Ali H, Wong TS. Carbon dioxide capture and utilization using biological systems: opportunities and challenges. *Journal of Bioprocessing and Biotechniques.* 2014;4:1-15.
[32] Zhao H, Luo X, Zhang H, Sun N, Wei W, Sun Y. Carbon-based adsorbents for post-combustion capture: A review. *Greenhouse Gases: Science and Technology*. 2018;8:11-36
[33] Fan LS, Zeng L, Wang W, Luo S. Chemical looping processes for CO_2 capture and carbonaceous fuel conversion–prospect and opportunity. *Energy & Environmental Science* 2012;5:7254-80.
[34] Laboratory NET. *www.netl.doe.gov* (accessed 15 December 2019).
[35] Rahman FA, Aziz MMA, Saidur R, Bakar WAWA, Hainin M, Putrajaya R, et al. Pollution to solution: Capture and sequestration of carbon dioxide (CO_2) and its utilization as a renewable energy source for a sustainable future. *Renewable and Sustainable Energy Reviews.* 2017;71:112-26.
[36] Idem R, Supap T, Shi H, Gelowitz D, Ball M, Campbell C, et al. Practical experience in post-combustion CO_2 capture using reactive solvents in large pilot and demonstration plants. *International Journal of Greenhouse Gas Control*. 2015;40:6-25.
[37] Vega F, Cano M, Camino S, Fernández LMG, Portillo E, Navarrete B. Solvents for carbon dioxide capture. Carbon Dioxide Chemistry, Capture and Oil Recovery. Intech open limited, London,UK. 2018.

[39] Mondal MK, Balsora HK, Varshney P. Progress and trends in CO_2 capture/separation technologies: a review. *Energy*. 2012;46:431-41.
[40] Zhang Z, Li Y, Zhang W, Wang J, Soltanian MR, Olabi AG. Effectiveness of amino acid salt solutions in capturing CO_2: A review. *Renewable and Sustainable Energy Reviews.* 2018;98:179-88.
[41] Koutsianos A, Barron AR, Andreoli E. CO_2 capture partner molecules in highly loaded PEI sorbents. *The Journal of Physical Chemistry C*. 2017;121:21772-81.
[42] Spigarelli BP, Kawatra SK. Opportunities and challenges in carbon dioxide capture. *Journal of CO_2 Utilization.* 2013;1:69-87.
[43] Ramasubramanian K, Ho WW. Recent developments on membranes for post-combustion carbon capture. *Current Opinion in Chemical Engineering.* 2011;1:47-54.
[44] Kentish SE, Scholes CA, Stevens GW. Carbon dioxide separation through polymeric membrane systems for flue gas applications. *Recent Patents on Chemical Engineering.* 2008;1:52-66.
[45] Kenarsari SD, Yang D, Jiang G, Zhang S, Wang J, Russell AG, et al. Review of recent advances in carbon dioxide separation and capture. *RSC Advances*. 2013;3:22739-73.
[46] Clodic D, Younes M. A new method for CO_2 capture: Frosting CO_2 at atmospheric pressure. *Greenhouse Gas Control Technologies-6th International Conference: Elsevier*; 2003;1:155-60.
[47] Tuinier M, Van Sint Annaland M, Kramer GJ, Kuipers J. Cryogenic CO_2 capture using dynamically operated packed beds. *Chemical Engineering Science*. 2010;65:114-9.
[48] Aaron D, Tsouris C. Separation of CO_2 from flue gas: a review. *Separation Science and Technology*. 2005;40:321-48.
[49] Packer M. Algal capture of carbon dioxide; biomass generation as a tool for greenhouse gas mitigation with reference to New Zealand energy strategy and policy. *Energy Policy*. 2009;37:3428-37.
[50] Eslamimanesh A, Mohammadi AH, Richon D, Naidoo P, Ramjugernath D. Application of gas hydrate formation in separation processes: A review of experimental studies. *The Journal of Chemical Thermodynamics.* 2012;46:62-71.
[51] Leung DY, Caramanna G, Maroto-Valer MM. An overview of current status of carbon dioxide capture and storage technologies. *Renewable and Sustainable Energy Reviews*. 2014;39:426-43.
[52] Singh S, Srivastava VC, Mall ID. Fixed-bed study for adsorptive removal of furfural by activated carbon. *Colloids and Surfaces A: Physicochemical and Engineering Aspects.* 2009;332:50-6.
[53] Ribeiro R, Grande C, Rodrigues A. Electric swing adsorption for gas separation and purification: A review. *Separation Science and Technology*. 2014;49:1985-2002.
[54] Nie L, Mu Y, Jin J, Chen J, Mi J. Recent developments and consideration issues in solid adsorbents for CO_2 capture from flue gas. *Chinese Journal of Chemical Engineering*. 2018;26:2303-17.
[55] Wang J, Huang L, Yang R, Zhang Z, Wu J, Gao Y, et al. Recent advances in solid sorbents for CO_2 capture and new development trends. *Energy and Environmental Science*. 2014;7:3478-518.
[56] Treybal RE. Mass Transfer Operations. New York. 1980;466.

[57] Wahby A, Ramos-Fernández JM, Martínez-Escandell M, Sepúlveda-Escribano A, Silvestre-Albero J, Rodríguez-Reinoso F. High surface area carbon molecular sieves for selective CO_2 adsorption. *ChemSusChem*. 2010;3:974-81.
[58] Sharuddin SDA, Abnisa F, Daud WMAW, Aroua MK. A review on pyrolysis of plastic wastes. *Energy Conversion and Management*. 2016;115:308-26.
[59] Arenillas A, Rubiera F, Parra JB, Ania CO & Pis JJ. Surface modification of low cost carbons for their application in the environmental protection. *Applied Surface Science*. 2005;252:619-24.
[60] Choma J, Marszewski M, Osuchowski L, Jagiello J, Dziura A, and Jaroniec M. Adsorption properties of activated carbons prepared from waste CDs and DVDs. *ACS Sustainable Chemistry & Engineering*. 2015;3:733-42.
[61] Clausse M, Merel J, Meunier F. Numerical parametric study on CO_2 capture by indirect thermal swing adsorption. *International Journal of Greenhouse Gas Control*. 2011;5:1206-13.
[62] Xu X, Song C, Andresen JM, Miller BG, Scaroni AW. Novel polyethylenimine-modified mesoporous molecular sieve of MCM-41 type as high-capacity adsorbent for CO_2 capture. *Energy & Fuels*. 2002;16:1463-9.
[63] Bonenfant D, Kharoune M, Niquette P, Mimeault M, Hausler R. Advances in principal factors influencing carbon dioxide adsorption on zeolites. *Science and Technology of Advanced Materials.* 2008;9:1-7.
[64] Song C, Ling Y, Jin L, Zhang M, Chen DL, He Y. CO_2 adsorption of three isostructural metal–organic frameworks depending on the incorporated highly polarized heterocyclic moieties. *Dalton Transactions.* 2016;45:190-7.
[65] Sengupta S, Amte V, Das AK, Yadav M, Mandal S, Nerivetla S, et al. Circulating Fluid-Bed Studies for CO_2 Capture from Flue Gas using K_2CO_3/Al_2O_3 Adsorbent. *Energy & Fuels*. 2018;32:8594-604.
[66] Yang RT. Adsorbents: Fundamentals and Applications: John Wiley & Sons; 2003.
[67] Deng S, Hu B, Chen T, Wang B, Huang J, Wang Y, Yu G. Activated carbons prepared from peanut shell and sunflower seed shell for high CO_2 adsorption. *Adsorption*. 2015;21:125-33.
[68] Wei H, Deng S, Hu B, Chen Z, Wang B, Huang J, Yu G. Granular bamboo-derived activated carbon for high CO_2 adsorption: the dominant role of narrow micropores. *ChemSusChem*. 2012;5:2354-60.
[69] Tiwari D, Bhunia H, Bajpai PK. Development of chemically activated N-enriched carbon adsorbents from urea-formaldehyde resin for CO_2 adsorption: Kinetics, isotherm, and thermodynamics. *Journal of Environmental Management*. 2018;218:579-92.
[70] Li JR, Sculley J, Zhou HC. Metal-organic frameworks for separations. *Chemical reviews*. 2012;112:869-932.
[71] Zhen HG, Mao H, Haq IU, Li SH, Ahmad A, Zhao ZP. In-situ SIFSIX-3-Cu growth into melamine formaldehyde sponge monolith for CO_2 efficient capture. *Separation and Purification Technology*. 2020;233:116042.
[72] Yoo DK, Yoon TU, Bae YS, Jhung SH. Metal-organic framework MIL-101 loaded with polymethacrylamide with or without further reduction: effective and selective CO_2 adsorption with amino or amide functionality. *Chemical Engineering Journal*. 2020;380:122496.
[73] Siegelman RL, Milner PJ, Forse AC, Lee J-H, Colwell KA, Neaton JB, et al. Water enables efficient CO_2 capture from natural gas flue emissions in an oxidation-resistant diamine-

appended metal–organic framework. *Journal of the American Chemical Society*. 2019;141:13171-86.
[74] Alessi A, Buscarino G, Agnello S, Sciortino L, Messina F, Cannas M, Gelardi FM, Boscaino R. Aging of MCM41, MSU-H and MSU-F mesoporous systems investigated through the Raman spectroscopy. *AIP Conference Proceedings. AIP Publishing* 2014;1624:3-9.
[75] Kumar S, Malik M, Purohit R. Synthesis methods of mesoporous silica materials. *Materials Today: Proceedings*. 2017;4:350-7.
[76] Xu X, Andresen JM, Song C, Miller BG, Scaroni AW. Preparation of novel CO_2 "molecular basket" of polymer modified MCM-41. *Division of Fuel Chemistry*. 2002;47:67-8.
[77] Xu X, Song C, Miller BG, Scaroni AW. Influence of moisture on carbon dioxide separation from simulated flue gas by a novel molecular basket adsorbent. *Preprint Papers American Chemical Society, Division of Fuel Chemistry*. 2004;49:300.
[78] Zeleňák V, Skřínska M, Siperstein FR, Patti A. Phase evolution during one-pot synthesis of amine modified mesoporous silica materials: Preparation, properties, carbon dioxide adsorption. *Applied Surface Science*. 2019;476:886-96.
[79] Peng HL, Zhang JB, Zhang JY, Zhong FY, Wu PK, Huang K, Fan JP, Liu F. Chitosan-derived mesoporous carbon with ultrahigh pore volume for amine impregnation and highly efficient CO_2 capture. *Chemical Engineering Journal*. 2019;359:1159-65.
[80] Dey R, Gupta R, Samanta A. Carbon dioxide capture under post combustion conditions using amine-functionalized SBA-15: Kinetics and multicyclic performance. *Separation Science and Technology*. 2018;53:2683-94.
[81] Hemingway BS, Robie RA. Thermodynamic properties of zeolites: Low-temperature heat capacities and thermodynamic functions for phillipsite and clinoptilolite. Estimates of the thermochemical properties of zeolitic water at low temperature. *American Mineralogist*. 1984;69:692-700.
[82] Siriwardane RV, Shen M-S, Fisher EP, Losch J. Adsorption of CO_2 on zeolites at moderate temperatures. *Energy & Fuels*. 2005;19:1153-9.
[83] Li Y, Yi H, Tang X, Li F, Yuan Q. Adsorption separation of CO_2/CH_4 gas mixture on the commercial zeolites at atmospheric pressure. *Chemical Engineering Journal*. 2013;229:50-6.
[84] Madden D, Curtin T. Carbon dioxide capture with amino-functionalised zeolite-β: A temperature programmed desorption study under dry and humid conditions. *Microporous and Mesoporous Materials* 2016;228:310-7.
[85] Chen C, Kim SS, Cho W-S, Ahn WS. Polyethylenimine-incorporated zeolite 13X with mesoporosity for post-combustion CO_2 capture. *Applied Surface Science*. 2015;332:167-71
[86] Jiang Q, Rentschler J, Sethia G, Weinman S, Perrone R, Liu K. Synthesis of T-type zeolite nanoparticles for the separation of CO_2/N_2 and CO_2/CH_4 by adsorption process. *Chemical Engineering Journal*. 2013;230:380-8.
[87] Shakarova D, Ojuva A, Bergström L, Akhtar F. Methylcellulose-directed synthesis of nanocrystalline zeolite NaA with high CO_2 uptake. *Materials*. 2014;7:5507-19.
[88] Nguyen TH, Kim S, Yoon M, Bae TH. Hierarchical zeolites with amine-functionalized mesoporous domains for carbon dioxide capture. *Chem Sus Chem*. 2016;9:455-61.
[89] Wang Y, Du T, Song Y, Che S, Fang X, Zhou L. Amine-functionalized mesoporous ZSM-5 zeolite adsorbents for carbon dioxide capture. *Solid State Sciences*. 2017;73:27-35.
[90] Brandani F, Ruthven DM. The effect of water on the adsorption of CO_2 and C_3H_8 on type X zeolites. *Industrial & Engineering Chemistry Research*. 2004;43:8339-44.

[91] Maji TK, Mostafa G, Chang H-C, Kitagawa S. Porous lanthanide-organic framework with zeolite-like topology. *Chemical Communications.* 2005:2436-8.
[92] Papa E, Medri V, Paillard C, Contri B, Murri AN, Vaccari A, et al. Geopolymer-hydrotalcite composites for CO_2 capture. *Journal of Cleaner Production*. 2019;237:117738.
[93] Chen SP, Sun X, Luo X, Liang Z. CO_2 Adsorption on premodified Li/Al hydrotalcite impregnated with polyethylenimine. *Industrial & Engineering Chemistry Research*. 2018;58:1177-89.
[94] Khalkhali M, Zhu X, Shi Y, Liu Q, Choi P, Zhang H. Structure and CO_2 physisorption capacity of hydrotalcite-derived oxide. *Journal of CO_2 Utilization*. 2020;36:64-75.
[95] Bhatta LKG, Subramanyam S, Chengala MD, Olivera S, Venkatesh K. Progress in hydrotalcite like compounds and metal-based oxides for CO_2 capture: a review. *Journal of Cleaner Production.* 2015;103:171-96.
[96] Salaudeen SA, Acharya B, Dutta A. CaO-based CO_2 sorbents: A review on screening, enhancement, cyclic stability, regeneration and kinetics modelling. *Journal of CO_2 Utilization*. 2018;23:179-99.
[97] Guo Y, Tan C, Sun J, Li W, Zhao C, Zhang J, et al. Nanostructured MgO sorbents derived from organometallic magnesium precursors for post-combustion CO_2 capture. *Energy & Fuels*. 2018;32:6910-7.
[98] Guo Y, Tan C, Wang P, Sun J, Li W, Zhao C, et al. Magnesium-based basic mixtures derived from earth-abundant natural minerals for CO_2 capture in simulated flue gas. *Fuel*. 2019;243:298-305.
[99] Granados-Pichardo A, Granados-Correa F, Sánchez-Mendieta V, Hernández-Mendoza H. New CaO-based adsorbents prepared by solution combustion and high-energy ball-milling processes for CO_2 adsorption: Textural and structural influences. *Arabian Journal of Chemistry*. 2017;13:171-183.
[100] Gao N, Chen K, Quan C. Development of CaO-based adsorbents loaded on charcoal for CO_2 capture at high temperature. *Fuel.* 2020;260:116411.
[101] Sengupta S, Amte V, Dongara R, Das AK, Bhunia H, Bajpai PK. Effects of the adsorbent preparation method for CO_2 capture from flue gas using K_2CO_3/Al_2O_3 adsorbents. *Energy & Fuels*. 2015;29:287-97.
[102] Sethia G, Sayari A. Comprehensive study of ultra-microporous nitrogen-doped activated carbon for CO_2 capture. *Carbon*. 2015;93:68-80.
[103] Hesas RH, Arami-Niya A, Daud WMAW, Sahu J. Microwave-assisted production of activated carbons from oil palm shell in the presence of CO_2 or N_2 for CO_2 adsorption. *Journal of Industrial and Engineering Chemistry*. 2015;24:196-205.
[104] Olivares-Marín M, Drage T, Maroto-Valer MM. Novel lithium-based sorbents from fly ashes for CO_2 capture at high temperatures. *International Journal of Greenhouse Gas Control*. 2010;4:623-29.
[105] Ribeiro RP, Grande CA, Rodrigues AE. Adsorption of water vapor on carbon molecular sieve: Thermal and electrothermal regeneration study. *Industrial & Engineering Chemistry Research*. 2011;50:2144-56.
[106] Creamer AE, Gao B. Carbon-based adsorbents for postcombustion CO_2 capture: a critical review. *Environmental Science & Technology*. 2016;50:7276-89.
[107] Liu Z, Grande CA, Li P, Yu J, Rodrigues AE. Multi-bed vacuum pressure swing adsorption for carbon dioxide capture from flue gas. *Separation and Purification Technology*. 2011;81:307-17.

[108] Dantas TL, Luna FM, Silva Jr IJ, de Azevedo DC, Grande CA, Rodrigues AE, Moreira RF. Carbon dioxide–nitrogen separation through adsorption on activated carbon in a fixed bed. *Chemical Engineering Journal*. 2011;169:11-9.
[109] Plaza MG, García S, Rubiera F, Pis J, Pevida C. Post-combustion CO_2 capture with a commercial activated carbon: Comparison of different regeneration strategies. *Chemical Engineering Journal*. 2010;163:41-7.
[110] Nasri NS, Hamza UD, Ismail SN, Ahmed MM, Mohsin R. Assessment of porous carbons derived from sustainable palm solid waste for carbon dioxide capture. *Journal of Cleaner Production*. 2014;71:148-57.
[111] Hu Z, Srinivasan M, Ni Y. Novel activation process for preparing highly microporous and mesoporous activated carbons. *Carbon*. 2001;39:877-86.
[112] Maroto-Valer MM, Lu Z, Zhang Y, Tang Z. Sorbents for CO_2 capture from high carbon fly ashes. *Waste Management*. 2008;28:2320-8.
[113] Han J, Zhang L, Zhao B, Qin L, Wang Y, Xing F. The N-doped activated carbon derived from sugarcane bagasse for CO_2 adsorption. *Industrial Crops and Products*. 2019;128:290-7.
[114] Wu X, Zhang C, Tian Z, Cai J. Large-surface-area carbons derived from lotus stem waste for efficient CO_2 capture. *New Carbon Materials*. 2018;33:252-61.
[115] Li Y, Xu R, Wang X, Wang B, Cao J, Yang J, et al. Waste wool derived nitrogen-doped hierarchical porous carbon for selective CO_2 capture. *RSC Advances*. 2018;8:19818-26.
[116] Olivares-Marín M, García S, Pevida C, Wong M, Maroto-Valer M. The influence of the precursor and synthesis method on the CO_2 capture capacity of carpet waste-based sorbents. *Journal of Environmental Management.* 2011;92:2810-7.
[117] cpcb. https://cpcb.nic.in/ (accessed 12 January 2020).
[118] Kunwar B, Cheng H, Chandrashekaran SR, Sharma BK. Plastics to fuel: A review. *Renewable and Sustainable Energy Reviews.* 2016;54:421-8.
[119] Choi S, Drese JH, Jones CW. Adsorbent materials for carbon dioxide capture from large anthropogenic point sources. *ChemSusChem: Chemistry & Sustainability Energy & Materials*. 2009;2:796-854.
[120] Okan M, Aydin HM, Barsbay M. Current approaches to waste polymer utilization and minimization: A review. *Journal of Chemical Technology & Biotechnology*. 2019;94:8-21.
[121] Li Z, Wang K, Song J, Xu Q, Kobayashi N. Preparation of activated carbons from polycarbonate with chemical activation using response surface methodology. *Journal of Material Cycles and Waste Management.* 2014;16:359-66.
[122] Tiwari D. Studies on carbon dioxide capture using polymer based carbon adsorbents. *PhD Thesis.* 2018;Thapar Institute of Engineering and Technology, Patiala, India.
[123] Sneddon G, McGlynn JC, Neumann MS, Aydin HM, Yiu HH, Ganin AY. Aminated poly (vinyl chloride) solid state adsorbents with hydrophobic function for post-combustion CO_2 capture. *Journal of Materials Chemistry A.* 2017;5:11864-72.
[124] Fu Z, Jia J, Li J, Liu C. Transforming waste expanded polystyrene foam into hyper-crosslinked polymers for carbon dioxide capture and separation. *Chemical Engineering Journal.* 2017;323:557-64.
[125] Ge C, Song J, Qin Z, Wang J, Fan W. Polyurethane foam-based ultramicroporous carbons for CO_2 capture. *ACS Applied Materials & Interfaces*. 2016;8:18849-59.
[126] Lo SH, Raja DS, Chen CW, Kang YH, Chen JJ, Lin CH. Waste polyethylene terephthalate (PET) materials as sustainable precursors for the synthesis of nanoporous MOFs, MIL-47, MIL-53 (Cr, Al, Ga) and MIL-101 (Cr). *Dalton Transactions*. 2016;45:9565-73.

[127] Lu AH, Hao GP, Zhang XQ. Porous carbons for carbon dioxide capture. Porous materials for carbon dioxide capture: Springer Berlin Heidelberg; 2014.
[128] Iijima S. Helical microtubules of graphitic carbon. *Nature*.1991;354:56-8.
[129] Hata K, Futaba DN, Mizuno K, Namai T, Yumura M, Iijima S. Water-assisted highly efficient synthesis of impurity-free single-walled carbon nanotubes. *Science.* 2004;306:1362-4.
[130] Su F, Lu C, Chen H-S. Adsorption, desorption, and thermodynamic studies of CO_2 with high-amine-loaded multiwalled carbon nanotubes. *Langmuir*. 2011;27:8090-8.
[131] Ngoy JM, Wagner N, Riboldi L, Bolland OA CO_2 capture technology using multi-walled carbon nanotubes with polyaspartamide surfactant. *Energy Procedia*. 2014;63:2230-48.
[132] Deng M, Park HG. Spacer-assisted amine-coiled carbon nanotubes for CO_2 capture. *Langmuir*. 2019;35:4453-9.
[133] Olivares-Marin MM-V, M. M. Preparation of a highly microporous carbon from a carpet material and its application as CO_2 sorbent. *Fuel Processing Technology*. 2011;92:322-9.
[134] Tiwari D, Goel C, Bhunia H, Bajpai PK. Dynamic CO_2 capture by carbon adsorbents: kinetics, isotherm and thermodynamic studies. *Separation and Purification Technology*. 2017;181:107-22.
[135] Tiwari D, Bhunia H, Bajpai PK. Epoxy based oxygen enriched porous carbons for CO_2 capture. *Applied Surface Science*. 2017;414:380-9.
[136] Tiwari D, Goel C, Bhunia H, Bajpai PK. Novel nanostructured carbons derived from epoxy resin and their adsorption characteristics for CO_2 capture. *RSC Advances*. 2016;6:97728-38.
[137] Sneddon G, McGlynn JC, Neumann MS, Aydin HM, Yiu HH, Ganin AY. Aminated poly (vinyl chloride) solid state adsorbents with hydrophobic function for post-combustion CO_2 capture. *Journal of Materials Chemistry A.* 2017;5:11864-72.
[138] Goel C, Bhunia H, Bajpai PK. Synthesis of nitrogen doped mesoporous carbons for carbon dioxide capture. *RSC Advances*. 2015;5:46568-82.
[139] Tiwari D, Bhunia H, Bajpai PK. Adsorption of CO_2 on KOH activated, N-enriched carbon derived from urea formaldehyde resin: Kinetics, isotherm and thermodynamic studies. *Applied Surface Science*. 2018;439:760-71.
[140] Lagergren S. About the theory of so-called adsorption of soluble substances. *Kungliga Svenska Vetenskapsakademiens Handlingar*. 1898; 24:1-39.
[141] Ho YS, McKay G. Pseudo-second order model for sorption processes. *Process Biochemistry*. 1999;34:451-65.
[142] Ho YS. Absorption of heavy metals from waste streams by peat: *Ph. D. Thesis*; University of Birmingham, 1995.
[143] Zeldowitsch J. The catalytic oxidation of carbon monoxide on manganese dioxide. *Acta Physicochim URSS.* 1934;1:364-449.
[144] Serna-Guerrero R, Sayari A. Modeling adsorption of CO_2 on amine-functionalized mesoporous silica. 2: Kinetics and breakthrough curves. *Chemical Engineering Journal*. 2010;161:182-90.
[145] Shen C, Grande CA, Li P, Yu J, Rodrigues AE. Adsorption equilibria and kinetics of CO_2 and N_2 on activated carbon beads. *Chemical Engineering Journal*. 2010;160:398-407.
[146] Freundlich HMF. Over the adsorption in solution. *Journal of Physical Chemistry*. 1906;57:385-471.

[147] Langmuir I. The constitution and fundamental properties of solids and liquids. Part I. Solids. *Journal of The American Chemical Society*. 1916;38:2221-95.
[148] Temkin MI, Pyzhev V. Kinetics of ammonia synthesis on promoted iron catalyst. *Acta Physicochimica URSS*. 1940;12:327-56.
[149] Salvestrini S, Leone V, Iovino P, Canzano S, Capasso S. Considerations about the correct evaluation of sorption thermodynamic parameters from equilibrium isotherms. *The Journal of Chemical Thermodynamics*. 2014;68:310-6.
[150] Goel C, Kaur H, Bhunia H, Bajpai PK. Carbon dioxide adsorption on nitrogen enriched carbon adsorbents: Experimental, kinetics, isothermal and thermodynamic studies. *Journal of CO_2 Utilization.* 2016;16:50-63.
[151] Guo B, Chang L, Xie K. Adsorption of carbon dioxide on activated carbon. *Journal of Natural Gas Chemistry*. 2006;15:223-9.
[152] Singh G, Lakhi KS, Ramadass K, Kim S, Stockdale D, Vinu A. A combined strategy of acid-assisted polymerization and solid state activation to synthesize functionalized nanoporous activated biocarbons from biomass for CO_2 capture. *Microporous and Mesoporous Materials.* 2018;271:23-32.
[153] Sun Y, Zhao J, Wang J, Tang N, Zhao R, Zhang D, Guan T, Li K. Sulfur-doped millimeter-sized microporous activated carbon spheres derived from sulfonated poly (styrene-divinylbenzene) for CO_2 capture. *The Journal of Physical Chemistry C*. 2017;121:10000-9.
[154] Querejeta N, Gil MV, Pevida C, Centeno TA. Standing out the key role of ultramicroporosity to tailor biomass-derived carbons for CO_2 capture. *Journal of CO_2 Utilization*. 2018;26:1-7.
[155] Xu C, Hedin N. Microporous adsorbents for CO_2 capture - a case for microporous polymers? *Materials Today*. 2014;17:397-403.
[156] Bragg R, Hammond M. X-ray study of pyrolytic graphites and glassy carbons. *Carbon*. 1965;3:340.
[157] Bratek W, Świątkowski A, Pakuła M, Biniak S, Bystrzejewski M, Szmigielski R. Characteristics of activated carbon prepared from waste PET by carbon dioxide activation. *Journal of Analytical and Applied Pyrolysis*. 2013;100:192-8.
[158] Sajjadi S-A, Mohammadzadeh A, Tran HN, Anastopoulos I, Dotto GL, Lopičić ZR, et al. Efficient mercury removal from wastewater by pistachio wood wastes-derived activated carbon prepared by chemical activation using a novel activating agent. *Journal of Environmental Management.* 2018;223:1001-9.
[159] Parra JB, Ania CO, Arenillas A, Rubiera F, Pis JJ, Palacios JM. Structural changes in polyethylene terephthalate (PET) waste materials caused by pyrolysis and CO_2 activation. *Adsorption Science & Technology*. 2006;24:439-50.
[160] Kaur B, Gupta RK, Bhunia H. Chemically activated nanoporous carbon adsorbents from waste plastic for CO_2 capture: Breakthrough adsorption study. *Microporous and Mesoporous Materials.* 2019;282:146-58.
[161] Madejová J. FTIR techniques in clay mineral studies. Vibrational Spectroscopy. 2003;31:1-10.
[162] Gnanasambandam R, Proctor A. Determination of pectin degree of esterification by diffuse reflectance Fourier transform infrared spectroscopy. *Food Chemistry*. 2000;68:327-32.
[163] Cuhadaroglu D, Uygun OA. Production and characterization of activated carbon from a bituminous coal by chemical activation. *African Journal of Biotechnology*. 2008;7:3703-10.

[164] Coates J. Interpretation of infrared spectra, a practical approach. *Encyclopedia of Analytical Chemistry*. 2000;12:10815-37.
[165] Ahmida K, Darmoon M, Al-Tohami F, Erhayem M, Zidan M. Effect of Physical and Chemical Preparation on Characteristics of Activated Carbon from Agriculture Solid Waste and their Potential Application. *International Conference of Chemical, Biological & Environmental Engineering*. 2015;5-6.
[166] Idris-Hermann KT, Raoul TTD, Giscard D, Gabche AS. Preparation and characterization of activated carbons from bitter kola (*Garcinia kola*) nut shells by chemical activation method using H_3PO_4; KOH and $ZnCl_2$. *Chemical Science International Journal.* 2018;23,1-15.
[167] Lua AC, Yang T. Effect of activation temperature on the textural and chemical properties of potassium hydroxide activated carbon prepared from pistachio-nut shell. *Journal of Colloid and Interface Science.* 2004;274:594-601.
[168] Mihajlović M, Petrović J, Kragović M, Stojanović M, Milojković J, Lopičić Z, et al. Effect of KOH activation on hydrochar surface: FTIR analysis. *Radiation and Applications.* 2017;20:65-67.
[169] Bou M, Martin J, Le Mogne T, Vovelle L. Chemistry of the interface between aluminium and polyethyleneterephthalate by XPS. *Applied Surface Science*. 1991;47:149-61.
[170] Laszlo K, Szűcs A. Surface characterization of polyethyleneterephthalate (PET) based activated carbon and the effect of pH on its adsorption capacity from aqueous phenol and 2, 3, 4-trichlorophenol solutions. *Carbon*. 2001;39:1945-53.
[171] Puziy A, Poddubnaya O, Socha R, Gurgul J, Wisniewski M. XPS and NMR studies of phosphoric acid activated carbons. *Carbon*. 2008;46:2113-23.
[172] Wiśniewski M, Terzyk AP, Gauden PA, Kaneko K, Hattori Y. Removal of internal caps during hydrothermal treatment of bamboo-like carbon nanotubes and application of tubes in phenol adsorption. *Journal of Colloid and Interface Science.* 2012;381:36-42.
[173] Park SJ, Jin SY. Effect of ozone treatment on ammonia removal of activated carbons. *Journal of Colloid and Interface Science.* 2005;286:417-9.
[174] Singh J, Bhunia H, Basu S. Synthesis of porous carbon monolith adsorbents for carbon dioxide capture: Breakthrough adsorption study. *Journal of the Taiwan Institute of Chemical Engineers*. 2018;89:140-50.
[175] Hayashi Ji, Horikawa T, Takeda I, Muroyama K, Ani FN. Preparing activated carbon from various nutshells by chemical activation with K_2CO_3. *Carbon*. 2002;40:2381-6.
[176] Singh J, Basu S, Bhunia H. Dynamic CO_2 adsorption on activated carbon adsorbents synthesized from polyacrylonitrile (PAN): Kinetic and isotherm studies. *Microporous and Mesoporous Materials*. 2019;280:357-66.
[177] Sreńscek-Nazzal J, Narkiewicz U, Morawski A, Wróbel R, Gęsikiewicz-Puchalska A, Michalkiewicz B. Modification of commercial activated carbons for CO_2 adsorption. *Acta Physica Polonica, A.* 2016;129.
[178] Pevida C, Drage T, Snape CE. Silica-templated melamine-formaldehyde resin derived adsorbents for CO_2 capture. *Carbon*. 2008;46:1464-74.
[179] Goel C, Bhunia H, Bajpai PK. Novel nitrogen enriched porous carbon adsorbents for CO_2 capture: Breakthrough adsorption study. *Journal of Environmental Chemical Engineering.*. 2016;4:346-56.

[180] Goel C, Bhunia H, Bajpai PK. Mesoporous carbon adsorbents from melamine-formaldehyde resin using nanocasting technique for CO_2 adsorption. *Journal of Environmental Sciences.* 2015;32:238-48.
[181] Nabgan B, Abdullah TA, Tahir M, Nabgan W, Gambo Y, Ibrahim M, Saeh I, Moghadamian K. Evaluation of theoretical and experimental mass transfer limitation in steam reforming of phenol-PET waste to hydrogen production over Ni/La-promoted Al_2O_3 catalyst. *Journal of Environmental Chemical Engineering*. 2017;5:2752-60.
[182] Nabgan B, Abdullah TA, Tahir M, Nabgan W, Triwahyono S, Jalil AA, Gambo Y, Ibrahim M, Moghadamian K. Pellet size dependent steam reforming of polyethylene terephthalate waste for hydrogen production over Ni/La promoted Al_2O_3 catalyst. *International Journal of Hydrogen Energy*. 2017;42:21571-85.
[183] Gunathilake C, Jaroniec M. Mesoporous calcium oxide–silica and magnesium oxide–silica composites for CO_2 capture at ambient and elevated temperatures. *Journal of Materials Chemistry A.* 2016;4:10914-24.
[184] Rehman A, Park SJ. Tunable nitrogen-doped microporous carbons: Delineating the role of optimum pore size for enhanced CO_2 adsorption. *Chemical Engineering Journal*. 2019;319:731-742.
[185] Moura PA, Vilarrasa-Garcia E, Maia DA, Bastos-Neto M, Ania CO, Parra JB, Azevedo DC. Assessing the potential of nanoporous carbon adsorbents from polyethylene terephthalate (PET) to separate CO_2 from flue gas. *Adsorption*. 2018;24:279-91.
[186] Adibfar M, Kaghazchi T, Asasian N, Soleimani M. Conversion of poly (ethylene terephthalate) waste into activated carbon: Chemical activation and characterization. *Chemical Engineering & Technology*. 2014;37:979-86.
[187] Przepiórski J , Czyżewski A , Pietrzak R, Morawski AW. MgO/CaO-loaded activated carbon for carbon dioxide capture: Practical aspects of use. *Industrial & Engineering Chemistry Research*. 2013;52:6669-77.
[188] Vargas D, Giraldo L, Erto A, Moreno-Piraján J. Chemical modification of activated carbon monoliths for CO_2 adsorption. *Journal of Thermal Analysis and Calorimetry*. 2013;114:1039-47.
[189] Chiou MS, Li HY. Equilibrium and kinetic modeling of adsorption of reactive dye on cross-linked chitosan beads. *Journal of Hazardous Materials*. 2002;93:233-48.
[190] Fauth D, Gray M, Pennline H, Krutka H, Sjostrom S, Ault A. Investigation of porous silica supported mixed-amine sorbents for post-combustion CO_2 capture. *Energy & Fuels.* 2012;26:2483-96.
[191] Szekely J. Evans, and HY Sohn, Gas–Solid Reactions. Academic Press, New York; 1976.
[192] Esteves IA, Lopes MS, Nunes PM, Mota JP. Adsorption of natural gas and biogas components on activated carbon. *Separation and Purification Technology*. 2008;62:281-96.
[193] Brems A, Baeyens J, Vandecasteele C, Dewil R. Polymeric cracking of waste polyethylene terephthalate to chemicals and energy. *Journal of the Air & Waste Management Association*. 2011;61:721-31.
[194] Sengupta S. Studies on CO_2 capture using adsorption from simulated refinery flue gas. *Ph.D. Thesis.* 2016; Thapar Institute of Engineering and Technology, Patiala, India .
[195] Sengupta S, Reddy SA, Dongara R, Das AK, Bhunia H, Bajpai PK. Improvement in regeneration properties and multicycle stability for K_2CO_3/Al_2O_3 adsorbents for CO_2 removal from flue gas. *Energy & Fuels.* 2014;28:5354-62.

[196] Delgado JA, Uguina MA, Sotelo JL, Ruiz B. Fixed-bed adsorption of carbon dioxide-helium, nitrogen-helium and carbon dioxide-nitrogen mixtures onto silicalite pellets. *Separation and Purification Technology*. 2006;49:91-100.
[197] Shafeeyan MS, Daud WMAW, Shamiri A. A review of mathematical modeling of fixed-bed columns for carbon dioxide adsorption. *Chemical Engineering Research and Design*. 2014;92:961-88.
[198] Siahpoosh M, Fatemi S, Vatani A. Mathematical modeling of single and multi-component adsorption fixed beds to rigorously predict the mass transfer zone and breakthrough curves. *Iranian Journal of Chemistry and Chemical Engineering*. 2009;28:25-44.
[199] Sharma M, Vyas RK, Singh K. Theoretical and experimental analysis of reactive adsorption in a packed bed: parallel and branched pore-diffusion model approach. *Industrial & Engineering Chemistry Research*. 2016;55:5945-54.
[200] Ben-Mansour R, Habib MA, Bamidele OE, Basha M, Qasem NA, Peedikakkal A, Laoui T, Ali M. Carbon capture by physical adsorption: materials, experimental investigations and numerical modeling and simulations-A review. *Applied Energy*. 2016;161:225-55.
[201] Won W, Lee S, Lee K-S. Modeling and parameter estimation for a fixed-bed adsorption process for CO_2 capture using zeolite 13X. *Separation and Purification Technology*. 2012;85:120-9.
[202] Dantas TL, Luna FM, Silva Jr IJ, Torres AE, de Azevedo DC, Rodrigues AE, Moreira RF. Carbon dioxide–nitrogen separation through pressure swing adsorption. *Chemical Engineering Journal*. 2011;172:698-704.
[203] Knox JC, Ebner AD, LeVan MD, Coker RF, Ritter JA. Limitations of breakthrough curve analysis in fixed-bed adsorption. *Industrial & Engineering Chemistry Research*. 2016;55:4734-48.
[204] Glueckauf E, Coates J. 241. Theory of chromatography. Part IV. The influence of incomplete equilibrium on the front boundary of chromatograms and on the effectiveness of separation. *Journal of the Chemical Society*. 1947:1315-21.
[205] Babu B, Gupta S. Modeling and simulation of fixed bed adsorption column: effect of velocity variation. *i-Manager's Journal on Future Engineering and Technology*. 2005;1:60.
[206] Hwang KS, Jun JH, Lee WK. Fixed-bed adsorption for bulk component system. Non-equilibrium, non-isothermal and non-adiabatic model. *Chemical Engineering Science.* 1995;50:813-25.
[207] Bird RB, Stewart WE, Lightfoot EN. Transport Phenomena, John Wiley & Sons. New York. 1960.
[208] Wakao N, Funazkri T. Effect of fluid dispersion coefficients on particle-to-fluid mass transfer coefficients in packed beds: correlation of Sherwood numbers. *Chemical Engineering Science*. 1978;33:1375-84.
[209] Ruthven DM. Principles of adsorption and adsorption processes: John Wiley & Sons; 1984.
[210] Chou CT, Chen CY. Carbon dioxide recovery by vacuum swing adsorption. *Separation and Purification Technology*. 2004;39:51-65.
[211] Sadiku MN, Obiozor C. A simple introduction to the method of lines. *International Journal of Electrical Engineering Education*. 2000;37:282-96.
[212] Mahmmod QY, Mohammed AS, Abdullah ZM Improving Parallel Solutions For Method of Lines to 1-D Heat Equation by using Five Point Finite Differene. *Tikrit Journal of Pure Science*. 2018;23:144-52.

[213] Cavenati S, Grande CA, Rodrigues AE. Separation of $CH_4/CO_2/N_2$ mixtures by layered pressure swing adsorption for upgrade of natural gas. *Chemical Engineering Science*. 2006;61:3893-906.
[214] Rios RB, Correia LS, Bastos-Neto M, Torres AEB, Hatimondi SA, Ribeiro AM, et al. Evaluation of carbon dioxide-nitrogen separation through fixed bed measurements and simulations. *Adsorption*. 2014;20:945-57.

LIST OF PUBLICATIONS

Publications

1. In Peer-reviewed (SCI) journals

1.1 Related to Ph.D. work

i. **Balpreet Kaur**, Raj Kumar Gupta, and Haripada Bhunia, "Chemically activated nanoporous carbon adsorbents from waste plastic for CO_2 capture: Breakthrough adsorption study" Microporous and Mesoporous Materials, 2019, 282, 146-158. (Impact Factor: 4.182)

ii. **Balpreet Kaur**, Raj Kumar Gupta, and Haripada Bhunia, "CO_2 capture on activated carbon from PET (polyethylene terephthalate) waste: kinetics and modeling studies" Chemical Engineering Communications, 2019, 207(8), 1031-1047. (Impact Factor: 1.431)

1.2 In related area

i. **Balpreet Kaur**, Jasminder Singh, Raj Kumar Gupta, and Haripada Bhunia, " Porous carbons derived from polyethylene terephthalate (PET) waste for CO_2 capture studies" Journal of Environmental Management, 2019, 242, 68-80. (Impact Factor: 4.865)

2. In conference

i. **Balpreet Kaur**, Raj Kumar Gupta and Haripada Bhunia, "Carbon Dioxide Capture and Utilization: A Review", 71st Annual session of Indian Institute of Chemical Engineers, CHEMCON- 2018, National Institute of Technology, Jalandhar, India, December 27-30, 2018

REPRINTS OF PUBLISHED ARTICLES

Microporous and Mesoporous Materials 282 (2019) 146–158

Contents lists available at ScienceDirect

Microporous and Mesoporous Materials

journal homepage: www.elsevier.com/locate/micromeso

Chemically activated nanoporous carbon adsorbents from waste plastic for CO_2 capture: Breakthrough adsorption study

Balpreet Kaur, Raj Kumar Gupta, Haripada Bhunia*

Department of Chemical Engineering, Thapar Institute of Engineering and Technology (Deemed to be University), Patiala, 147004, Punjab, India

ARTICLE INFO

Keywords:
PET waste
Chemical activation
CO_2 adsorption
Breakthrough curves
Adsorption isotherm
Thermodynamics

ABSTRACT

This paper describes the preparation of O-enriched porous carbonaceous adsorbents derived from low cost, abundantly available polyethylene terephthalate (PET) waste with high carbon content by directly carbonising at different temperatures (500–800 °C) and then chemically activating using variable impregnation ratios of KOH to carbon. The prepared carbon adsorbents were characterized for their textural and surface chemical properties using nitrogen sorption, CHN, FTIR, XRD, SEM, HRTEM, and XPS techniques. Further, to assess their CO_2 adsorption-desorption performance under dynamic conditions, breakthrough experiments were conducted in a fixed-bed adsorption set up. Porous carbon obtained at 700 °C with KOH to carbon mass ratio of 3 (Act-3-700) exhibited best textural properties with BET surface area of 1690 m^2g^{-1} and micropore volume of 0.78 $cm^3 g^{-1}$ and showed highest CO_2 uptake of 1.31 mmol g^{-1} at 30 °C and 12.5% CO_2 concentration. Four adsorption–desorption cycles establish the adsorbent's remarkable stability and regeneration. Furthermore, fractional order kinetic model explained the CO_2 adsorption kinetics and Freundlich isotherm showed superior fit with the adsorption equilibrium data suggesting heterogeneous nature of the adsorbent surface. Negative values of Gibbs free energy ΔG° and adsorption enthalpy ΔH° indicate the spontaneous and exothermic nature of adsorption process.

1. Introduction

In the present era, one of the major threats to environment is climate change and the well known and accepted basis for this is green house gas (GHG) emissions. The most abundantly emitted GHGs are carbon dioxide (56%) and methane (18%) [1–3]. CO_2 is the key contributor promoting global warming and subsequently affecting the climate as manifested by frequent occurrence of floods and droughts, progressive rise in temperature and sea levels, heat waves and melting of glaciers [4]. Concentration of CO_2 has uplifted from ~280 ppm from the preindustrial period [3,5] to ~408 ppm currently [6]. Capturing of CO_2 from major point sources, such as coal-fired power plants (contributing 40% of total CO_2 emissions), gas processing units, refineries, etc and its sequestration (CCS) is recognized as an important wayout to address this problem [7]. To economically sequester CO_2, it is imperative to comprise cost-effective capture for which the adsorption-based post-combustion CO_2 capture has been identified as a promising alternative due to its lower energy requirements, cost effectiveness, and simplicity in use at a broad range of temperatures. However, the main challenge in successfully commercializing adsorption technology is the development of effective and low cost adsorbents. Up till today an extensive range of materials have been prepared and analyzed for CO_2 adsorption namely amines [8], zeolites [9], metal-organic-frameworks (MOFs) [10,11], silicas [12], metal oxide-based adsorbents [13], and activated carbons from biomass and synthetic polymers [14–16]. In comparison to these adsorbents, the distinctive properties of carbon-based materials such as high surface area, excellent regenerability over multi-cycle adsorption/desorption, superior mechanical and thermal stability and non-expensive preparation make them exclusively promising for CO_2 adsorption. Presence of high carbon content together with absence of mineral matter and impurities makes PET waste a highly potential precursor of carbon materials [17]. Moreover, PET waste takes around 500–700 years to biodegrade, therefore environmentalists are seriously concerned about its disposal [18]. Various studies on carbon adsorbents using PET waste as precursor in removal of pollutants from wastewater [19–22], natural gas adsorption [23] and as electrode material in supercapacitors [24] are available but very limited reports are available on their application in capturing of CO_2. Different routes for synthesis of adsorbents from plastic wastes have been proposed and attempted such as gasification/pyrolysis, direct carbonization supplemented with physical or chemical activation and hydrothermal carbonization [17,25,26]. Parra et al. [17,27] prepared

* Corresponding author.
E-mail addresses: balpreet.kaur@thapar.edu (B. Kaur), rkgupta@thapar.edu (R.K. Gupta), hbhunia@thapar.edu (H. Bhunia).

https://doi.org/10.1016/j.micromeso.2019.03.025
Received 8 January 2019; Received in revised form 22 February 2019; Accepted 16 March 2019
Available online 21 March 2019
1387-1811/

CHEMICAL ENGINEERING COMMUNICATIONS
2020, VOL. 207, NO. 8, 1031–1047
https://doi.org/10.1080/00986445.2019.1635466

Taylor & Francis
Taylor & Francis Group

CO_2 capture on activated carbon from PET (polyethylene terephthalate) waste: Kinetics and modeling studies

Balpreet Kaur, Raj Kumar Gupta, and Haripada Bhunia

Department of Chemical Engineering, Thapar Institute of Engineering and Technology (Deemed to be University), Patiala, Punjab, India

ABSTRACT

CO_2 emissions from flue gases can be restricted via a promising post-combustion capture technique, namely, adsorption. In the present work, behavior of adsorbents, prepared from PET (polyethylene terephthalate) waste, for CO_2 capture studies was investigated to understand the fixed bed adsorption dynamics. The effect of activation on textural properties, surface functional groups and elemental composition was studied through nitrogen adsorption/desorption, XPS, FTIR, and EDX analysis. Thermal stability of adsorbent samples was also evaluated. The kinetics of the adsorption process was studied using Lagergren's pseudo-first-order model, pseudo-second, fractional order, Elovich, and Avrami models. Freundlich isotherm fit confirmed the heterogeneous nature of adsorbent's surface. Adsorption column breakthrough profiles were modeled using linear driving force (LDF) approximation for mass transfer. Model equations were solved using the Method of lines in MATLAB environment. Results show that the model closely approximated the column breakthrough curves for different CO_2 concentrations (5–12.5%) and different adsorption temperatures (30–100 °C).

KEYWORDS

Breakthrough curves; CO_2 capture; LDF model; method of lines; PET waste

Introduction

Carbon dioxide (CO_2) emissions in consequence of fossil fuel burning, are considered to be the major contributors to global climate change (Goel et al., 2016). In recent years, the concentration of CO_2 in the atmosphere has sharply increased and surpassed levels of ~414 ppm (CO_2.earth, 2019). This value is expected to rise up to a level of 550 ppm by 2100 if fossil-fuel burning continues at the present rate (Tiwari et al., 2016). It is a general consensus that these levels should not exceed 350 ppm (Wennersten et al., 2015). Progressive increase in CO_2 concentration at current pace will adversely impact the global environment causing droughts, rise in temperature of earth's surface, augment in acidity of sea water and simultaneously causing financial losses too which are anticipated to be about 5–20% of the global gross domestic product (Tiwari et al., 2017; Qasem and Ben-Mansour, 2018). Carbon dioxide capture and storage (CCS) has proved to be a promising technique for reducing CO_2 emissions in the environment. Precombustion decarbonization, oxy-fuel combustion, and post-combustion are three different ways to put CCS technological advances into practice. Among these, post-combustion capture of CO_2 on solid adsorbents is more advantageous due to its low capital cost and lesser energy requirement. Also, this technology can be retrofitted in the existing power plants. Furthermore, the fixed bed adsorption process can be implemented at an industrial level using well-established technologies (temperature swing or pressure swing adsorption).

Physical properties of an adsorbent play a crucial role in capturing CO_2. An effective adsorbent is expected to possess following characteristics: low cost, high capacity, selectivity, easy regenerabilty, stability, faster kinetics, and good abrasive

CONTACT Raj Kumar Gupta rkgupta@thapar.edu Department of Chemical Engineering, Thapar Institute of Engineering and Technology (Deemed to be University), Patiala, Punjab 147004, India.
Color versions of one or more of the figures in the article can be found online at www.tandfonline.com/gcec.
Supplemental data for this article is available online at https://doi.org/10.1080/00986445.2019.1635466.

Journal of Environmental Management 242 (2019) 68–80

Contents lists available at ScienceDirect

Journal of Environmental Management

journal homepage: www.elsevier.com/locate/jenvman

Research article

Porous carbons derived from polyethylene terephthalate (PET) waste for CO_2 capture studies

Balpreet Kaur[a], Jasminder Singh[b], Raj Kumar Gupta[a], Haripada Bhunia[a,*]

[a] Department of Chemical Engineering, Thapar Institute of Engineering and Technology (Deemed to be University), Patiala, 147004, Punjab, India
[b] School of Chemistry and Biochemistry, Thapar Institute of Engineering and Technology (Deemed to be University), Patiala, 147004, Punjab, India

ARTICLE INFO

Keywords:
PET waste
KOH activation
CO_2 uptake
Adsorption kinetics
Adsorption isotherm
Thermodynamics

ABSTRACT

Oxygen augmented carbon adsorbent has been developed using polyethylene terephthalate (PET) waste by first carbonizing at different temperatures (500–800 °C) and then chemically activating using different ratios of KOH: PET (mass ratio 1 to 4). The textural characterization divulges the effect of activation in terms of the development of the high surface area and micropore volume of 1690 $m^2 g^{-1}$ and 0.78 $cm^3 g^{-1}$ respectively, for the optimum sample (PET-3-700). Elemental analysis of PET-3-700 illustrates the presence of 34.33% oxygen and XPS results confirmed the occurrence of oxygen moieties which enhance the basicity of the adsorbent and promote CO_2 capture. The CO_2 adsorption capacity of prepared carbons was determined thermogravimetrically under dynamic conditions, at different concentrations of CO_2 (6–100%) and temperatures. The maximum CO_2 uptake capacity of 2.31 mmol g^{-1} was exhibited by PET-3-700 at an adsorption temperature of 30 °C under 100% pure CO_2 flow. Four adsorption-desorption cycles corroborate almost complete regenerability of the prepared adsorbent. Adsorption kinetics at all adsorption conditions was described best by fractional order kinetic model. Freundlich isotherm fit indicates the surface of adsorbent being heterogeneous and low values of isosteric heat shows physisorption behavior of the process. Negative values of thermodynamic parameters indicate exothermic and feasible nature of adsorption process.

1. Introduction

The industrial revolution has caused a huge impact on the environment and damaged its essential domains including land, water, and air. The major effect is due to air pollution caused by it. This effect has further created disturbance in many natural processes including sea level rise, melting of glaciers, etc. (Robinson et al., 2007) and the major anthropogenic gas which is a key contributor to disorder is carbon dioxide (CO_2). Ironically, its concentration in our environment is increasing from decades with current level being 406 ppm (CO_2.earth, 2018) and if the trend continues it may reach up to 570 ppm by 2100 (Yu et al., 2008). According to Intergovernmental Panel on Climate Change the rise in CO_2 concentration up to these levels may cause a rise in mean global temperature (~1.9 °C), average sea level (~3.8 m) and ocean acidification consequently leading to detrimental effects on climate change and marine life (McCarthy et al., 2001; Stewart and Hessami, 2005). So, presently initiatives need to be taken to combat this problem in order to prevent any further damage to our environment. Also, this captured CO_2, as a renewable carbon feedstock can be converted into valuable products such as fine chemicals (urea, carbonates, acrylates, etc) and transportation fuels. It can also be utilized as feedstock in pharmaceuticals, polymer synthesis, beverages and inorganic chemicals (Al-Mamoori et al., 2017).

Among the diverse available technologies namely absorption, membrane separation, cryogenic distillation, and adsorption, absorption technique using alkanolamine and monoethanol amine is being used at large scale (Chatti et al., 2009) but there are many drawbacks of this technology such as corrosion of equipment and high energy requirement. Consequently, there is a need for the development of better option than the currently existing ones for controlling CO_2 emissions. Adsorption technology which is based on the molecular interaction between the adsorbate molecules and the adsorbent surface is yet another promising and viable technique for capturing CO_2 due to its cost-effectiveness, high CO_2 uptake and low energy requirements of the selected porous adsorbents (Siriwardane et al., 2001). Some special type of materials notably zeolites (Bonenfant et al., 2008), pyrogenic carbon (Creamer and Gao, 2016), amine modified precursors (Chatti et al., 2009), metal-organic-frameworks (MOFs) (Song et al., 2014,

* Corresponding author.
E-mail addresses: balpreet.kaur@thapar.edu (B. Kaur), jasminder.singh91@gmail.com (J. Singh), rkgupta@thapar.edu (R.K. Gupta), hbhunia@thapar.edu (H. Bhunia).

https://doi.org/10.1016/j.jenvman.2019.04.077
Received 5 November 2018; Received in revised form 5 March 2019; Accepted 19 April 2019